Recent advances in modeling and simulation of nanofluid flows-Part I Fundamentals and theory

O. Mahian, L. Kolsi, M. Amani, Patrice Estellé, G. Ahmadi, C. Kleinstreuer, J.S. Marshall, M. Siavashi, R.A. Taylor, H. Niazmand, et al.

Recent Advances in Modeling and Simulation of Nanofluid Flows-Part I: Fundamental and Theory

Omid Mahian [a,b,c*], Lioua Kolsi[d,e], Mohammad Amani [f], Patrice Estellé [g], Goodarz Ahmadi[h], Clement Kleinstreuer[i], Jeffrey S. Marshall[j], Majid Siavashi[k], Robert A. Taylor[l], Hamid Niazmand[m], Somchai Wongwises[c,n], Tasawar Hayat[o,p], Arun Kolanjiyil[i], Alibakhsh Kasaeian[q], Ioan Pop[r]

*Corresponding author email: omid.mahian@gmail.com

[a] *School of Chemical Engineering and Technology, Xi'an Jiaotong University, Xi'an, Shaanxi 710049, China*

[b] *Center for Advanced Technologies, Ferdowsi University of Mashhad, Mashhad, Iran*

[c] *Fluid Mechanics, Thermal Engineering and Multiphase Flow Research Laboratory(FUTURE Lab.), Department of Mechanical Engineering, Faculty of Engineering, King Mongkut's University of Technology Thonburi, Bangmod, Bangkok 10140, Thailand*

[d] *Dept. Mech. Engineering, College of Engineering, Hail University, Hail City, Saudi Arabia*

[e] *Laboratory of metrology and energy system, National engineering school, Monastir, University of Monastir, Tunisia*

[f] *Mechanical and Energy Engineering Department, Shahid Beheshti University, Tehran, Iran*

[g] *Univ Rennes, LGCGM, EA3913, F-35000 Rennes, France*

[h] *Department of Aeronautical and Mechanical Engineering, Clarkson University, NY, USA*

[i] *Department of Mechanical and Aerospace Engineering, North Carolina State University, Raleigh, USA.*

[j] *Department of Mechanical Engineering, University of Vermont, Burlington VT, USA*

[k] *Applied Multiphase Fluid Dynamics Laboratory, School of Mechanical Engineering, Iran University of Science and Technology, Tehran, Iran*

[l] *School of Mechanical and Manufacturing Engineering, School of Photovoltaics and Renewable Energy Engineering, University of New South Wales, Kensington, New South Wales, Australia*

[m] *Department of Mechanical Engineering, Ferdowsi University of Mashhad, Mashhad, Iran*

[n] *The Academy of Science, The Royal Institute of Thailand, Sanam Suea Pa, Dusit, Bangkok 10300, Thailand*

[o] *Nonlinear Analysis and Applied Mathematics (NAAM) Research Group, Department of Mathematics, Faculty of Science, King Abdulaziz University, Jeddah 121589, Saudi Arabia*

[p] *Department of Mathematics, Quaid-i-Azam University 45320, Islamabad 44000, Pakistan*

[q] *Faculty of New Sciences and Technologies, University of Tehran, Tehran, Iran*

[r] *Faculty of Mathematics, University of Cluj, R-3400 Cluj, CP 253, Romania*

Abstract

It has been more than two decades since the discovery of nanofluids-mixtures of common liquids and solid nanoparticles less than 100 nm in size. As a type of colloidal suspension, nanofluids are typically employed as heat transfer fluids due to their favorable thermal and fluid properties. There have been numerous numerical studies of nanofluids in recent years (more than 1000 in both 2016 and 2017, based on Scopus statistics). Due to the small size and large numbers of nanoparticles that interact with the surrounding fluid in nanofluid flows, it has been a major challenge to capture both the macro-scale and the nano-scale effects of these systems without incurring extraordinarily high computational costs. To help understand the state of the art in modeling nanofluids and to discuss the challenges that remain in this field, the present article reviews the latest developments in modeling of nanofluid flows and heat transfer with an emphasis on 3D simulations. In part I, a brief overview of nanofluids (fabrication, applications, and their achievable thermo-physical properties) will be presented first. Next, various forces that exist in particulate flows such as drag, lift (Magnus and Saffman), Brownian, thermophoretic, van der Waals, and electrostatic double layer forces and their significance in nanofluid flows are discussed. Afterwards, the main models used to calculate the thermophysical properties of nanofluids are reviewed. This will be followed with the description of the main physical models presented for nanofluid flows and heat transfer, from single-phase to Eulerian and Lagrangian two-phase models. In part II, various computational fluid dynamics (CFD) techniques will be presented. Next, the latest studies on 3D simulation of nanofluid flow in various regimes and configurations are reviewed. The present review is expected to be helpful for researchers working on numerical simulation of nanofluids and also for scholars who work on experimental aspects of nanofluids to understand the underlying physical phenomena occurring during their experiments.

Keywords: Nanofluids, thermophysical properties, dynamics of nanoparticles, physical models

Table of Contents

1- Introduction

Amelioration of heat transfer rate in thermal systems has been always one of the primary concerns of scientists. Let's start with a simple example. Consider the engine of an automobile. The friction between moving and stationary parts in the engine leads to temperature rise in the system, so a lubricant (Engine oil) is used for cooling the components. The engine performance improves if we can increase the lubricant ability in heat removal. But the question is, how can this be done? One solution is the augmentation of oil thermal conductivity; in this way its ability for cooling purposes increases. The thermal conductivity of solids is much greater than that of fluids. Figure 1 has been drawn to show the difference between thermal conductivity of liquids including water and oil with some solids such as ceramics, metals, and graphene (which is known as a semi-metal). As seen, thermal conductivity of metals and graphene are hundreds of times higher than that of liquids. As shown in Fig. 1, some solids like graphene have very high thermal conductivity (thousands of times higher than liquids) which makes them a suitable option to employ in thermal systems.

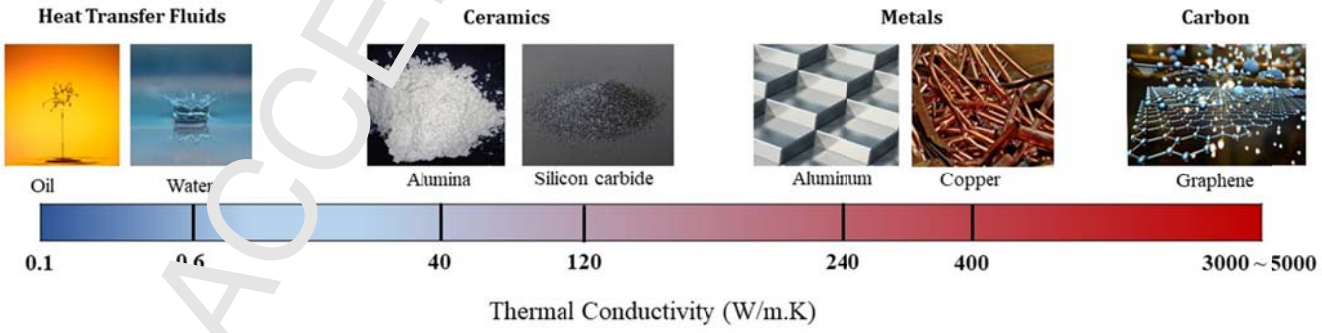

Figure 1. Thermal conductivity of some common liquids and solids, the high thermal conductivity of solids gives the idea to mix them with liquids to enhance the effective thermal conductivity.

From the above discussion, one idea for thermal conductivity enhancement of oil could be adding solid particles at low concentrations to the base fluid to augment the effective thermal conductivity. However, what sizes of particles are most suitable? Using particles with diameters in the millimeter or even micrometer range results in the eventual sedimentation of suspended particles unless the particles are perfectly neutrally buoyant. Gravitational effects are minimized because of solid particles with the smallest possible size, in the nanoscale size range. The stability of nanoparticle-based liquids is much greater than that of microparticle-based liquids; moreover, at a given mass of solid particles, the contact surface area between nanoparticles is bigger than that of microparticles, which leads to faster thermal response of the particles to change in liquid temperature in mixtures containing nanoparticles. Figure 2 compares the diameter of typical carbon nanotubes with the size of some well-known things such as an ant and a single grain of salt to better visualize the size of a nanoparticle. As seen, the diameter of a carbon nanotube can be 1 million times smaller than that of a single grain of salt.

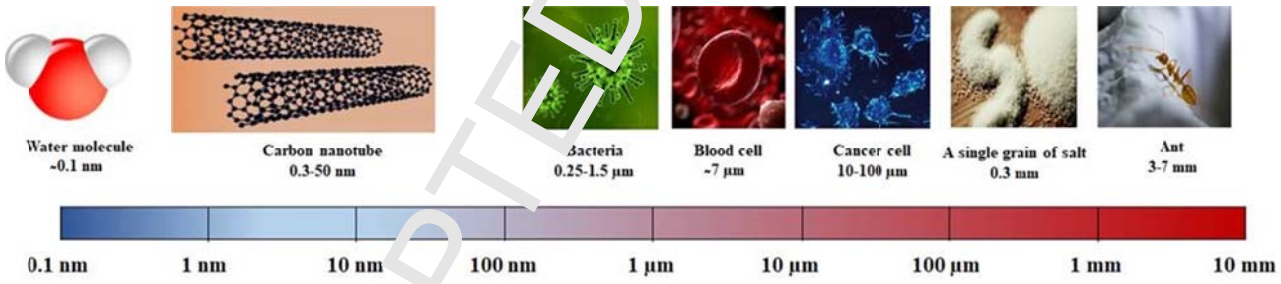

Figure 2. Comparison between sizes of carbon nanotubes as a typical nanoparticle with other things

1.1. What is a nanofluid?

In 1993, Masuda et al. [1] measured thermal conductivity and viscosity of three different water-based suspensions containing Al_2O_3, TiO_2, and SiO_2 nanoparticles (particles with a size between 1 and 100 nm). They reported that both thermal conductivity and viscosity of the water become greater than

before by adding nanoparticles. Later in 1995, Choi [2] selected the name "nanofluid" for a mixture of nanoparticles and a liquid. It should be kept in mind that nanofluids are not prepared simply by adding nanoparticles to water or oil and stirring the mixture, similar to mixing sugar and tea, but rather the formation of a nanofluid requires special physical and chemical processes in order to produce a uniform and efficient dispersion of particles for long-term applications. Use of surfactant (non-covalent functionalization), functionalization of nanoparticles, control of pH and sonication are some primary approaches for increasing the stability of nanofluids [3]. Figure 3 presents the main physical and chemical approaches that might be used to prepare stable nanofluids. The most suitable method for preparing stable nanofluids is determined based on the nanoparticles type and the choice of the base liquid.

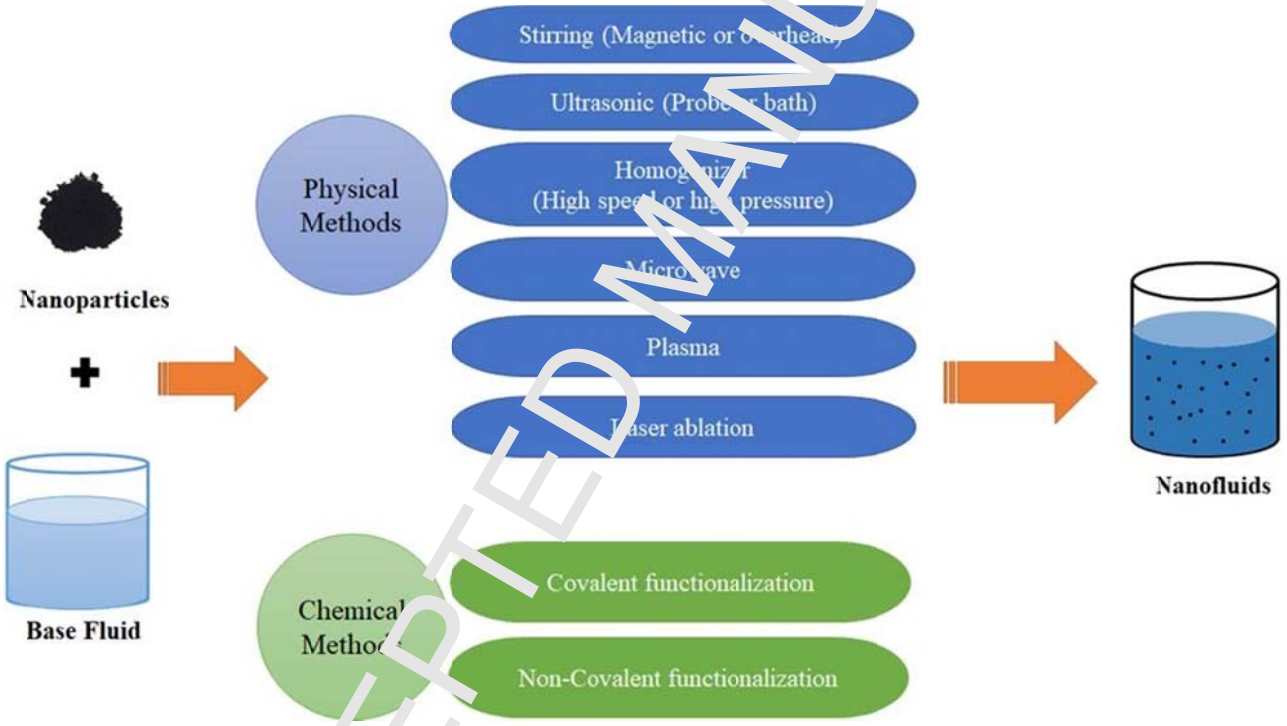

Figure 3. Nanofluid preparation is not just mixing nanoparticles and a liquid but special physical and chemical techniques are needed to have a stable nanofluid.

1.2. How has the research on nanofluids evolved?

After the initial introduction of nanofluids, many researchers assessed the potential of various nanofluids for heat transfer enhancement. Figure 4 indicates how the research on nanofluids evolved

from its introduction in 1995 up to the present time, and which subject areas have been of most interest during this time period. The results were extracted from the Scopus database by searching "nanofluid" or "nanofluids" in the article title, abstract, and keywords (date of extract: 16 April 2018). As seen in Fig. 4(a), after 2005 the number of articles per year increased remarkably year by year, so that by 2017 it reached more than 2000 papers. Regression analysis of data for the years between 1995 and 2017 shows that a polynomial of degree 4 can be fit to the data with high accuracy. If this trend were to continue, by polynomial expression it is predicted that the number of articles per year on nanofluids will exceed 3800 in 2020. Figure 4 (b) shows a word cloud of the most prevalent subject areas to which nanofluids have been applied. As indicated, Engineering, Physics, Chemical Engineering and Materials Science have been the subject areas in which nanofluids were most widely engaged.

1.3. What applications are suitable for nanofluids?

Indeed, in most applications in which conventional fluids are used for cooling or heating purposes, nanofluids can be used to replace single-phase fluids. Nanofluids can be used in solar collectors and photovoltaic systems, car radiators, refrigerators, boilers, medicine-drug delivery, cooling of electronic equipment, lubrication of components, heating and cooling of buildings, desalination, CO_2 absorption, porous media, aerospace, oil recovery, and any type of liquid-based heat exchanger [4–18]. Figure 5 gives an overview of primary nanofluid applications.

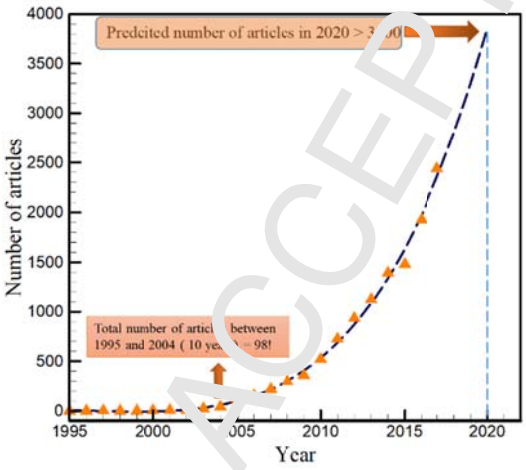

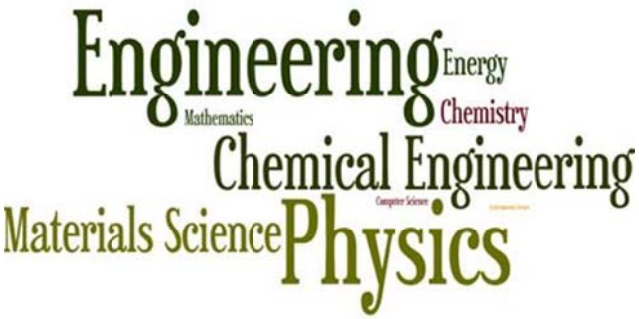

a) b)

Figure 4. Research in field of nanofluids, (a) number of articles per year (b) word cloud of most popular subject areas (done with wordle.net); information extracted from Scopus

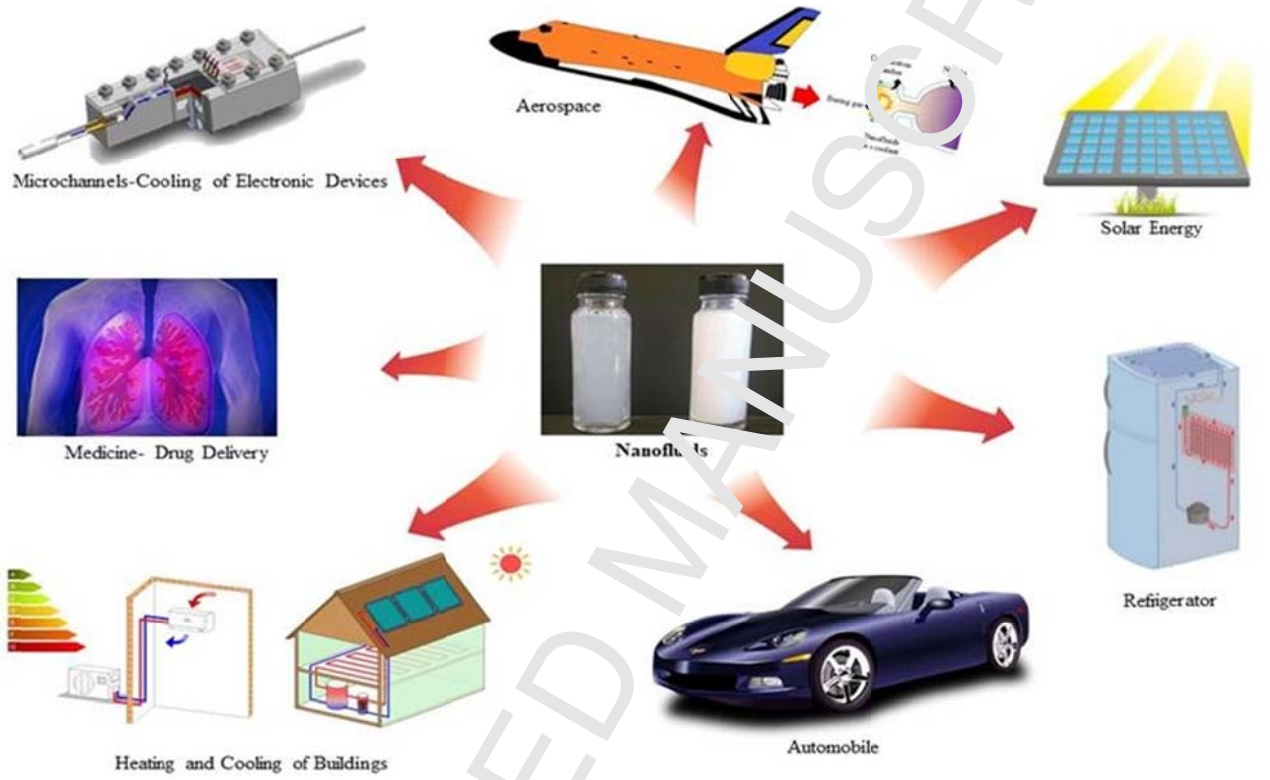

Figure 5. Some applications of nanofluids in a glance

1.4. What are the advantages and disadvantages of nanofluids?

Generally, by using a nanofluid the rate of heat exchange in thermal systems is enhanced because of higher thermal conductivity of nanofluids compared to the base fluid. Therefore, to transfer a specified value of heat, the size of a thermal system can be reduced by using nanofluids to enhance heat transfer rate, implying a more compact system and saving in material weight and expense. In comparison with microfluids, nanofluids have a higher stability and a better ability to enhance heat conduction. On the other hand, nanofluids have some disadvantages which can be listed as follows [19]:

- Nanofluids have a relatively high cost of production.

- Preservation of nanofluids for long-term use without aggregation and sedimentation of nanoparticles is a challenge.
- The higher viscosity of nanofluids compared to base fluids leads to increases in required pumping power and increases the rate of frictional heating.
- Use of nanofluids can increase rates of corrosion and erosion of components that come into contact with the nanofluids.

1.5. What is the aim of present review article?

As mentioned in the section 1.4, one of the challenges of using nanofluids is high cost of production. Therefore, it is reasonable that before applying nanofluids in a real situation, the effects of nanofluids on the system performance are physically modeled. Up to now, some interesting review articles and books have been published on physical modeling of nanofluids, including Refs. [20–27].

The present article aims to comprehensively investigate the latest developments in modeling of nanofluid flow, focusing on physical phenomena affecting the heat and fluid flow of nanofluids. The review is presented in two parts. In the present part (part I), various mathematical models and the main physical phenomena that affect the heat transfer rate in nanofluid flows are reviewed. In part II, an overview of common computational fluid dynamics (CFD) approaches and software used for solving nanofluid flows is presented. Finally, three-dimensional studies on modeling of nanofluids are reviewed, focusing on differences between 2D and 3D simulations, physical models and solution method effects. Figure 6 summarizes the main questions that the review aims to answer in parts I and II.

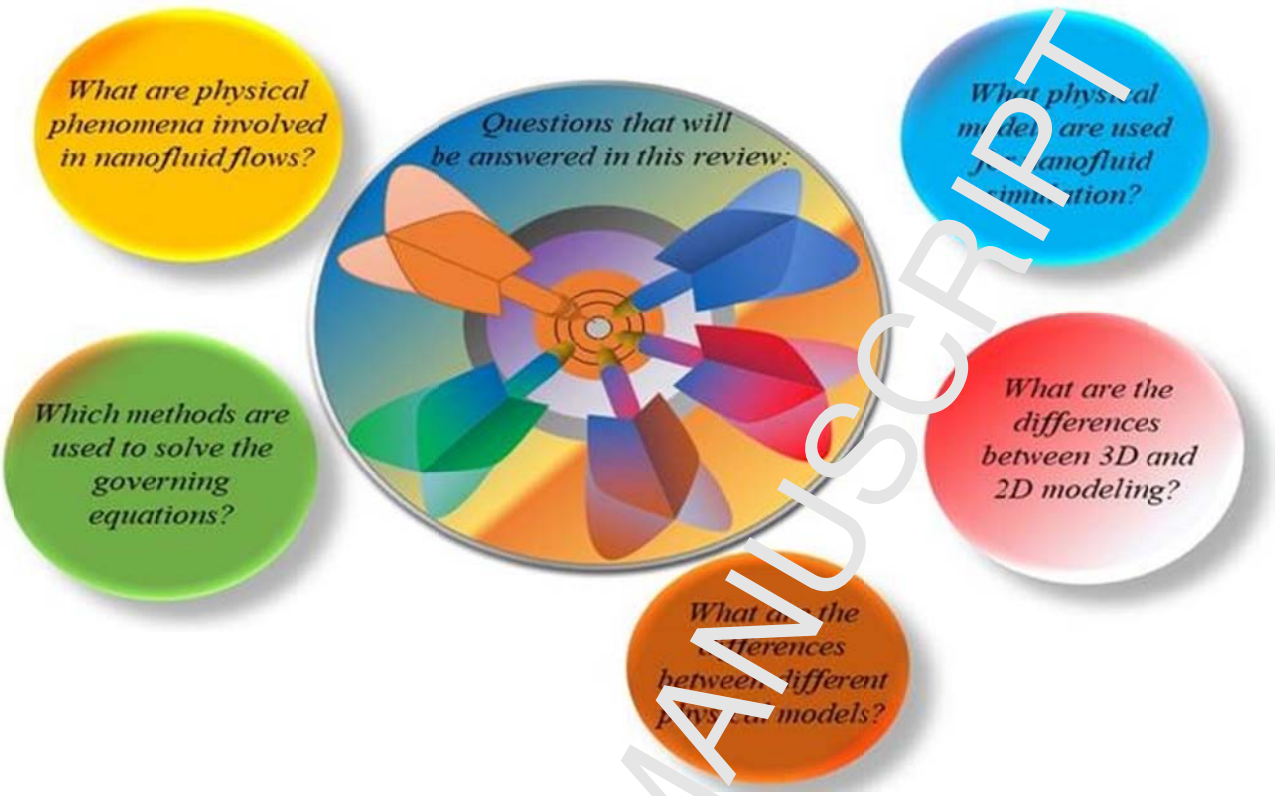

Figure 6. The main questions that will be answered in the present work

2. Dynamics of nanoparticle motion in a liquid

Knowledge of the dynamics of nanoparticles in the base liquid is a prerequisite for accurately describing the processes of heat transfer in nanofluid flows. There are a wide range of forces that act on particles suspended in a fluid, but only a fraction of these forces are significant for nanofluids due to the small particle size. In general, forces acting on particles suspended in a fluid include those induced by:

1- The base liquid

2- Surrounding walls and solid surfaces

3- Other nanoparticles

4- External magnetic or electric fields (if any)

5- An acoustic field (if any)

Figure 7 summarizes the main acting forces on a general suspended particle in a fluid flow. In following sections, we present definitions of forces summarized in Fig. 7 and discuss which ones are most important and which ones can be neglected in nanofluid flows.

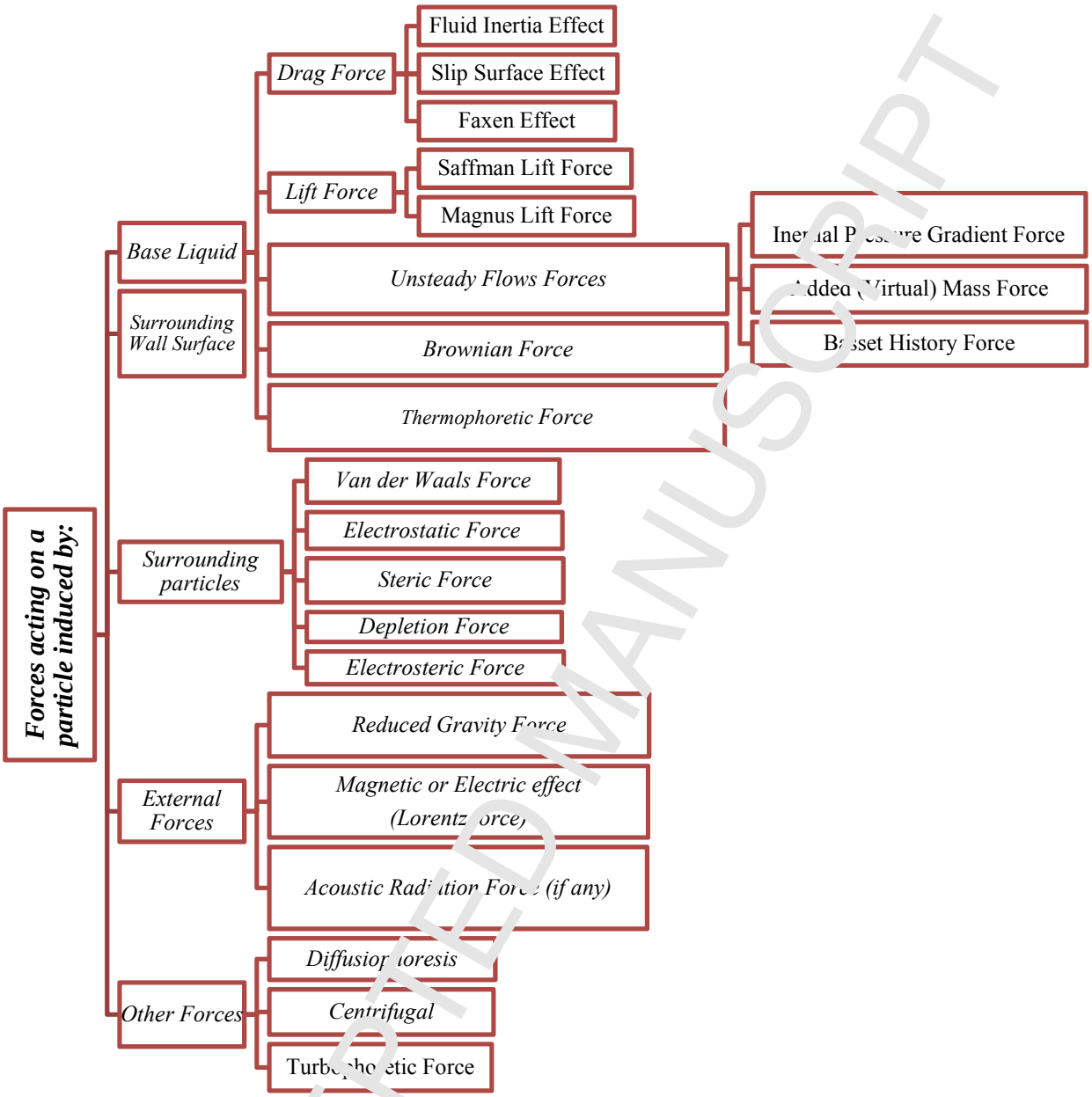

Figure 7. Forces acting on a general particle suspended in a fluid flow by different sources

2.1. Forces acting on a nanoparticle by the base liquid

2.1.1. Drag force

When a spherical nanoparticle with a vector velocity of $\boldsymbol{V}_p$ and a diameter of d_p moves through a viscous liquid with a velocity of $\boldsymbol{V}_f$ and a viscosity of μ_f, a force opposite to the motion direction of the particle due to relative velocity between the particle and the liquid is created which is called "drag force". The drag force based on Stokes law, which is modified by a friction factor (f), is given by [28]:

$$\boldsymbol{F}_D = -3\pi d_p \mu_f \boldsymbol{V}_s f \tag{1}$$

where $\boldsymbol{V}_s = \boldsymbol{V}_p - \boldsymbol{V}_f$ is the particle slip velocity, defined as the relative velocity of the particle with respect to the fluid. The friction factor, defined as $f = C_I C_C C_F$, takes into account the effects of fluid inertia (C_I), slip flow (C_C) and crowding by fluid particles (C_F). It should be noted that the Faxen effect, which takes into account the non-uniformity effects of the incident fluid velocity profile ($\boldsymbol{V}_f$), is not included in Eq.(1) because it is generally negligible due to the ultra-fine size of nanoparticles [29]. The above equation can be rewritten as:

$$C_D = \frac{F_D}{\frac{1}{2}\rho V_s^2 A} = \frac{24}{\mathrm{Re}_p} f \tag{2}$$

where F_D is the drag force magnitude, C_D is the drag coefficient, V_s is the slip velocity magnitude, A is the cross-sectional area of the nanoparticle ($\pi d_p^2/4$) and Re_p is the particle Reynolds number, defined as:

$$\mathrm{Re}_p = \frac{\rho_f V_s d_p}{\mu_f}. \tag{3}$$

It should be noted that setting the friction factor at $f = 1$ recovers the original Stokes relation. Also, the inertial coefficient (C_I) depends on the particle Reynolds number, so for a small particle Reynolds number (Re_p <1), we can let $C_I = 1$. However, for higher particle Reynolds numbers, in the range of 1-800 (transition regime), it should be corrected by the Schiller-Naumann relation [30]:

$$C_I = 1 + 0.15\,\mathrm{Re}_p^{0.687} \tag{4}$$

The comparison between experimental data and Eq.(4) shows good agreement [28]. Other experimental correlations are also suggested for higher Reynolds numbers, but for nanofluid flows the

mentioned range for particle Reynolds number is sufficient and higher values are not expected to occur. Concerning typical range of particle Reynolds number in nanofluids, Sekrani et al. [31] performed a series of numerical simulations for alumina nanoparticles with a size of 47 nm dispersed in water with concentrations up to 1.8% under laminar flow (100≤ Re ≤1600) in a 2D channel. They indicated that for the range of their simulations, Re_p changes between 3.5×10^{-5} and 6×10^{-4} (i.e., much smaller than 1). The slip velocity magnitude for the experiments of [31] can then be estimated using Eq. (3) using the values of water properties.

As a particle gets very small, the no-slip assumption on the particle surface can begin to break down, necessitating a slip correction to the drag force expression. The Knudsen number is a dimensionless parameter that determines the significance of slip between particles and the base fluid, and it is defined as the ratio of the mean-free-path of fluid molecules to the particle diameter ($Kn=\lambda/d_p$). The Cunningham relation [32] approximates the slip correction coefficient for small Knudsen numbers as the following:

$$C_C = \frac{1}{1+3.26\,Kn} \tag{5}$$

Slip correction becomes important if Kn exceeds 0.01. For nanoparticle suspensions in a gas, particle slip relative to the fluid can be very important. However, for liquid nanofluid flows the slip effect on drag is generally not very important due to the small values of mean-free-path in a liquid. The effect of crowding by fluid particles is important in fluidized beds and flow through packed beds. This effect should not be relevant in dilute fluid flows, as is the case with many nanofluids, for which we can set $C_F=1$.

2.1.1.1. Wall effect on drag coefficient

Here, we consider two cases shown in Figure 8. In the first case, a particle migrates with a low Reynolds number (creeping flow) towards a wall, for which case the drag coefficient is given by [33]:

$$C_D = \frac{24}{\mathrm{Re}_p}\left(1+\frac{d_p}{2h_p}\right) \tag{6}$$

where h_p stands for the distance between the center of the particle and the wall surface.

In the case that a particle moves parallel to wall surface, Faxen suggested the following expression to calculate the drag coefficient [28]:

$$C_D = \frac{24}{\mathrm{Re}_p}\left[1-\frac{9}{16}\left(\frac{d_p}{2h_p}\right)+\frac{1}{8}\left(\frac{d_p}{2h_p}\right)^3-\frac{45}{256}\left(\frac{d_p}{2h_p}\right)^4-\frac{1}{16}\left(\frac{d_p}{2h_p}\right)^5\right]^{-1} \quad (7)$$

$C_D = \frac{24}{\mathrm{Re}_p}\left(1+\frac{d_p}{2h_p}\right)$

$C_D = \frac{24}{\mathrm{Re}_p}\left[1-\frac{9}{16}\left(\frac{d_p}{2h_p}\right)+\frac{1}{8}\left(\frac{d_p}{2h_p}\right)^3-\frac{45}{256}\left(\frac{d_p}{2h_p}\right)^4-\frac{1}{16}\left(\frac{d_p}{2h_p}\right)^5\right]^{-1}$

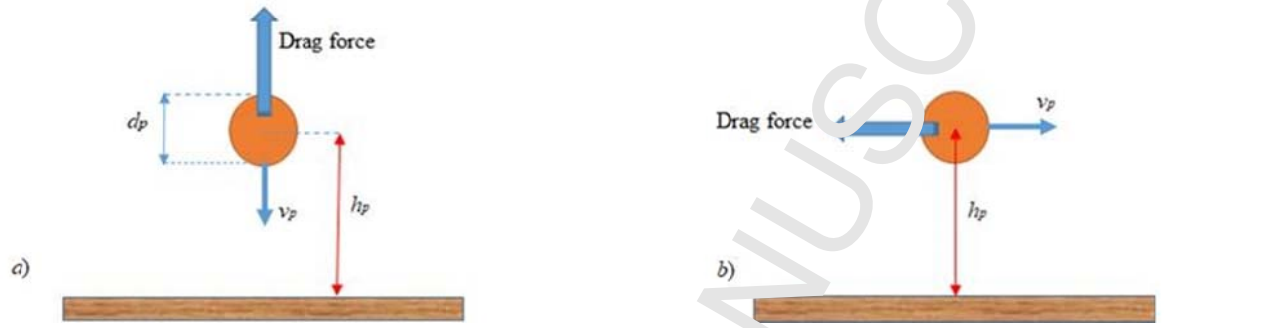

Figure 8. Drag coefficient when (a) particle moves toward wall, (b) particle moves parallel to wall.

2.1.2. Lift force

Lift force (also called lateral force) acting on a nanoparticle moving in a liquid is composed of two independent forces, typically referred to as the **Saffman** and **Magnus** lift forces.

2.1.2.1. Saffman force

Consider a nanoparticle moving in a uniform shear flow where the movement directions of particle and fluid are the same (say, the *x*-direction). The shear-induced force that acts on a particle moving with the fluid elements is called the **Saffman force.** Saffman [34,35] presented the following equation for the lift force (in the *y*-direction) due to shear flow:

$$F_{LS} = 6.46\,\mu_f (d_p/2)^2 V_s (\rho_f G/\mu_f)^{1/2}, \quad (8)$$

Where G is the fluid shear rate.

2.1.2.2. Magnus force

A rotating particle in a flowing fluid experiences an aerodynamic lift force that was first studied by Rubinow and Keller [36], and which is referred to as the Magnus lift force. The rotation may be induced by collision between particles with each other or collision between a particle and a wall surface. If we again consider a flow in the *x*-direction, such that the rotational velocity of the particle is given by $\Omega\mathbf{k}$, where **k** is the basis unit vector in the *z*-direction, the Magnus force will be a force in the *y*-direction given by:

$$F_{LM} = \pi\rho_f (d_p/2)^3 V_s \left(\Omega - \frac{11}{8\pi}G\right) \tag{9}$$

Saffman employed an asymptotic analysis to write the total lift force acting on a particle in a shear flow is the sum of the Saffman and Magnus forces, or:

$$F_L = 6.46\,\mu_f (d_p/2)^2 V_s (\rho_f G/\mu_f)^{1/2} + \pi\rho_f (a_p/2)^3 V_s \left(\Omega - \frac{11}{8\pi}G\right). \tag{10}$$

2.1.2.3. Scale of lift force compared to drag force

As pointed out in the scaling analysis by Marshall and Li [29], the ratio of the Saffman lift to the fluid drag varies in proportion to $\mathrm{Re}_G^{1/2}$ and the ratio of the Magnus lift to the fluid drag force varies in proportion to Re_G, where $\mathrm{Re}_G = \rho_f a_p^2 G/\mu_f$ is the shear Reynolds number. Since $\mathrm{Re}_G << 1$ for a nanofluid flow, the lift force on the particles is negligible. It is worth noting that the Magnus force is much smaller than the Saffman force for nanofluid flows.

2.1.3. Unsteady Flows Forces

Unsteady flow forces on particles can be divided into three groups including inertial pressure gradient force, added (virtual) mass force, and Basset history force, which are defined as follows.

2.1.3.1. Inertial pressure gradient force

Consider a spherical particle with a diameter of d_p and volume of $V = \frac{\pi}{6}d_p^3$ immersed in a liquid with density of ρ_f. The force acting on the particle due to pressure gradient is obtained by integration over the volume [29]:

$$\boldsymbol{F}_p = -\int_V \nabla p \, dv = -V\nabla p = -\frac{\pi}{6} d_p^3 \nabla p \tag{11}$$

On the other hand, the momentum equation in simple form is written as:

$$\rho_f \frac{D\boldsymbol{V}_f}{Dt} = -\nabla p + \nabla \cdot \left[\mu_f \left(\nabla \boldsymbol{V}_f + \left(\nabla \boldsymbol{V}_f \right)^T \right) \right] \tag{12}$$

In the above equation, $D\boldsymbol{V}_f / Dt$ is the material derivative and the viscous term can be neglected for high fluid Reynolds numbers, outside the boundary layer, therefore we have:

$$\nabla p = -\rho_f \frac{D\boldsymbol{V}_f}{Dt} \tag{13}$$

The final form for the inertial pressure gradient force becomes:

$$\boldsymbol{F}_p = \rho_f \frac{D\boldsymbol{V}_f}{Dt} (\frac{\pi}{6} d_p^3) \tag{14}$$

One of the important applications in which inertial pressure gradient force appears is in vortex flow fields, where it is responsible for drawing particles that are lighter than the surrounding fluid (such as gas bubbles) into the vortex core.

2.1.3.2. Added (Virtual) Mass Force

The force acting on an accelerating particle in a liquid is higher than the force acting on the same particle in vacuum because of the need to also accelerate the surrounding fluid elements that are set in motion by the particle. Added (virtual) mass force is the additional force that is needed to act on a particle inside a fluid to change its velocity in comparison with the case in which the particle moves in vacuum in an inviscid flow. It is obtained as [29]:

$$\boldsymbol{F}_A = -c_M \rho_f \left(\frac{\pi}{6} d_p^3 \right) \left(\frac{d\boldsymbol{V}_p}{dt} - \frac{D\boldsymbol{V}_f}{Dt} \right) \tag{15}$$

where c_M is the added mass coefficient and for a sphere is equal to 0.5. The first derivative on the right-hand side of (15) is the time derivative with respect to the particle, whereas the second derivative is the material derivative with respect to the fluid. Although the above equation has been derived for inviscid flows, it has been shown to remain accurate also for viscous flows over a wide range of Re numbers.

2.1.3.3. Basset History Force

Boussinesq-Basset history force, or simply Basset force (sometimes simply called the 'unsteady drag force'), is an unsteady force due to velocity change of a suspended particle in a viscous flow. This force

can affect the drift rate of particles significantly in vortex flows. It is calculated by the following equation derived by Boussinesq (1885) and Basset (1888) [29]:

$$\boldsymbol{F}_{BH} = \mu_f d_d \int_{-\infty}^{t} \left(\frac{3}{2}\right)\left(\frac{\pi\rho_f d_p^2}{\mu_f (t-t')}\right)^{1/2} \left(\frac{d\boldsymbol{V}_f}{dt'} - \frac{d\boldsymbol{V}_p}{dt'}\right) dt' \tag{16}$$

where $(t-t')$ is the time delay of the acceleration term.

2.1.3.4. Scales of Unsteady Flows Forces

The order of magnitude of the pressure gradient force with respect to the particle inertia is proportional to the density ratio (ρ_f/ρ_p). As the added mass force given by (15) also follows a similar scaling relationship. Therefore, the importance of pressure gradient and added (virtual) mass forces become more important for nanoparticles with lower density. We will investigate the importance of these two forces for different nanofluids. Consider five common nanoparticles including Cu, Al_2O_3, TiO_2, SiO_2, and CNTs with densities of 8933, 3970, 4250, 2220, and 1250 kg/ m^3 [37] and three conventional base fluids including ethylene glycol (EG), water, and oil with approximate densities of 1100, 1000 and 900 kg/m^3. The lowest value of ρ_f/ρ_p =0.1 belongs to Cu/ Oil nanofluid, and the highest value of 0.81corresponds to CNTs/EG; therefore, for nanofluids such as CNTs/EG the inertial pressure gradient and added (virtual) mass forces are not negligible compared to particle inertia. Figure 9 shows the order of magnitude of pressure gradient and added (virtual) mass forces with respect to particle inertia for a wide range of nanoparticle densities.

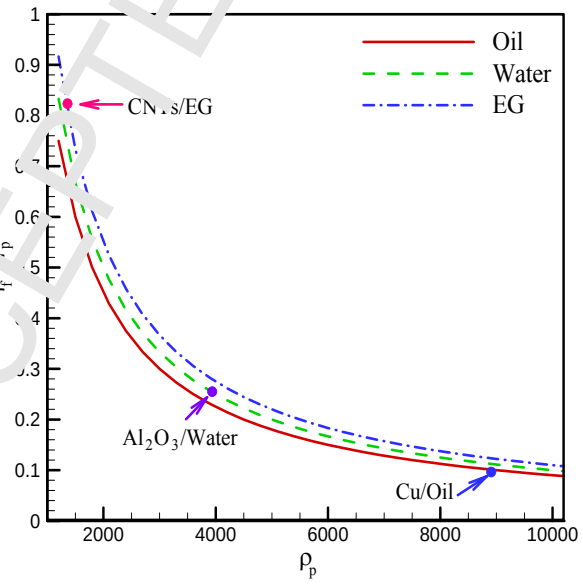

Figure 9. The order of magnitude of inertial pressure gradient and added (virtual) mass forces with respect to particle inertia (proportional with ρ_f/ρ_p) for common nanofluids

The ratio of the Basset history force to the fluid drag force is given by [29] as:

$$\frac{F_{BH}}{F_D} = O\left(\frac{\rho_f d_p V_s}{\mu_f}\right)^{1/2} = O\left(\mathrm{Re}_p\right)^{1/2} \tag{17}$$

where V_s is the particle slip velocity. As seen, the Basset history force is negligible in nanofluid flows because of the ultrafine size of nanoparticles.

2.1.4. Brownian force

In 1827, Brown, a botanist, was probably the first one who observed by microscope the collisions between grains of pollen of a plant with water molecules which leads to random motion of grains in water [38]. In general, Brownian motion (called also pedesis) is defined as the random motion of solid particles inside a fluid due to collisions between solid particles and fluid molecules. In nanofluids, heat and mass transfer might be enhanced significantly due to micro-convection and mechanical agitation which are induced mainly by Brownian motion of nanoparticles in the base fluid [39].

Figure 10 shows schematically the Brownian motion of a solid particle in a vessel filled with a liquid, and the position of the particle versus time. As seen, the position of the particle changes rapidly with time, therefore Brownian force is a time dependent force. In this regard, Li and Ahmadi [40] suggested to simulate the Brownian force as a white noise process with zero mean and finite variance. They proposed the following equation to obtain the components of Brownian force [40]:

$$\frac{F_{Bi}}{m_p} = \zeta_i \sqrt{\frac{\pi S_o}{\Delta t}} \tag{18}$$

where at every time step, ζ_i is selected from a population of zero mean unit variance Gaussian random variable, Δt is the time-step used for integration of particle equation of motion, and S_o is a spectral intensity function, which is related to the diffusion coefficient and is given as:

$$S_0 = \frac{216\upsilon_f \kappa_B T}{\pi^2 \rho_f d_p{}^5 \left(\frac{\rho_p}{\rho_f}\right)^2 C_c} \tag{19}$$

where κ_B is Boltzmann constant equal to 1.38064852 × 10^{-23} m^2 kg/ s^2 K, υ_f is kinematic viscosity of fluid and C_c is the Cunningham coefficient.

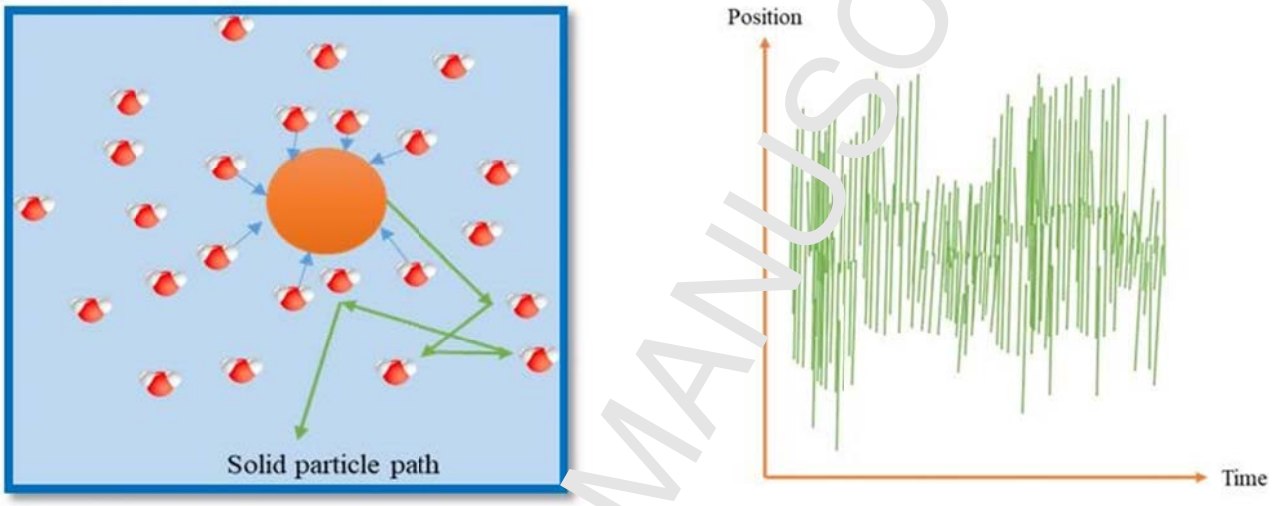

Figure 10. Schematic of the Brownian motion of a solid particle immersed in a liquid

In separate studies, Einstein and Smoluchowski [29,41,42] proved that after passing a specified time (t) where $t >> \frac{m_p}{3\pi d_p \mu_f}$ (in the case of nanoparticles the time may be just a hundredth of a second), particles diffuse from a region having high concentration of particles towards a region with a lower concentration via Brownian motion. In this regard, if concentration ϕ is assumed to be a function of time and space, the diffusion equation for particles can be written as:

$$\frac{\partial \phi}{\partial t} = D_B \nabla^2 \phi \tag{20}$$

where the Brownian diffusion coefficient D_B (m^2/s) is defined as [43]:

$$D_B = \frac{\kappa_B T C_c}{3\pi \mu_f d_p} \tag{21}$$

The above equation is called the Stokes-Einstein relation. It is worth mentioning that the Stokes-Einstein relation is used to identify the size of particles where D_B can be measured experimentally via dynamic light scattering.

The equation for Brownian force presented by Li and Ahmadi [40] can be rewritten in terms of D_B as:

$$\frac{F_{Bi}}{m_p} = \varsigma_i \frac{\mu_f}{\rho_p d_p^2 C_c} \sqrt{\frac{648 D_B}{\Delta t}} \tag{22}$$

The magnitude of the Brownian force per unit mass affects the heat transfer rate. The value of the Brownian force per unit mass, as well as the diffusion coefficient, increases with decreasing size of the nanoparticles and increasing temperature.

2.1.5. Thermophoretic Force

Thermophoresis (also known as thermomigration, thermodiffusion, the Soret effect, or the Ludwig–Soret effect) can be viewed as a consequence of the asymmetry imposed on Brownian motion by a temperature gradient. In nanofluids, the thermophoresis phenomenon acts to migrate particles from a region with higher temperature (hot zone) to a region with lower temperature (cold zone) [44]. Figure 11 shows the thermophoresis phenomenon schematically.

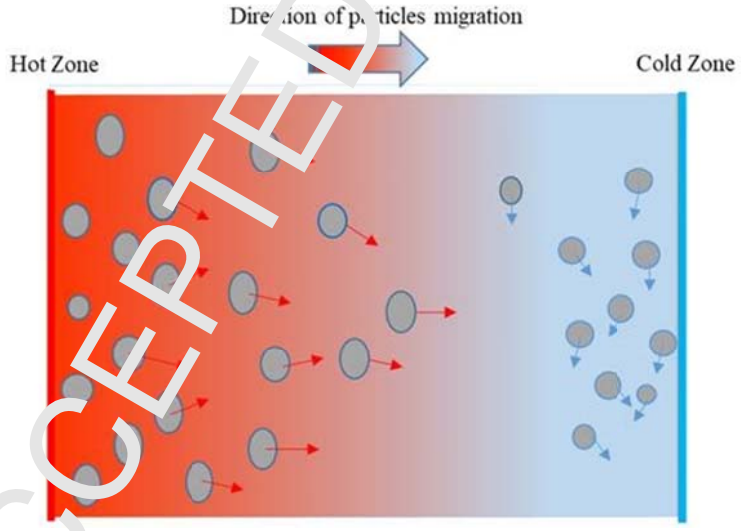

Figure 11. Schematic of thermophoresis phenomenon

Most of studies available in the literature deal with thermophoretic force in gas-solid suspensions, and relatively few studies has been done on solid-liquid suspensions (nanofluids). In this section, we first

review three models that have been derived for solid-gas mixtures, but which are sometimes also used for solid-liquid mixtures. Epstein [45] was probably the first study that developed a relation for particle velocity and force induced by thermophoresis in solid-gas mixtures by considering continuum conditions. Epstein [45] obtained the following relationship for the theromophoresis force:

$$\boldsymbol{F}_T = -\frac{9}{2}\pi d_p \left(\frac{k_f}{2k_f + k_p}\right)\frac{\mu_f^2}{\rho_f}\frac{\nabla T}{T_f} \tag{23}$$

where T_f is the mean temperature of the fluid and ∇T is the fluid temperature gradient, k_f and k_p are respectively the fluid and particle thermal conductivity. According to the Stokes' law, Epstein [45] suggested that the steady thermophoretic velocity can be obtained as:

$$\boldsymbol{V}_T = -\frac{3}{2}\left(\frac{k_f}{2k_f + k_p}\right)\frac{\mu_f}{\rho_f}\frac{\nabla T}{T_f} \tag{24}$$

In writing this expression, Epstein [45] has assumed that thermophoretic force is the sole resistance force that balances the drag force.

Later, Brock [46] suggested the following expressions for obtaining thermophoretic force and velocity, respectively as:

$$\boldsymbol{F}_T = -3\pi\frac{\mu_f^2 d_p}{\rho_f}\left(\frac{2C_s(k_f + k_p Kn)}{(1+3C_m Kn)(2k_f + k_p + 2k_p C_t Kn)}\right)\frac{\nabla T}{T_f} \tag{25}$$

$$V_T = -\left(\frac{2C_s(k_f + k_p Kn)}{(1+3C_m Kn)(2k_f + k_p + 2k_p C_t Kn)}\right)\frac{\mu_f}{\rho_f}\frac{\nabla T}{T_f} \tag{26}$$

where $C_s = 0.75$, $C_m = 1.14$, and $C_t = 2.18$. The above equations were obtained by including thermal slip at the interface of gas and particles.

Talbot et al. [47] presented more accurate equations for thermophoretic force and velocity in solid-gas mixtures as:

$$\boldsymbol{F}_T = -3\pi\frac{\mu_f^2 d_p}{\rho_f}\left(\frac{2C_s(k_f + k_p Kn)\left[1 + Kn[1.2 + 0.41\exp(-0.88/Kn)]\right]}{(1+3C_m Kn)(2k_f + k_p + 2k_p C_t Kn)}\right)\frac{\nabla T}{T_f} \tag{27}$$

$$\boldsymbol{V}_T = -\left(\frac{2C_s(k_f + k_p Kn)\left[1 + Kn[1.2 + 0.41\exp(-0.88/Kn)]\right]}{(1+3C_m Kn)(2k_f + k_p + 2k_p C_t Kn)}\right)\frac{\mu_f}{\rho_f}\frac{\nabla T}{T_f} \tag{28}$$

where $C_s = 1.17$, $C_m = 1.14$, and $C_t = 2.18$. It is noted that the above equations reduce to that of Epstein [45] in the limit of vanishing Knudsen number.

He and Ahmadi [48] proposed a semi-empirical model to account the thermophoresis force (even for the non-continuum regimes) with large Knudsen numbers (Kn>1). They modified the equation of Cha-McCoy-Wood (CMW), calling it the MCMW model, and presented the following relation for the thermophoresis force:

$$\boldsymbol{F}_T = 1.15 \frac{Kn}{4\sqrt{2}\alpha\left(1+\frac{\pi_1}{2}Kn\right)}\left[1-\exp\left(-\frac{\alpha}{Kn}\right)\right]\left(\frac{4}{3\pi}\phi\pi_1 Kn\right)^{1/2} f_B\left(\frac{d_p^2}{d_m^2}\right)\nabla T \tag{29}$$

where d_m is the molecular diameter, and α and π_1 are given by:

$$\alpha = 0.22\left[\frac{\frac{\pi}{6}\phi}{1+\frac{\pi_1}{2}Kn}\right]^{1/2} \tag{30}$$

$$\pi_1 = 0.18\frac{36/\pi}{\left(2-S_n+3\frac{\lambda}{r}\right)\frac{\lambda}{r}+S_n} \tag{31}$$

As mentioned, the above equations for thermophoretic force were derived for solid-gas mixtures; however, Michaelides [49] argued that special relations should be obtained for thermophoretic force in solid-liquid mixtures for the following reasons:

- The Knudsen number (the ratio of mean free path, λ, to particle diameter) should be small enough in a solid-liquid mixture so that the continuum assumption is valid. Consequently, the size of particles that can be dispersed in liquids via Brownian motion are much smaller than in gases because the mean free path for liquid molecules is much less than that of gas molecules (e.g. $\frac{\lambda_{air}}{\lambda_{water}} >> 10$).
- The trend of variations of viscosity with temperature for liquids is the inverse of the trend in gases. With increasing temperature, liquid viscosity reduces while in gases the viscosity increases with temperature.

In this regard, Michaelides [49] suggested the following correlations to obtain thermophoretic force and velocity:

Thermophoretic force:

$$\boldsymbol{F}_T = -6\pi d_p A \left(\frac{d_p}{d_{p0}} \right)^{-B} \frac{\mu_f^2}{\rho_f} \frac{\nabla T}{T_f} \tag{32}$$

Thermophoretic velocity:

$$\boldsymbol{V}_T = -A \left(\frac{d_p}{d_{p0}} \right)^{-B} \frac{\mu_f}{\rho_f} \frac{\nabla T}{T_f} \tag{33}$$

where $d_{p_0} = 2\ nm$. Also, A and B are constants that have been obtained for 20 different nanofluids [49]. Table 1 provides the coefficients of A and B.

Table 1. Constant coefficients of (A, B) to obtain thermophoretic force for common nanofluids [49].

Base fluid / Nanoparticle	Water	Engine Oil	Ethylen Glycol	R-134
Aluminum	(1264, 1.417)	(3.092[illegible] 1.242)	(14.615,1.869)	(4401,1.774)
Aluminum Oxide	(1227,1434)	(7.1026,1.579)	(5.1095, 1.621)	(6270, 1.819)
CNTs	(945.5, 1.263)	(5.804[illegible] 1.445)	(3.6765, 1.406)	(8580, 1.894)
Copper	(2039, 1.870)	([illegible]139[illegible], 1.724)	(2.3558, 1.587)	(4191,1.659)
Gold	(3155, 1.799)	(6.6483,1.917)	(4.2431,1.672)	(2721,1.603)

2.1.6. Scaling Analysis

A scaling analysis for micrometer-scale particulate flows is given by Marshall and Li [29], and scaling analyses for nanofluids are given by Buongiorno [21] and Savithiri et al.[50]. It is generally the case for *micrometer-scale* particulate flows that the particle motion in the fluid, in the absence of collision or external electric, magnetic or gravitational fields, is controlled primarily by a balance between particle inertia and fluid drag. Other forces, such as added mass force or inertial pressure gradient force, can often have the same magnitude as the particle inertia for liquid flows, and for purposes of a

scaling analysis these forces are typically lumped in with inertia. In addition to drag and inertia, secondary forces such as Saffman and Magnus lift forces, Bassett history force, Brownian force, etc., can influence particle motion in a non-negligible way, but are usually smaller than the dominant drag and inertia forces.

For *nanometer-scale* particulate flows (nanofluids), the fluid drag remains of primary importance, but the inertia decreases sufficiently rapidly with particle size that other forces may become of a similar, or greater, order of magnitude as the inertia. In examining the relative scale of the fluid forces on the nanoparticles, we recall our previous argument that the lift force and the Basset history force are negligible for nanofluids due to the very small particle sizes. The particle Reynolds number is small, so that the inertial correction to the drag force can be omitted. For liquid nanoparticle flows, usually the Knudsen number is also small, so that the slip correction on the drag force can be omitted. Furthermore, we will assume that the nanoparticle density is of a similar magnitude to that of the surrounding fluid, so that the inertial pressure gradient force and the added mass force are of the same order of magnitude as the particle inertia (and these forces are therefore lumped in with inertia for simplicity). The two forces of particular interest in nanoparticle flows, with the potential of displacing particle inertia in balancing the drag force, are the Brownian force and the thermophoretic force, which are examined in more detail below.

The significance of Brownian force compared to particle inertia is determined by the value of the particle Peclet number, Pe_p, which is defined by

$$Pe_p = V_s d_p / D_B . \tag{34}$$

In this equation, $V_s = \left| \boldsymbol{V}_p - \boldsymbol{V}_f \right|$ is the particle slip velocity, d_p is the particle diameter, and D_B is the Brownian diffusion coefficient given by Eq. (21). The ratio of Brownian force to particle inertia scales like [29]:

$$\frac{F_B}{F_i} = O\left(\mathrm{Pe}_p^{-1/2} \right) \tag{35}$$

so that the Brownian force is significant for $Pe_p \le O(1)$. The slip velocity V_s associated with particle inertia scales as the product of the fluid free stream velocity U and the Stokes number St. The Stokes number is defined as the ratio of the particle time scale τ_p to the fluid time scale $\tau_f = L/U$, so that

$$\mathrm{St} \equiv \frac{\tau_p}{\tau_f} = \frac{\rho_p U d_p^2}{18 \mu_f L} \tag{36}$$

where L is a characteristic fluid length scale. Using the estimate $V_s = O(\mathrm{St}\, U)$ for slip velocity, the particle Peclet number can be written in terms of constant quantities as

$$Pe_p = O(\mathrm{St}\, U d_p / D_B)\,. \tag{37}$$

The significance of the thermophoretic force compared to the particle inertia can be assessed by equating the force ratio to the ratio of the thermophoretic drift velocity magnitude V_T to the inertial slip velocity magnitude $V_s = O(St\, U)$, giving:

$$\frac{F_T}{F_i} = \frac{V_T}{V_s} = O\left(\frac{V_T}{St\, U}\right) = O\left(\frac{A}{\mathrm{Re}_f\, St}\frac{\Delta T_f}{T_f}\right) \tag{38}$$

where $\mathrm{Re}_f = \rho_f U L / \mu_f$ is the Reynolds number of the ambient fluid flow. In writing Eq. (38), we made use of the data in Table 1 for the two constants A and B in Eq. (32), which indicates that B = O(1) but that A varies in magnitude from O(1) to O(10^4) for different nanofluids.

A typical example illustrating the significance of Brownian and thermophoretic forces in nanofluids is given by the problem of 10 nm diameter aluminum particles in water, for which Table 1 gives $A = 1264$. We assume a temperature difference $\Delta T_f = 10\,\mathrm{K}$, an ambient temperature $T_f = 300\,\mathrm{K}$, a fluid length scale $L = 1\,\mathrm{cm}$, and a fluid velocity scale $U = 1\,\mathrm{m/s}$. The Brownian diffusion coefficient for this problem is $D_B \cong 4\times10^{-11}$ m^2/s and the fluid kinematic viscosity is $\nu_f \cong 10^{-6}$ m^2/s. The fluid Reynolds number is $\mathrm{Re}_f = 10^4$ and the Stokes number is $St = 5\times10^{-10}$. Our estimates Eqs. (35) and (38) of the ratio of Brownian force and thermophoretic force to particle inertia yield for this example

$$\frac{F_b}{F_i} = O\left(\mathrm{Pe}_p^{-1/2}\right) \cong O(2.7\times10^3) \tag{39}$$

$$\frac{F_T}{F_i} = O\left(\frac{A}{\mathrm{Re}_f\, St}\frac{\Delta T_f}{T_f}\right) \cong O(8.4\times10^6) \tag{40}$$

Both the Brownian force and the thermophoretic force are observed to be significantly larger than the particle inertia. For this particular example the thermophoretic force dominates, and would therefore balance the drag force to determine the particle motion, but the balance between Brownian and thermophoretic force in general depends on the problem details and the materials used.

The readers may refer to Refs. [21] and [50] to see more examples of scale analysis.

2.2. Inter-particle forces

Interparticle forces become important especially when the number of particles in a specific volume of mixture increases, however, if the concentration of particles in the system is small, the interparticle forces acting between non-adhesive particles – ignoring agglomeration or aggregation of particles – may be safely neglected. Of course in systems of adhesive particles, collisions will eventually occur even in dilute suspensions, giving rise to formation of particle agglomerates. In these suspensions of adhesive particles, interparticle forces are therefore necessary at all values of the bulk particle concentration. In this section, we first study the criterion that determines the range in which interparticle forces are negligible in systems of non-adhesive particles, or for short-time computations of systems of adhesive particles, and in the next section various interparticle forces are discussed.

2.2.1. Dilute and dense nanofluids

Based on the solid volume fraction of nanoparticles dispersed in the base fluid, nanofluids (solid-liquid mixtures) can be classified into two general groups including: diluted and dense [51,52]. Solid volume fraction (or nanofluid volume concentration) is defined as the ratio of solid nanoparticles volume to the total volume of mixture. Mathematically it can be written as:

$$\phi(\%) = \frac{\text{Nanoparticle volume}}{\text{Total volume}} = \frac{(m_p/\rho_p)}{(m_p/\rho_p)+(m_f/\rho_f)} \times 100 \qquad (41)$$

A nanofluid can be considered to be a dilute mixture when its volume concentration is less than 0.1% [51,52]. Interparticle forces can be safely neglected for a dilute nanofluid provided that adhesive forces are not present. For concentrations higher than 0.1% the nanofluid is dense. The dense flow is also divided into two groups. When $0.1 \le \phi(\%) \le 10$ collision between particles is dominated and when $\phi \ge 10\%$ contact is dominated in the flow [52]. Due to the heterogeneous distribution of nanoparticles

that may be created by aggregation and sedimentation of nanoparticles, in nanofluid flows we may have both dilute and dense flows in different regions of the flow field at the same time. It may be interesting to estimate the minimum distance between two spherical nanoparticles in ideal conditions so that the suspension is considered dilute (i.e., with almost no collision between particles). For a case with two spherical particles with the same diameter (d_p) and where the distance between the particle centers is l_p, the relation between particle diameter, distance between the two particles and volume fraction of the nanoparticles is [52]:

$$\frac{l_p}{d_p} = \left(\frac{\pi}{6\phi} \right)^{\frac{1}{3}} \tag{42}$$

Based on the definition of dilute flow in which the volume concentration should be less than 0.1% and using the above equation we find that the ratio of particle distance to particle diameter ($\frac{l_p}{d_p}$) should be more than almost 8 to have a dilute nanofluid. Figure 12 illustrates schematically the concepts of dilute and dense flows and the associated range of volume fraction [52].

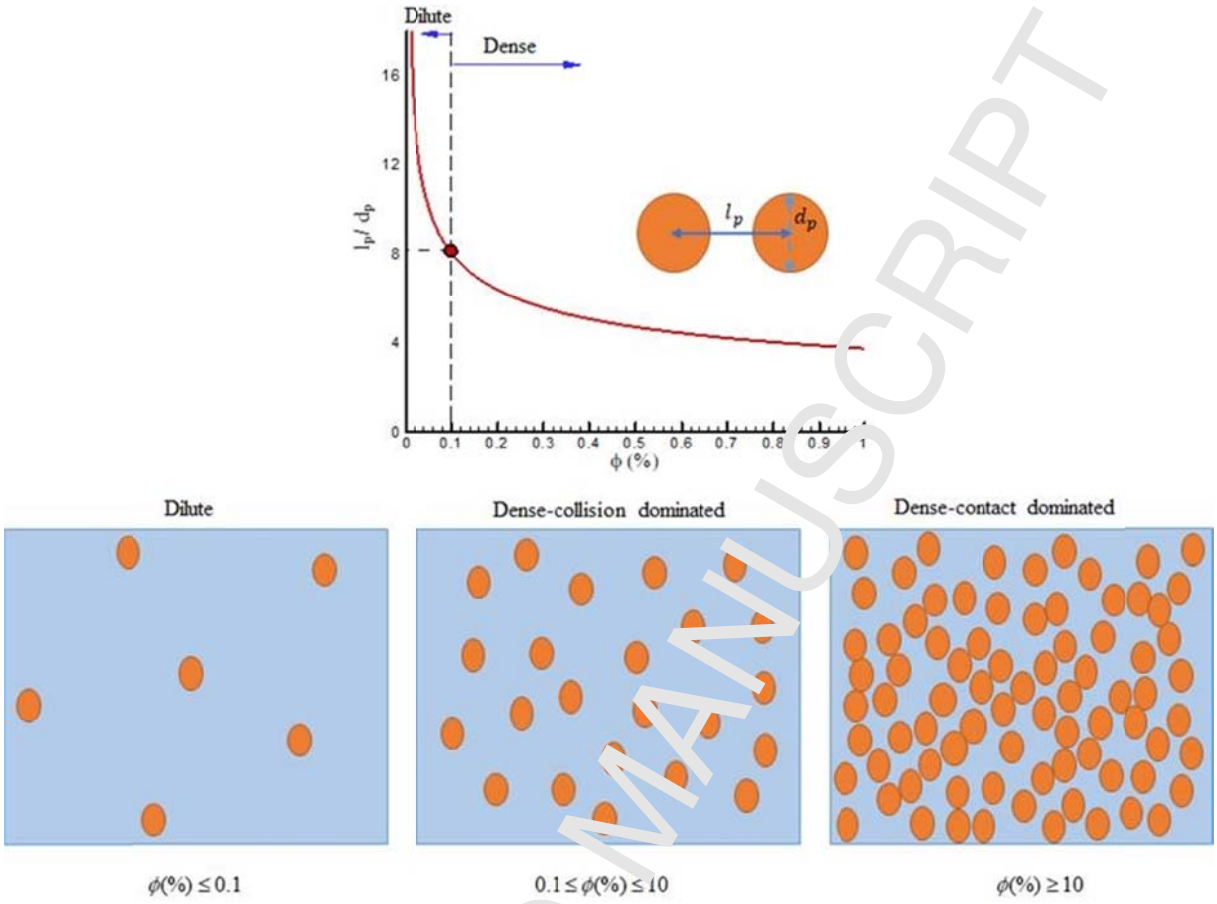

Figure 12. Concepts of dilute and dense flows based on solid volume fraction of particles.

2.2.2. Van der Waals Force

Van der Waals force appears between molecules or tiny particles and acts generally as an attractive force. Van de Waals force itself is composed of three forces: dispersion interaction (London force), dipole–dipole interaction (Keesom force) and dipole-induced dipole interaction (Debye force)[53]. The van der Waals force may be significant in a wide range of distances ranging from atomic scale (0.2 nm) to greater than 10 mm [54,55]. The Hamaker theory [56] is used to estimate the van der Waals force between different materials. The van der Waals force between two rigid (non-deforming) spheres formed of the same material is given by [36]:

$$F_{Van} = -\frac{A_H}{6z_p^2}\frac{r_{p_1} r_{p_2}}{r_{p_1} + r_{p_2}} \tag{43}$$

where z_p is the distance between surfaces of two spheres(the shortest distance), and r_{p_1} and r_{p_2} are radii of spheres. Also, A_H is Hamaker constant that depends on the materials of the spheres. If the spheres are made from different materials (we face with this in hybrid nanofluids), the coefficient A_H is replaced by $A_{H\,12}$ so that it is estimated as[28]:

$$A_{H12} = \sqrt{A_{H11} A_{H22}} \tag{44}$$

where $A_{H\,11}$ is Hamaker constant for the first sphere and $A_{H\,22}$ is Hamaker constant for the second sphere. If the two spheres are dispersed in a medium (like a fluid) the Hamaker constant can be estimated as:

$$A_{H132} = \left(\sqrt{A_{H11}} - \sqrt{A_{H33}}\right)\left(\sqrt{A_{H22}} - \sqrt{A_{H33}}\right) \tag{45}$$

where $A_{H\,33}$ is the Hamaker constant for the medium (fluid). Hamaker constant for some materials is given in Table 2.

Table 2. Hamaker constant for some materials[52].

Material	Hamaker constant (A_H) ($J\times10^{20}$)
Water	4.38
Al_2O_3	15.5
Cu	28.4
Au	45.5

The van der Waals force between a sphere and a plane can be estimated as [36]:

$$F_{Van} = -\frac{A_H r_p}{6z^2} \tag{46}$$

The above equations for van der Waals force assume that the particles are perfect spheres. Since the van der Waals force acts only over very short distances, even tiny deformation of a sphere upon collision can have a significant effect on the van der Waals force. The influence of particle deformation is quite important for micrometer-scale and larger particles, but of only moderate importance for nanoscale particles. A more extensive review of van der Waals force between deforming spheres is given by [18]. The van der Waals force is one of the reasons behind the aggregation of particles (since they act mainly as an attractive force); therefore, the stability of nanofluids is critically dependent on accurate modeling of this force [53].

2.2.3. Electrostatic double layer force

The presence of ions in the base fluid (e.g., electrolytes, such as salt water) can result in the formation of an electrical double layer around charged particles. This electrostatic double layer will induce a

force of very small range which can be modeled using the Hogg–Healy–Fuerstenau (HHF) formula [57]:

$$E_{Edl} = \frac{\varepsilon r_{p_1} r_{p_2} (\psi_{01}^2 + \psi_{02}^2)}{4(r_{p_1} + r_{p_2})} \left[\frac{2\psi_{01}\psi_{02}}{(\psi_{01}^2 + \psi_{02}^2)} \ln\left[\frac{1+\exp(-\kappa z_p)}{1-\exp(-\kappa z_p)} \right] + \ln(1-\exp(-2\kappa z_p)) \right] \quad (47)$$

$$F_{Edl} = -\frac{d\vec{E}}{dz_p}$$

Here E_{Edl} is the particle–particle electrostatic interaction potential energy, ψ_{01} and ψ_{02} are the particle surface potentials, ε is the dielectric constant of the solution, and κ^{-1} is the Debye length (double layer thickness). The above relation is a good approximation when particle surface potentials are less than 50-60 mV. The above relation can also be modified to estimate the interaction force between a particle and a wall by assuming one of the particle radii tends to infinity. Contrary to the van der Waals force, electrostatic double layer forces are repulsive in nature; therefore, they decrease the agglomeration of nanoparticles, and, hence, enhance the stability of a nanofluid [53].

2.2.4. Other interparticle forces

Other interparticle forces such as steric, electrosteric, depletion, capillary, solvation, structural or hydration forces can affect the stability of nanofluids. For example, steric force can prevent the aggregation of nanoparticles. Steric force leads to absorption of a layer of organic molecules at the surface of particles. Depending on the thickness and density of the layer, attractive forces and consequently the aggregation rate reduce [53]. Interested readers may refer to Refs. [53,55,58].

2.2.5. DLVO theory and nanofluid stability

Based on independent studies of Derjaguin and Landau (1941) and Verwey and Overbeek (1948), a quantitative theory known as DLVO was established to demonstrate the stability of colloidal dispersions [53,55]. The theory of DLVO combines the effects of two opposite forces i.e. van der Waals attraction and the electrostatic double layer repulsion to describe the dispersion stability. Indeed in DLVO theory other forces are ignored. Figure 13 (replotted based on a figure given in [53]) shows schematically the DLVO theory concept. At the primary minimum point, the amount of attraction

between particles is maximized; therefore, the suspension is unstable (strongly flocculated or irreversible aggregation). At the energy barrier point, the repulsive force is maximized; therefore, the suspension attains a stable condition. At the secondary minimum point, the amount of attractive forces is less than at the primary minimum point, giving rise to a weakly flocculated or reversible aggregation.

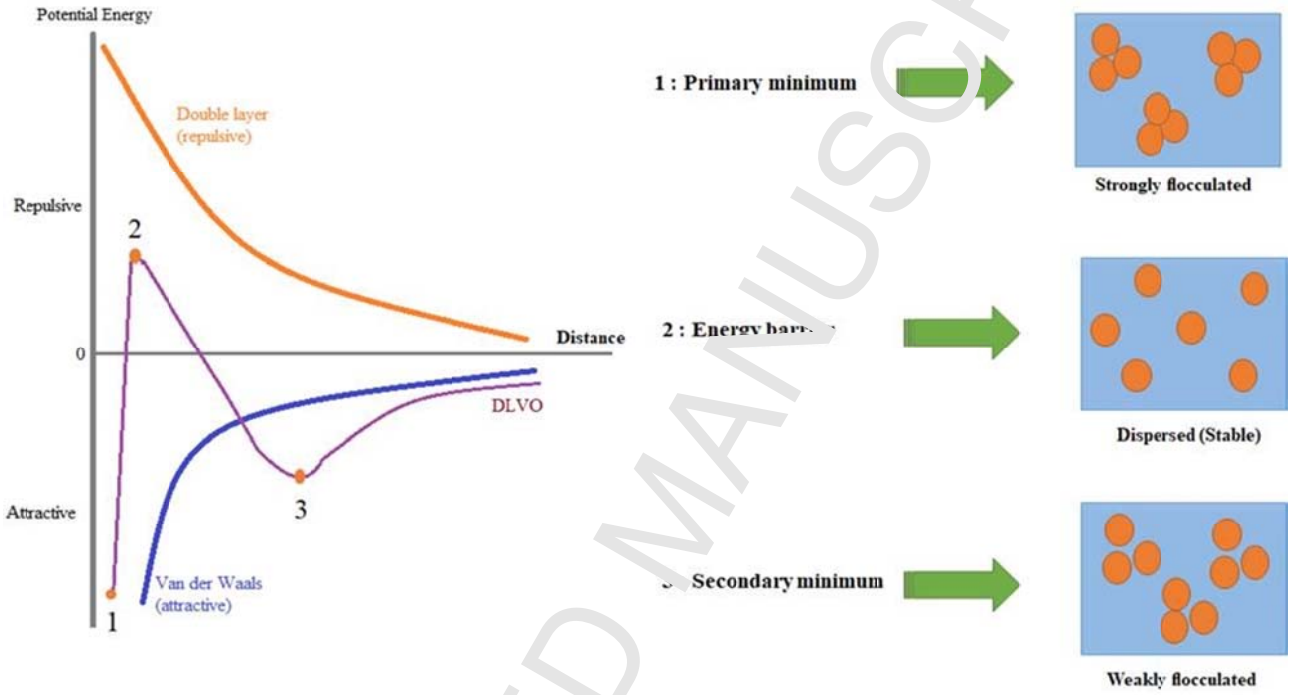

Figure 13. DLVO theory can be used to describe the stability of suspensions.

2.3. External forces

Sources such as gravity, magnetic, electric fields, and acoustic oscillations can create forces which affect the flow and heat transfer fields in a nanofluid-based thermal system. Here, an overview of these forces is presented.

2.3.1. Reduced gravity force

The reduced gravity force is the outcome of gravitational and buoyancy (obtained from Archimedes' law) forces. It can be obtained by the following relation [29]:

$$\mathbf{F}_G = \left(\pi \frac{d_p^3}{6}\right)\left(\rho_f - \rho_p\right) g \tag{48}$$

The reduced gravity force can be neglected usually in nanofluid flows due to ultrafine size of nanoparticles.

2.3.2. Lorentz force

If a fluid with an electrical conductivity of σ (with dimension of 1/Ω.m) flows in a duct under an external electrical field of $\mathbf{E}$ and magnetic field of $\mathbf{B}$, a force is applied to elements of the fluid called Lorentz force. Lorentz force affects the velocity magnitude and temperature field in the thermal equipment. Lorentz force is defined as [59]:

$$\mathbf{F}_{Lz} = \mathbf{J} \times \mathbf{B} = \sigma(\mathbf{E} + \mathbf{V} \times \mathbf{B}) \times \mathbf{B} \tag{49}$$

In the above, $\mathbf{V}$ is fluid velocity vector, and $\mathbf{J}$ is current density (with dimension of A/m^2). In the case of magnetohydrodynamic (MHD) flows, by neglecting the electrical field and assuming that the external magnetic field has a constant strength of B_0, the Lorentz force simplifies to:

$$\mathbf{F}_{Lz} = \sigma \mathbf{B}_0^2 \mathbf{V} \tag{50}$$

For MHD flows, a dimensionless number called "Hartmann number" comes into play, which can be defined as:

$$Ha = B_0 L_c \sqrt{\frac{\sigma}{\mu}} \tag{51}$$

where L_c is the characteristic length (for example, the diameter of a tube) and μ is the viscosity of the working fluid.

For nanofluids, the corresponding electrical conductivity can be calculated based on the Maxwell model that is used to calculate the thermal conductivity of nanofluids (See section 3.1.1.1).

2.3.3. Acoustic radiation force

The energy of sound waves (acoustic waves) can also be used to enhance the performance of thermal systems. The force (time averaged) acting on particles by acoustic waves (e.g., an ultrasound field) is called acoustic radiation force [60]. For a particle dispersed in a fluid, the acoustic radiation force is a nonlinear function of acoustic pressure, velocity of particle, sound velocity and fluid density [60,61].

Many studies have been done to determine the radiation force on particles (either elastic or rigid) in a fluid (for example see Refs. [60,61]). However, based on the best knowledge of authors, there is no CFD study on nanofluid-based systems in which the interaction of radiation force with other forces acting on nanoparticles in nanofluid flows has been assessed. However, since the acoustic radiation force is proportional to the particle volume, it would be expected to be small compared to forces such as drag (that are proportional to the particle diameter) for these very small particle sizes.

2.4. Other forces

There are some other forces such as diffusiophoresis, centrifugal, and turbophoresis that may be found in the literature. Here, an overview of these forces is given.

Diffusiophoresis phenomenon happens due to concentration gradients of solution. In this phenomenon, due to diffusiophoresis force, nanoparticles migrate from a zone with high concentration to a zone with lower concentration. Since diffusiophoresis requires two base fluids, it is not common in nanofluid systems (which historically have just one base fluid component [21]).

Another force included in some studies is the centrifugal force. One should note that centrifugal force is related not to the rotation of the particle about a fixed point, but rather to the rotation of the reference frame about a fixed point. It is necessary to include the centrifugal force only if computations are needed to be done in a rotating reference frame (for example, consider nanofluid on a rotating circular disk). If instead, an inertial reference frame is used, the centrifugal force on the particle is contained within the particle inertia. The centrifugal force for a coordinate system that rotates with an angular velocity of Ω_S can be expressed as [62]:

$$\mathbf{F}_{Cl} = \left(\frac{\rho_f}{\rho_p} - 1 \right) m_p \Omega_S^2 r \tag{52}$$

where r stands for the position of nanoparticle times the unit vector in the radial direction.

Turbophoresis is a phenomenon in which the particles tend to migrate towards a region with less turbulent fluctuations. Since turbulent fluctuations decrease very close to a wall, the possibility of particle sedimentation on the wall increases through this phenomenon [63]. For turbulent flow in a pipe, turbophoretic force can be evaluated as[64]:

$$\begin{cases} \mathbf{F}_{Tu} = -\rho_p \dfrac{\pi d_p^3}{6}\left(\dfrac{d\left\langle v_p'^2\right\rangle}{dy}\right) \\ V_{Tu} = -\tau_p\left(\dfrac{d\left\langle v_p'^2\right\rangle}{dy}\right) \end{cases} \tag{53}$$

in the above, $\left\langle v_p'^2\right\rangle$ is the particle mean square fluctuation velocity in the normal direction and $\tau_p = \dfrac{\rho_p d_p^2}{18\mu_f}$ is the particle relaxation time as defined earlier.

3. An overview of nanofluids thermophysical properties

In this section, the main models available for thermophysical properties of nanofluids are first presented, and then the importance of using proper models in flow and heat transfer simulations is highlighted.

3.1. Thermophysical properties

3.1.1. Thermal conductivity (k_{nf})

Thermal conductivity characterizes the ability of a material to conduct heat, and it is measured in units of W/mK. The thermal conductivity of nanofluids is generally higher than that of conventional liquids. Here, the most used theoretical models and experimental correlations for thermal conductivity presented in the literature are reviewed.

3.1.1.1. Theoretical models

The Maxwell model [65,66] is probably the first model presented for the thermal conductivity k_{nf} of solid-liquid dispersions, where we set

$$k_{nf} = \frac{k_p + 2k_f + 2\phi(k_p - k_f)}{k_p + 2k_f - \phi(k_p - k_f)}k_f \tag{54}$$

and k_f and k_p are the thermal conductivities of the base fluid and the nanoparticles, respectively. This model is valid for spherical particles with small concentration ($\phi << 1$).

Bruggeman [65,67] presented the following model by considering interactions between spherical particles:

$$\frac{k_{nf}}{k_f} = \frac{(3\phi - 1)\frac{k_p}{k_f} + \{3(1-\phi) - 1\} + \sqrt{\Delta}}{4}; \quad (55)$$

$$where: \Delta = \left[(3\phi - 1)\frac{k_p}{k_f} + \{3(1-\phi) - 1\}\right]^2 + 8\frac{k_p}{k_f}$$

Hamilton and Crosser [68] extended the Maxwell model by including a shape factor as follows:

$$k_{nf} = \frac{k_p + (n-1)k_f + (n-1)\phi(k_p - k_f)}{k_p + (n-1)k_f - \phi(k_p - k_f)} k_f \quad (56)$$

where n is the empirical shape factor, determined by $n = \frac{3}{\psi}$ in which ψ is the particle sphericity. The sphericity parameter is 1 for spherical particles and it reduces to 0.5 for cylindrical particles.

It is important to mention that the previous models, valid for large particle sizes and generally underestimate the thermal conductivity magnitude compared to real (experimental) data. However, they are still widely used in numerical simulations of nanofluid flows. To avoid these discrepancies, several attempts have been made to extend or renovate the previous models and take in consideration phenomena involved in heat conduction of nanoparticles and nanofluids such as nanolayer, nanoparticle interaction, aggregation and Brownian motion.

The following models are mainly developed for metallic and oxide nanoparticles which are also spherical in shape.

When nanoparticles are dispersed in a liquid, a thin layer of liquid is formed on the surface of nanoparticles called the "liquid nanolayer". Yu and Choi [69] considered this factor to derive a new thermal conductivity model as follows:

$$k_{nf} = \frac{k_p + 2k_f + 2(k_p - k_f)(1+\gamma)^3\phi}{k_p + 2k_f - 2(k_p - k_f)(1+\gamma)^3\phi} k_p \quad (57)$$

where γ is the ratio of liquid nanolayer thickness to radius of nanoparticles and it is usually assumed to be 0.1.

Xuan et al. [70] presented a model for nanofluid thermal conductivity by considering the aggregation and Brownian motion of nanoparticles, giving

$$\frac{k_{nf}}{k_f}=\frac{k_p+2k_f-2\phi(k_f-k_p)}{k_p+2k_f+\phi(k_f-k_p)}+\frac{\rho_p\phi c_{p,f}}{2k_f}\sqrt{\frac{2\kappa_B T_{ave}}{3\pi d_p\mu_f}} \tag{58}$$

where κ_B is the Boltzmann constant and d_p is nanoparticle diameter. Therefore, based on this model, the thermal conductivity of a nanofluid depends on the nanoparticle thermal conductivity, the volume fraction of nanoparticles, the temperature of the mixture, the size of the nanoparticles, and the properties of the base fluid, including thermal conductivity, viscosity and specific heat capacity.

Koo and Kleinstreuer [71] proposed the following model for nanofluid thermal conductivity (known as the K-K model):

$$k_{nf}=k_{static}+k_{Brownian} \tag{59}$$

This model is composed of two parts, referred to as static and dynamic. The static part (k_{static}) has the form

$$k_{static}=\left(1+\frac{3(k_p/k_f-1)\phi}{(k_p/k_f+2)-(k_p/k_f-1)\phi}\right)k_f \tag{60}$$

The dynamic part accounts for the effect of Brownian motion on nanoparticles ($k_{Brownian}$) and is calculated by:

$$k_{Brownian}=5\times10^4\sigma\phi(\rho c_p)_f\sqrt{\frac{\kappa_B T}{\rho_p d_p}}f(T,\phi) \tag{61}$$

where σ and f are two empirical functions and κ_B is the Boltzmann constant.

Li [72] developed the K-K model by combining functions σ and f and replacing it by a single function g, which results in the expression

$$k_{Brownian}=5\times10^4\phi(\rho c_p)_f\sqrt{\frac{\kappa_B T}{\rho_p d_p}}g(T,\phi,d_p) \tag{62}$$

where:

$$g(T,\phi,d_p)=(a_1+a_2\ln(d_p)+a_3\ln(\phi)+a_4\ln(\phi)\ln(d_p)+a_5\ln(d_p)^2)\ln(T)+ \\ (a_6+a_7\ln(d_p)+a_8\ln(\phi)+a_9\ln(\phi)\ln(d_p)+a_{10}\ln(d_p)^2) \quad (63)$$

The constants a_1-a_{10}, which may be either positive or negative, are determined based on the type of nanoparticle and base liquid.

Feng and Kleinstreuer [73] presented a more advanced model in which there is no need for any empirical function (called the F-K model). This model takes into account the Brownian motion and turbulent fluctuation effects. This model is valid for water-based nanofluids containing metal oxide nanoparticles with diameter in the interval 30 <d_p< 50 nm, volume fractions less than 5%, and absolute suspension temperatures lower than 350 K. The F-K model is written as:

$$k_{nf}=k_{static}+k_{mm} \quad (64)$$

in which k_{static} is the same as defined earlier in the K-K model and k_{mm} indicates the micro-mixing contribution caused by the Brownian motion. The parameter k_{mm} is given by

$$k_{mm}=49500\frac{\kappa_B\tau_P}{2m_p}.C_c.(\rho c_p)_{nf}.\phi^2.(T\ln T-T). \\ \frac{\exp(-\zeta\omega_n\tau_p)\,Sinh\left(\sqrt{\frac{(3\pi\mu_f d_p)^2}{4m_p^2}-\frac{K_{p-p}}{m_p}}\,\frac{m_p}{3\pi\mu_f d_p}\right)}{\tau_p\sqrt{\frac{(3\pi\mu_f d_p)^2}{4m_p^2}-\frac{K_{p-p}}{m_p}}} \quad (65)$$

Here, m_p is the particle mass. The parameter C_c is constant and equal to 38 for metal-oxide based nanofluids. Also, the damping coefficient ζ, natural frequency ω_n, and characteristic time interval τ_p are defined as

$$\zeta=\frac{3\pi d_p\mu_f}{2m_p\omega_n},\quad \omega_n=\sqrt{\frac{K_{P-P}}{m_p}},\quad \tau_p=\frac{m_p}{3\pi\mu_f d_p} \quad (66)$$

where K_{P-P} shows the magnitude of particle- particle interaction intensity and is estimated by

$$K_{P-P}=\rho_p\sqrt{d_p}\left(\frac{32.1724\times 273K}{T}-19.4849\right) \quad (67)$$

In 2014, Xu and Kleinstreuer [74] proposed a new model that is more accurate than the F-K model

and considers the effect of aggregates, it reads as:

$$k_{nf} = k_{static} + k_{mm} \tag{68}$$

where k_{static} reads as

$$k_{static} = k_f \left(1 + \frac{3\left(k_a/k_f - 1\right)\phi}{\left(k_a/k_f + 2\right) - \left(k_a/k_f - 1\right)\phi} \right) \tag{69}$$

In this equation, k_a is the effective thermal conductivity of the aggregates, as proposed by Nan et al. [75]:

$$k_a = k_{de} \cdot \frac{3 + \phi_b \left[2\beta_{11}\left(1 - L_{11}\right) + \beta_{33}\left(1 - L_{33}\right) \right]}{3 - \phi_b \left(2\beta_{11} L_{11} + \beta_{33} L_{33} \right)} \tag{70}$$

The thermal conductivity of the aggregate due to dead-end particles, $k_{de,}$ is defined based on the Bruggeman model[67].

The geometrical factors L_{11} and L_{33} are expressed in [75] as

$$L_{11} = p^2 \Big/ 2\left(p^2 - 1\right) - p^2 \cosh^{-1} \Big/ 2\left(p^2 - 1\right)^{1.5} \text{ and } L_{33} = 1 - L_{11} \tag{71}$$

The aspect ratio is $p = R_g / d_p$, and

$$\beta_{ii} = \left(k_{ii}^c - k_{de}\right) \Big/ \left[k_{de} + L_{ii}\left(k_{ii}^c - k_{de}\right) \right], \; i = 1, 3 \tag{72}$$

k_{ii}^c are equivalent thermal conductivities along corresponding symmetric axis of an ellipsoidal composite unit cell, with $k_{ii}^c = k_{bf} \left(1 + \gamma L_{ii} k_p / k_{bf}\right)$, $\gamma = \left(2 + 1/p\right)\alpha$, $\alpha = A_k / d_p$ with A_k is the Kapitza length. Also,

$$k_{de} = \left(3\phi_{de} - 1\right).k_{peff} + \left(2 - 3\phi_{de}\right).k_{bf} + \sqrt{\left(3\phi_{de} - 1\right)^2 .k_{peff}^2 + \left(2 - 3\phi_{de}\right)^2 k_{bf}^2 + 2\left[2 + 9\phi_{de}\left(1 - \phi_{de}\right)\right] k_{peff} k_{bf}} \tag{73}$$

and the improved parameter k_{mm} is:

$$k_{mm} = 19631.C_c \phi \frac{\kappa_B \tau_a}{m_a} \left(\rho c_p\right)_{nf} \left(\bar{T}.ln\bar{T} - \bar{T}\right) \tag{74}$$

In the above, C_c is a correction factor having a value about 1 for water-based nanofluids.

Prasher et al. [76] derived a correlation as follows:

$$\frac{k_{nf}}{k_f} = (1 + \Gamma \,\mathrm{Re}_b^m \,\mathrm{Pr}^{0.333}\,\phi) \times \left(\frac{\left[k_p(1+2\alpha) + 2k_f\right] + 2\phi\left[k_p(1-2\alpha) - k_f\right]}{\left[k_p(1+2\alpha) + 2k_f\right] - \phi\left[k_p(1-2\alpha) - k_f\right]} \right) \tag{75}$$

in which the random motion-induced convection is included. In the above relation Reynolds number due to Brownian motion is $\mathrm{Re}_b = \frac{\sqrt{18\kappa_b T / \pi\rho_p d_p}}{\upsilon_f}$, and α is the nanoparticle Biot number defined as $\alpha = 2R_b k_f / d_p$. Also, R_b is the thermal interface resistance equal to $0.77 \times 10^{-8}\, Km^2/W$ for water-based nanofluids, while Γ and m are empirical constants depending on nanoparticle type. For Al_2O_3 nanoparticles, $m = 2.5$ and $\Gamma = 40000$.

Another model that considers Brownian motion of nanoparticles is presented by Patel et al.[77] as follows:

$$\frac{k_{nf}}{k_f} = 1 + \frac{k_p A_p}{k_f A_f} + C_e k_p Pe \frac{A_p}{k_f A_f} \tag{76}$$

where C_e should be determined by experiments. In addition, A_p / A_f and Pe are obtained by:

$$\frac{A_p}{A_f} = \frac{d_f}{d_p}\frac{\phi}{(1-\phi)} \; and \; Pe = \frac{u_p d_p}{\alpha_f} \tag{77}$$

in which u_p is the Brownian motion velocity of nanoparticles:

$$u_p = \frac{\sqrt{\kappa_B T}}{\pi \mu_f a_p^2} \tag{78}$$

In another model, Amiri and Vafai considered the contribution of thermal dispersion to thermal conductivity model, this model reads as[78,79]:

$$k_f = k_{static} + k_d \tag{79}$$

Maxwell's model is used to estimate k_{static}, and the thermal conductivity induced by thermal dispersion (k_d) is estimated by:

$$k_d = C_e (\rho C_p)_{nf} \sqrt{v_x^2 + v_y^2}\, \phi\, d_p \tag{80}$$

where C_e is the constant obtained from experiments, v is the fluid velocity.

Several models have also been developed for the prediction of thermal conductivity of nanofluids containing carbon-based nanotubes.

Xue et al. [80] offered a model to obtain the thermal conductivity nanosuspensions containing carbon nano tubes (CNTs). The model originates from the classic model given by Maxwell. Moreover, it takes into account the influence of physical characteristics of CNTs, including axial ratio and space distribution, to obtain

$$k_{nf} = \frac{1-\phi+2\phi\dfrac{k_p}{k_p-k_{bf}}\ln\dfrac{k_p+k_{bf}}{2k_{bf}}}{1-\phi+2\phi\dfrac{k_{bf}}{k_p-k_{bf}}\ln\dfrac{k_p+k_{bf}}{2k_{bf}}}k_{bf} \tag{81}$$

Patel et al. [81] presented a model in which the thermal conductivity of CNT nanofluids was a function of nanofluid volume concentration, and both the base fluid molecular and nanoparticle radii, r_{bf} and r_p respectively, which reads as

$$k_{nf} = k_{bf}\left[1+\frac{k_p\phi r_{bf}}{k_{bf}(1-\phi)}\right] \tag{82}$$

Nan et al. [82] proposed the following model for CNTs based nanofluids:

$$k_{nf} = \frac{3+\phi(\beta_{11}+\beta_{33})}{3-\phi\beta_{11}}k_{bf} \tag{83}$$

where

$$\beta_{11} = \frac{2\left(k^c_{11}-k_{bf}\right)}{k^c_{11}+k_{bf}}\ ;\ \beta_{33} = \frac{k^c_{33}}{k_{bf}}-1 \tag{84}$$

and

$$k^c_{11} = \frac{k_p}{1+\dfrac{2a_k k_p}{dk_{bf}}}\ ;\ k^c_{33} = \frac{k_p}{1+\dfrac{2a_k k_p}{lk_{bf}}} \tag{85}$$

In the previous equations, k^c_{11} is thermal conductivity along transverse axis and k^c_{33} is the thermal conductivity along longitudinal axis of a thin interfacial thermal layer and depend on dimensions of CNT. Also, Kapitza radius $a_k = R_k k_{bf}$, with $R_k = 8\times10^{-8}$ m²K/W [83].

Murshed et al.[84] developed a model for CNTs nanofluids by considering the size of nanoparticle, nanosuspension volume concentration, and interfacial layer. It writes as

$$k_{nf} = \frac{(k_p - k_{lr})\phi k_{lr}(\gamma_1^2 - \gamma^2 + 1) + (k_p + k_{lr})\gamma_1^2[\phi\gamma^2(k_{lr} - k_{bf}) + k_{bf}]}{\gamma_1^2(k_p + k_{lr}) - (k_p - k_{lr})\phi(\gamma_1^2 + \gamma^2 - 1)} \quad (86)$$

with

$$\gamma_1 = 1 + t/r_p \ ; \ \gamma = 1 + t/d_p \quad (87)$$

k_{lr} represents the thermal conductivity of interfacial layer and t is the thickness of interfacial layer between nanoparticle and base fluid.

A comprehensive overview about thermal conductivity models of CNT based nanofluids is given in Ref. [85]. In addition, Estellé et al. [86] measured the thermal conductivity of CNTs/water nanofluids and compared the results with available models.

3.1.1.2. Experimental based correlations

With regards on experimental based correlations, they were mainly obtained for spherical metallic and oxide nanoparticles. Maiga et al. [87] presented two correlations based on experimental data for the thermal conductivity of Al_2O_3- water and Al_2O_3- EG nanofluids as follows:

Al_2O_3/water:

$$k_{nf} = (4.97\phi^2 + 2.72\phi + 1)k_f \quad (88)$$

Al_2O_3/ ethylene glycol:

$$k_{nf} = (28.905\phi^2 + 2.8273\ \phi + 1)k_f \quad (89)$$

The above correlations were developed for nanoparticles with a size of 28 nm.

Based on various experimental data for thermal conductivity of nanofluids, Corcione [88] developed the following correlation:

$$\frac{k_{nf}}{k_f} = 1 + 4.4\ \mathrm{Re}_p^{0.4}\ \mathrm{Pr}_f^{0.66}\left(\frac{T}{T_{freez}}\right)^{10}\left(\frac{k_p}{k_f}\right)^{0.03}\phi^{0.66} \quad (90)$$

where:

$$\mathrm{Re}_p = \frac{2\rho_f \kappa_B T}{\pi \mu_f^2 d_p} \quad (91)$$

The above relation is valid for nanoparticle sizes between 10-150 nm, volume fractions of 0.2-9%, and temperatures between 294 and 324 K. It should be noted that T_{freez} is the freezing temperature of the base fluid.

Khanafer and Vafai [65] proposed a general correlation for the thermal conductivity of Al_2O_3/water and CuO/water nanofluids as follows:

$$\frac{k_{nf}}{k_f} = 1 + 1.0112\phi + 2.4375\phi\left(\frac{47}{d_p(nm)}\right) - 0.0248\phi_p\left(\frac{k_p}{0.613}\right) \quad (92)$$

The above correlation is valid for nanoparticle size between 13nm and 80nm and volume fractions up to 15%.

Chon et al.[89] derived the following correlation for alumina/water nanofluids which is valid for the temperature range between 21 and 71 ^{o}C, and nanoparticle sizes between 11 and 150nm as follows:

$$\frac{k_{nf}}{k_f} = 1 + 64.7\phi^{0.7460}\left(\frac{d_f}{d_p}\right)^{0.3690}\left(\frac{k_p}{k_f}\right)^{0.7476} \mathrm{Pr}^{0.9955}\,\mathrm{Re}_p^{1.2321} \quad (93)$$

As seen, Re_p is included in the equation which implies Brownian motion has been taken into account in this correlation.

Ho et al. [90] derived the following empirical correlation for thermal conductivity of alumina/water nanofluids where the size of nanoparticles is 33 nm:

$$k_{nf} = k_{bf}(1 + 2.944\phi + 19.672\phi^2) \quad (94)$$

The above relation is valid for concentrations up to 4%.

A correlation developed by Sharma et al. [91,92] can be applied to all water-based nanofluids containing either metal or metal oxide nanoparticles where the particle diameter is between 20 and 150 nm, nanofluid temperature is between 20 and 70 °C, and maximum volume fraction of 4%. It reads as:

$$\frac{k_{nf}}{k_f} = 0.8938\left(1 + \frac{\phi}{100}\right)^{1.37}\left(1 + \frac{T_{nf}}{70}\right)^{0.2777}\left(1 + \frac{d_p}{150}\right)^{-0.0336}\left(\frac{\alpha_p}{\alpha_f}\right)^{0.01737} \quad (95)$$

In conclusion, it should be noted that most of articles on nanofluids indicate that the thermal conductivity increases with increases in volume concentration and temperature, and it decreases with increase in the particle size. It should also be mentioned that many other empirical correlations have been developed as shown in the literature, but they are specific to the kind of nanofluids tested, including the nature of the base fluid and the nanoparticles, the size and shape of the nanoparticles, the range of nanoparticle content, and the temperature.

To date, there is no universal model for the prediction of nanofluid thermal conductivity, which is a significant challenge in nanofluid research. The readers can refer to several papers such as Refs. [93–104] on the thermal conductivity of EG-based nanofluids and Refs. [105–113] on the thermal conductivity of water based nanofluids, as well as comprehensive reviews such as Refs. [114–123].

3.1.2. Viscosity (μ_{nf})

Viscosity is defined as the resistance of a liquid to flow and it is measured in terms of Pa.s (pascal*second) or N.S/m^2. When we say water flows faster than oil on an inclined glass it means viscosity (resistance) of water to flow is less than oil. Fluids can be divided into two groups, i.e. Newtonian and non-Newtonian fluids. A fluid is called a Newtonian fluid if (i) shear stress (the force per unit area applied to fluid) has a linear relationship with shear rate (called also deformation rate- $G = \partial V_f / \partial y$) and (ii) when shear stress is zero, the shear rate being also zero (see Fig. 14 (a)) at fixed temperature and pressure. For a Newtonian fluid, viscosity does not change with increase in shear rate (Fig. 14 (b)). Fluids such as water and air are simple instances of Newtonian fluids. However, in non-Newtonian fluids the viscosity follows the variations of shear rate. Non-Newtonian fluids can be categorized as (i) time-dependent, if shear rate varies with magnitude and amplitude of shear stress, and possibly time between two consecutive applied shear stress. Fluids with time-dependent viscosity can be classified as thixotropic (viscosity reduces with time) and rheopectic (viscosity increases with time) fluids. However, if shear rate only depends on current shear stress the fluid is classified as (ii) time-independent, and generally refer to purely viscous fluids. Non-Newtonian fluids can also present (iii) viscoelastic properties. Among non Newtonian fluids, one can distinguish shear-thinning (also called pseudoplastic) fluids and shear-thickening (also called dilatant) fluids, as shown in Fig.14. In addition, they can possess a yield stress, i.e. a minimum stress that should be applied for starting the flow. Toothpaste is a familiar non Newtonian fluid which is classified as Bingham plastic (see Fig. 14 (a)).

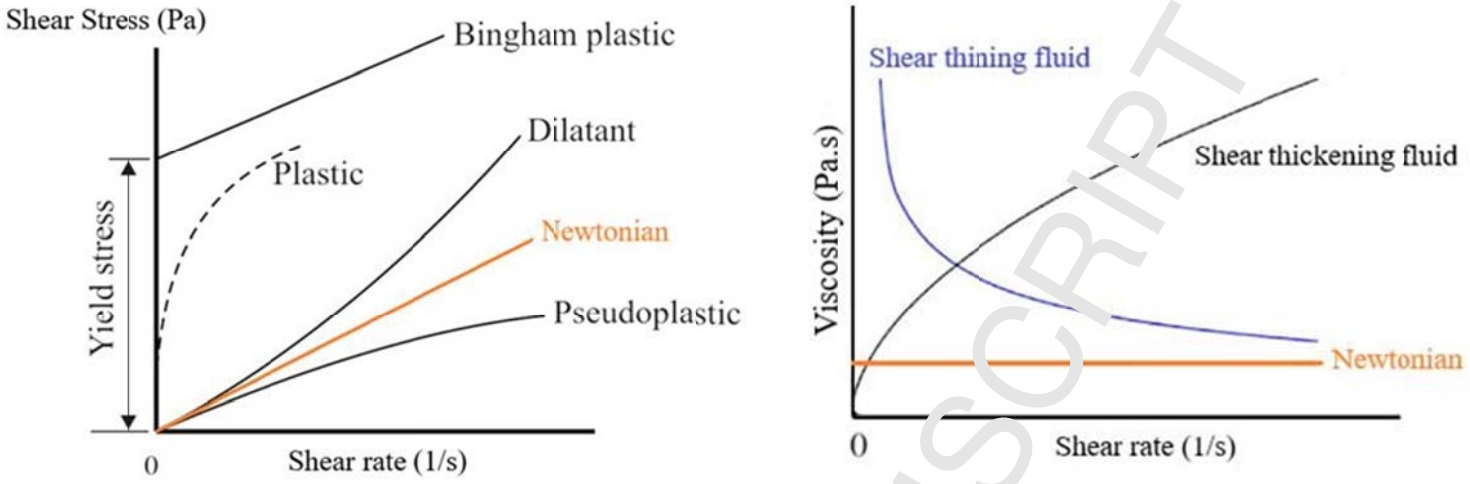

(*a*) (b)

Figure 14. Newtonian versus non-Newtonian fluid (a) shear stress variations with shear rate determines the fluid is Newtonian or non-Newtonian (b) Variation of viscosity with shear rate

The viscosity of nanofluids is generally higher than that of conventional liquids. With increases in the concentration of nanofluids, they may become non-Newtonian liquid. Here, a brief review is done on models presented for viscosity of nanofluids based on a Newtonian behavior or at a fixed shear rate. As for thermal conductivity, first models considered are issued from suspension theory of large spherical particles. However, they are also unable to predict viscosity enhancement of nanofluid viscosity with volume fraction.

3.1.2.1. Theoretical models

Einstein presented a model based on kinetic theory for mixtures of solids and liquids which is valid for volume fractions less than 1%. It gives the mixture effective viscosity as [65]

$$\mu_{nf} = \mu_f (1 + 2.5\phi) \tag{96}$$

Brinkman proposed the following model for particles(spherical)- useable up to 4% particle volume loadings [124]:

$$\mu_{nf} = \frac{\mu_f}{(1-\phi)^{2.5}} \tag{97}$$

For wider range in nanoparticle content, the model proposed by Krieger and Dougherty[125] for monodisperse spherical particles is more suitable. It reads as

$$\mu_{nf} = \mu_f \left(1 - \frac{\phi}{\phi_m}\right)^{-[\mu]\phi_m} \tag{98}$$

where the intrinsic viscosity [μ]= 2.5 for hard spheres and the maximum packing fraction ϕ_m is about 0.605. This equation reduces to the Maron-Pierce equation with exponent $[\mu]\phi_m$=2 [126].

The equations given in [125,126] were successfully used with nanofluids of different natures in the presence of aggregates[127–129], with the nanoparticle volume fraction being replaced by the aggregate volume fraction.

Masoumi et al. [130] presented a theoretical model for nanofluid viscosity as a function of nanoparticle size, nanofluid temperature, volume fraction of nanoparticles, nanoparticle density and viscosity of the base fluid as

$$\mu_{nf} = \mu_f + \frac{\rho_p}{72C}\left(\sqrt{\frac{18\kappa_B T}{\pi\rho_p d_p}}\right)\left(\frac{\phi}{\pi}\right) \tag{99}$$

where

$$C = \frac{1}{\mu_f}\left[\left(-0.000001133 d_p - 0.000002771\right)\phi + \left(0.00000009 d_p - 0.000000393\right)\right] \tag{100}$$

3.2.2.2 Experimental based correlations

By using experimental data for Al_2O_3-water nanofluids, Singh et al. [131] modified the Einstein model as

$$\mu_{nf} = \mu_f (1 + 10\phi) \tag{101}$$

Corcione [88]presented an empirical correlation for viscosity of nanofluids as a function of nanoparticles diameter (d_p) and the molecular diameter of base fluid (d_f) as

$$\frac{\mu_{nf}}{\mu_f} = \frac{1}{1 - 34.87(d_p/d_f)^{-0.3}\phi^{1.03}} \tag{102}$$

where the molecule diameter of base fluid can be calculated by knowing the molecular weight of base fluid(M) as

$$d_f = \left[\frac{6M}{N\pi\rho_{f,0}}\right]^{1/3} \quad (103)$$

Here, N is the Avogadro number ($6.022140857 \times 10^{23}$) and $\rho_{f,0}$ is the density of base fluid calculated at the temperature of 293 K. The above correlation is valid for nanoparticle sizes between 25 and 200 nm, concentrations between 0.01 and 7.1%, and temperatures between 293 and 333 K.

Maiga et al. [87] presented two experimental-based correlations for the viscosity of Al_2O_3-water and Al_2O_3-EG nanofluids, respectively, as

$$\mu_{nf} = (123\phi^2 + 7.3\phi + 1)\,\mu_f \quad (104)$$

$$\mu_{nf} = (306\phi^2 - 0.19\phi + 1)\,\mu_f \quad (105)$$

Rea et al. [132], using regression analysis of experimental data of Williams et al.[133], presented the following correlation for Al_2O_3/ water nanofluids that is valid for volume fractions less than 6 % and temperatures in the interval 20-80 ^oC:

$$\mu_{nf}(\phi,T) = \mu_f(T)\exp[4.91\phi(0.2092 - \rho)] \quad (106)$$

The water viscosity (μ_f) can be obtained by the following equation:

$$\mu_f = \mu_{ref}\left(\frac{T}{T_{ref}}\right)^n \exp\left[B\left(\frac{1}{T} - \frac{1}{T_{ref}}\right)\right] \quad (107)$$

where B= 4700 , n = 8.9, T_{ref} = 295 K and $\mu_{ref} = 959\times10^{-6}\,\frac{N.S}{m^2}$.

In a combined experimental and numerical study, Jang et al. [134]noted that the viscosity of nanofluids when the nanofluid flows in micro and mini tubes depends on the size of the tube. Therefore, they developed the Einstein model by including the effect of slip velocity of nanoparticles for nanofluid flow in micro and mini tubes as follows:

$$\frac{\mu_{nf}}{\mu_f} = (1+2.5\phi)\left[1+\eta\left(\frac{d_p}{D_m}\right)^{-2\varepsilon}\phi^{2/3(\varepsilon+1)}\right] \quad (108)$$

in which D_m is the inner diameter of microchannel (or minitube), and ε and η are empirically obtained constants which for Al_2O_3 nanoparticles are equal to-1/4 and 280, respectively.

Ho et al. [90] presented the following correlation based on their experimental data for viscosity of alumina/water nanofluids, where the size of nanoparticles is 33 nm (valid for $\phi \le 4\%$):

$$\mu_{nf} = \mu_f(1+4.93\phi+222.4\phi^2) \tag{109}$$

Sharma et al. [91,92] presented the following correlation for viscosity of water-based nanofluids containing either metal or metal oxide nanoparticles:

$$\frac{\mu_{nf}}{\mu_f} = \left(1+\frac{\phi}{100}\right)^{11.3}\left(1+\frac{T_{nf}}{70}\right)^{-0.038}\left(1+\frac{d_p}{170}\right)^{-0.061} \tag{110}$$

The above correlation is valid for particle diameters between 20 and 150 nm, nanofluid temperature between 20 and 70 °C, and maximum volume fraction of 4%.

It should be noted that most articles on nanofluids indicate that the viscosity increases with ϕ and the increase in the particle size and temperature lessens the viscosity.

Here, only a few models are presented as the literature on this topic is abundant. For a more comprehensive overview, the reader can refer to recent review papers on this specific topic [135–138] and other research papers [139–144].

Contrary to thermal conductivity and viscosity, only a few equations are available and useful for density, specific heat capacity and thermal coefficient expansion. They are mainly based on mixing rules.

3.1.3. Density (ρ_{nf})

Density is defined as the ratio of mass to volume of a substance and it is measured in terms of kg/m^3. For a nanofluid with a volume concentration of ϕ , the nanofluid density can be calculated as[145]

$$\rho_{nf} = \rho_f(1-\phi)+\rho_p\phi \tag{111}$$

3.1.4. Specific heat capacity ($c_{p,nf}$)

Specific heat capacity is the amount of heat that should be given to one kilogram of a substance to increase its temperature by 1 degree Kelvin, and it is measured in units of J/ kg.K. The specific heat capacity of nanofluids can be calculated by [65]

$$c_{p,nf} = \frac{\rho_f c_{p,f}(1-\phi)+\rho_p c_{p,p}\phi}{\rho_{nf}} \tag{112}$$

where $c_{p,f}$ and $c_{p,p}$ are, respectively, the specific heat capacities of base fluid and nanoparticles.

A common simplified model that is valid when the nanoparticle density is similar to that of the base fluid is given by

$$c_{p,nf} = (1-\phi)c_{p,f} + \phi c_{p,p} \tag{113}$$

Specific heat capacity significance is highlighted in solar collector applications where the demand is higher outlet temperature of collector.

3.1.5. Thermal expansion coefficient (β_{nf})

The volumetric thermal expansion coefficient for a nanofluid is the amount of change in nanofluid volume per one degree Kelvin increase in the temperature of the mixture, and it is measured in units of 1/K. The following relation is used to estimate the thermal expansion coefficient[65]:

$$\beta_{nf} = \frac{(1-\phi)(\rho\beta)_f + \phi(\rho\beta)_p}{\rho_{nf}} \tag{114}$$

Again, if the particle and fluid densities are similar, a common approximation of this expression is

$$\beta_{nf} = (1-\phi)\beta_f + \phi\beta_p \tag{115}$$

Significance of the thermal expansion coefficient is highlighted in natural and mixed convection problems.

3.1.6. Surface tension (γ_{nf})

Surface tension is the amount of force per unit length that is consumed for extending the surface of a liquid by overcoming the intermolecular forces (measured in units of N/m). Surface tension is a crucial parameter in the analysis of heat transfer phenomena such as pool boiling since it affects surface wettability and bubble growth [146]. On the measurement of surface tension of nanofluids, Ahammed et al. [147] measured the surface tension of graphene/water nanofluids and showed that with increasing the temperature and nanofluid concentration the surface tension decreases. They developed a correlation as:

$$\frac{\gamma_{nf}}{\gamma_f} = 0.493\left(\frac{T_\infty}{T_{nf}}\right)^{0.163}\left(\frac{1}{\phi}\right)^{0.0884} \tag{116}$$

where γ_{nf} is the surface tension of nanofluid, γ_f is the surface tension of base fluid, and T_∞ is the ambient temperature. The above relation is valid for temperatures ranging from 10 to 90 °C, and graphene volume fractions between 0.05% and 0.15%.

Similar trends of nanoparticle effect were also reported in [148] with graphene nanofluids while opposite effect of nanoparticle content was observed in [98] with different base fluids and nanoparticles. In another study, Chinnam et al. [149] presented a nanoparticle size dependent correlation for surface tension with four different nanoparticles, including Al_2O_3, ZnO, TiO_2 and SiO_2, suspended in a mixture of propylene glycol and water (60:40 PG/water) as follows:

$$\frac{\gamma_{nf}}{\gamma_f} = A_1\phi + A_2\left(\frac{T_0}{T_{nf}}\right) + A_3\left(\frac{d_p}{d_f}\right) + A_4 \tag{117}$$

where T_0 = 299 K, A_1 = -1.02219, A_2 = -0.27706, A_3 = 0.006635[illegible] and A_4 = 1.17344. Also, d_f is the molecular diameter of the base fluid. The above relation can be used for 303< T_{nf} < 343 K, 0.5 < ϕ (%)< 6 and 15< d_p (nm) < 50.

In a recent review, Estellé et al. [146] highlighted the role of surface tension in thermal engineering applications and investigated the effects of various parameters such as temperature, surfactant, morphology and concentration of particles, and base fluid type on the surface tension of nanofluids. There are some other correlations on the surface tension of nanofluids which are gathered by Estellé et al. [146].

3.2. On the importance of thermophysical models in modeling

A challenge in modeling of nanofluid flows is the choice and use of suitable models for property determination, specifically for thermal conductivity and viscosity. Figure 15 gives a summary of the effects of nanoparticle concentration, nanoparticle size, and nanofluid temperature on the thermal conductivity and viscosity of nanofluids, with trends that are valid for almost all nanofluids. However, it should be noted that just the prediction of trends by models (or correlations) is not sufficient, but it is vital to have the minimum uncertainty in the estimation of thermal conductivity and viscosity when the data are compared with experimental (real) data.

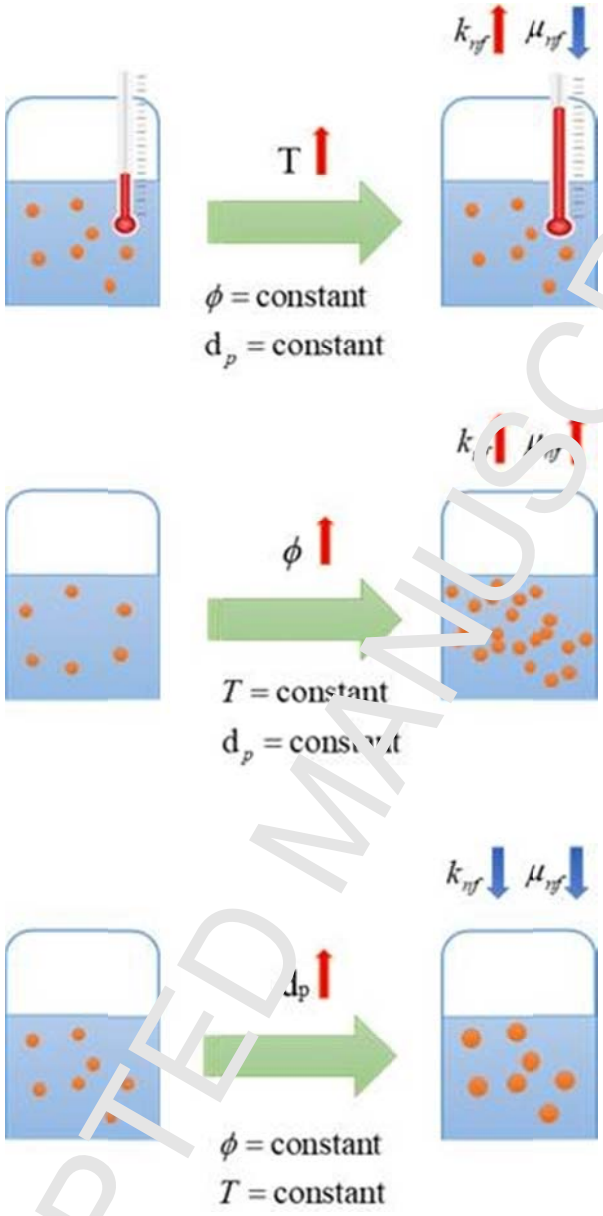

Figure 15. Variations of thermal conductivity and viscosity with temperature, volume fraction, and nanoparticle size. Note that almost all of studies on nanofluids have verified the above trend.

In this section, some work focusing on the impact of uncertainties in thermophysical properties on the results of nanofluid modeling are reviewed.

Mahian et al. [150] indicated that although using different thermophysical models has a significant effect on the values of heat transfer coefficient in solar collector tubes, there is no significant effect on the outlet temperature of solar collectors. Mahian et al. [151] found that using different thermophysical

models may lead to opposite predictions of entropy generation between two rotating cylinders. For natural convection in square and triangular cavities, Mahian et al. [152] noted that using classic models for thermophysical properties instead of experimental based correlations may give opposite predictions of heat transfer coefficient. Abu-Nada and Chamkha [153] also showed that different thermophysical models can give different trends for prediction of Nusselt number in natural convection of cavities. In other work, Abu-Nada [154] analyzed the role of different viscosity and thermal conductivity models on flow and heat transfer characteristics of Al_2O_3/water nanofluid natural convection flow in cavities.

Figure 16 highlights this note that using different thermophysical models may provide opposite trends for heat transfer coefficient variations.

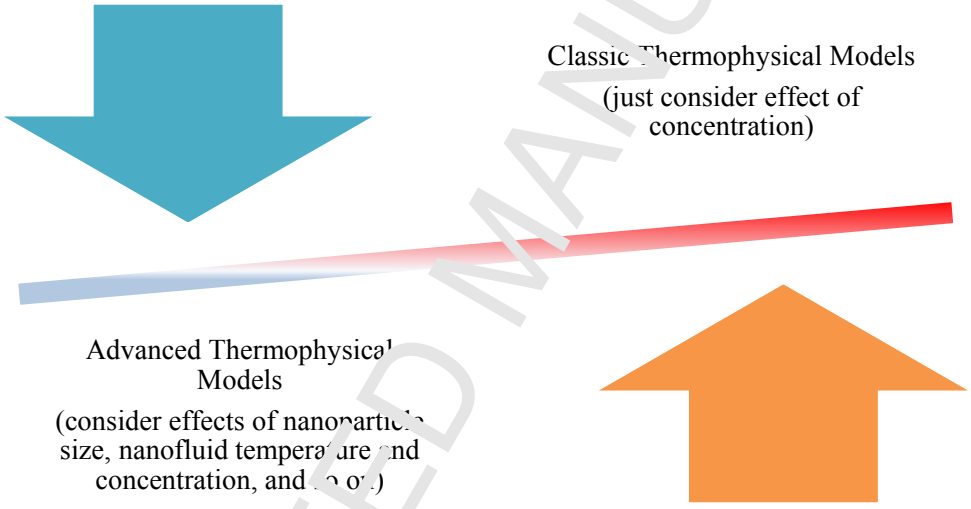

Figure 16. Using different thermophysical models may provide opposite trends for heat transfer coefficient variations

4. Physical models for nanofluid flow and heat transfer

In analysis of a thermal system, one seeks to solve for the velocity and temperature fields and to use these fields to determine integral measures such as heat transfer coefficient, Nusselt number, thermal

efficiency, and entropy generation rate of the system. In this section, we present the main physical models used to describe the nanofluid flow and heat transfer characteristics. We begin by reviewing the transport equations for conventional fluids, including continuity, the Navier Stokes equations, and the energy equation, which are used for evaluating the velocity, pressure, and temperature fields due to motion of a conventional fluid in an arbitrary geometry. This is followed by the extension of for the conservation laws to nanofluid flows.

4.1. Transport equations for conventional fluids

In the following equations, **V** is the velocity vector, p is the pressure, T is the temperature, **I** is the identity matrix and $\boldsymbol{F}$ is the summation of external body forces (due to gravity or magnetic field) discussed in section 2. The transport equations are written below for steady, Newtonian, incompressible flow of a conventional fluid with a density of ρ_f, a thermal conductivity of k_f, and a viscosity of μ_f. The continuity equation states the requirement of mass conservation for the fluid, and is given by:

$$\nabla \cdot (\rho_f \mathbf{V}) = 0 \tag{118}$$

The momentum equation is obtained by applying the Newton's second law applied to an element of a viscous fluid and is given by

$$\rho_f (\mathbf{V} \cdot \nabla)\mathbf{V} = -\nabla p + \nabla \cdot [\mu_f (\nabla \mathbf{V} + \nabla \mathbf{V}^T)] + \nabla \cdot [\lambda (\nabla \cdot \mathbf{V})\mathbf{I}] + \mathbf{F} \tag{119}$$

In the above equation λ is the second coefficient of viscosity due to viscous effects of volume changes, and usually can be considered to be negligible. However, $\lambda \approx -2\mu_f/3$ is a common approximation for this parameter, when it's not ignorable. In addition, $\rho_f (\nabla \cdot \mathbf{V})\mathbf{V}$ is the convective term, $-\nabla p$ is the pressure gradient, $\nabla \cdot [\mu_f (\nabla \mathbf{V} + \nabla \mathbf{V}^T)]$ is the viscous diffusion term where the viscosity is a function of temperature and nanoparticle concentration.

Considering the (very common) case of incompressible flow with constant viscosity and density and ignoring the second viscosity coefficient (λ), the momentum equation can be simplified as follows:

$$\rho_f (\boldsymbol{V} \cdot \nabla \boldsymbol{V}) = -\nabla p + \mu_f \nabla^2 \boldsymbol{V} + \boldsymbol{F} \tag{120}$$

The energy equation that indicates the temperature field (T) can be written as

$$\nabla \cdot (\rho_f c_{p,f} \mathbf{V} T) = \nabla \cdot (k_f \nabla T) + \Phi \tag{121}$$

In the above equation, the left side represents the thermal convection, $\nabla \cdot (k_f \nabla T)$ is the heat conduction and Φ is the viscous dissipation function, which arises from the work done against viscous forces and for a Newtonian incompressible viscous fluid and is given by:

$$\Phi = \mu_f \left\{ 2\left[\left(\frac{\partial u}{\partial x}\right)^2 + \left(\frac{\partial v}{\partial y}\right)^2 + \left(\frac{\partial w}{\partial z}\right)^2 \right] + \left(\frac{\partial v}{\partial x} + \frac{\partial u}{\partial y}\right)^2 + \left(\frac{\partial w}{\partial y} + \frac{\partial v}{\partial z}\right)^2 + \left(\frac{\partial u}{\partial z} + \frac{\partial w}{\partial x}\right)^2 \right\} + \lambda(\nabla . \boldsymbol{V})^2 \tag{122}$$

It is also worth mentioning that the viscous dissipation energy is usually ignored with respect to the other energy transfer terms. In the remainder of this section, we have neglected the viscous dissipation source term on the right side of the energy equation.

The component forms of the above equations are presented in Appendix A for different coordinate systems.

4.2. Transport equations for nanofluids

Considering the transport equations mentioned for conventional liquids, we will develop governing equations associated with different approaches for nanofluid flow modeling in the next sections. In this regard, Fig. 17 presents the main approaches for nanofluid flow modeling, which can be classified as either single-phase or two-phase approaches.

4.3. Single-phase approaches

A nanofluid is inherently a two-phase fluid (solid-liquid); however, for numerical simulations under certain conditions some appropriate assumptions can be made to model nanofluids as single-phase fluids.

In single-phase models the governing equations are solved only for an effective liquid phase. Single-phase based models can be divided into three main approaches including homogenous, thermal dispersion, and Buongiorno models. In the following each model is described in detail.

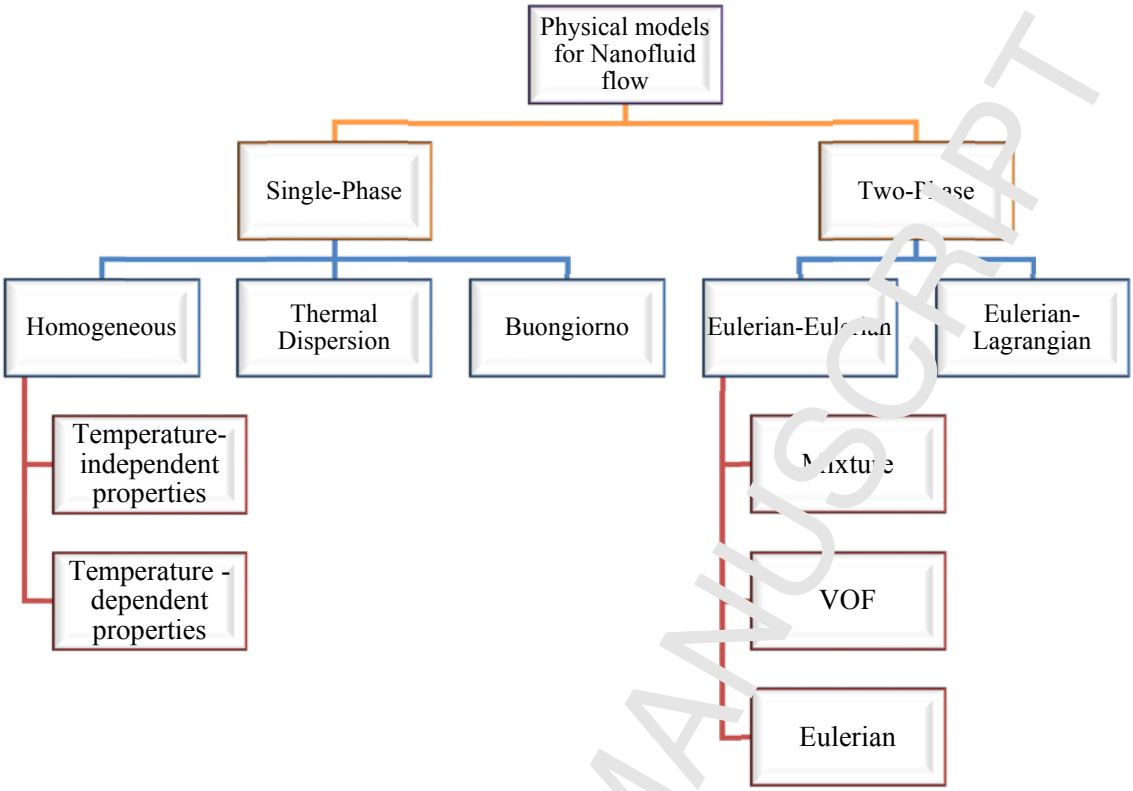

Figure 17. Main approaches for nanofluid flow modeling

4.3.1. Homogenous model

The simplest approach for modeling of nanofluid flow is the homogenous model. The main assumptions in this model are:

- The slip between the base liquid and the nanoparticles is negligible.

- The size of solid particles are ultrafine and dispersed uniformly throughout the base fluid.

- Solid and fluid phases are in hydrodynamic and thermal equilibrium.

The above assumptions imply that any interphase forces and thermal exchange between the fluid and the solid particles can be neglected. Therefore, the mixture of nanoparticles and the base fluid can be considered as a single-phase continuum with certain effective material properties. Figure 18 schematically describes the single-phase flow approximation for nanofluid flow in a tube.

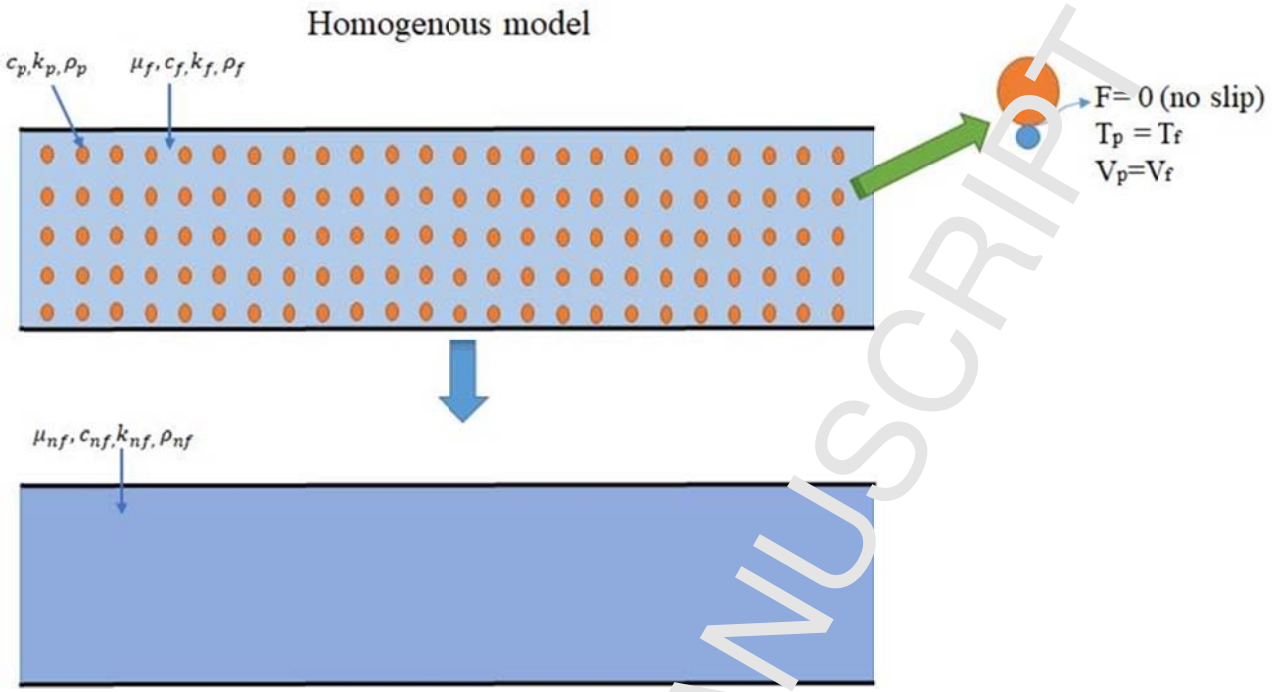

Figure 18. A schematic of the single-phase homogenous model in which effective properties of the mixture are used to capture the nanoparticle influence

The transport equations given in part 4.1, can be modified for nanofluids, considering negligible viscous dissipation and $\lambda = 0$, and applying the homogenous model as follows:

Continuity equation:

$$\nabla \cdot (\rho_{nf} \mathbf{V}) = 0 \tag{123}$$

Momentum equation for a nanofluid with variable viscosity:

$$\rho_{nf} (\mathbf{V} \cdot \nabla)\mathbf{V} = -\nabla p + \nabla \cdot [\mu_{nf} (\nabla \mathbf{V} + \nabla \mathbf{V}^T)] + \mathbf{F} \tag{124}$$

Regarding the momentum equation presented above, it should be noted that in many studies on nanofluids the viscosity is considered to be a function of temperature and concentration. In such a case, it is necessary to include $(\nabla \boldsymbol{V})^T$ in the viscous shear term.

Energy equation:

$$\nabla \cdot (\rho_{nf} c_{p,nf} \mathbf{V} T) = \nabla \cdot (k_{nf} \nabla T) + \Phi \tag{125}$$

Selecting suitable models for thermophysical properties of nanofluids (mainly thermal conductivity and viscosity) is the main challenge of this approach. The properties can be considered as constant (temperature-independent) or temperature–dependent, depending on the problem and the characteristics of the mixture. A large number of studies have been conducted regarding the modeling of the nanofluids by employing the homogenous single-phase model. Here, some studies that utilized homogenous model are reviewed briefly.

Saha and Paul [155] simulated the turbulent flow of water-based Al_2O_3 and TiO_2 nanofluids in a horizontal tube under constant heat flux boundary condition using homogenous single-phase model and temperature-dependent properties. Demir et al. [156] simulated forced convection of Al_2O_3 and TiO_2 based nanofluids in a heat exchanger with double tube structure. The homogenous single-phase model was used to solve the problem.

Namburu et al. [157] studied the turbulent flow of EG/water nanofluids having SiO_2, Al_2O_3, and CuO nanoparticles in a tube using homogenous single-phase model with temperature-dependent properties. Moraveji et al. [158] investigated the convective heat transfer of Al_2O_3/water nanofluid flow as a single-phase liquid in the developing region of a tube with constant heat flux. Manca et al. [159] analyzed the forced convection of alumina/water nanofluid in a two-dimensional channel under uniform heat flux using homogenous single-phase approach and the properties were assumed temperature-independent. Ahmed et al. [160] studied the laminar convective heat transfer from tube bank under constant wall temperature conditions in cross flow using Al_2O_3 nanofluid. Vajjha et al. [161] carried out a numerical analysis of fluid dynamic and heat transfer performance of ethylene glycol/water-based Al_2O_3 and CuO nanofluids in the flat tubes of a radiator.

For obtaining Nusselt number and heat transfer coefficient as indicators of heat transfer enhancement in some simple problems such as natural convection in enclosures where the walls have either constant temperature or adiabatic conditions, Abouali and Ahmadi [162] showed that there is no need to solve transport equations where the nanofluid is assumed as single-phase and homogenous. In such cases the heat transfer enhancement can be estimated simply just by calculating the ratio of nanofluid thermophysical properties to base fluid properties [162]:

$$\frac{Nu_{nf}}{Nu_f} = \left(\frac{k_{nf}}{k_f}\right)^{-m} \left(\frac{\mu_{nf}}{\mu_f}\right)^{-m} \left(\frac{c_{p,nf}}{c_{p,f}}\right)^{m} \left(\frac{\beta_{nf}}{\beta_f}\right)^{m} \left(\frac{\rho_{nf}}{\rho_f}\right)^{2m} \tag{126}$$

$$\frac{h_{nf}}{h_f} = \left(\frac{k_{nf}}{k_f}\right)^{1-m} \left(\frac{\mu_{nf}}{\mu_f}\right)^{-m} \left(\frac{c_{p,nf}}{c_{p,f}}\right)^{m} \left(\frac{\beta_{nf}}{\beta_f}\right)^{m} \left(\frac{\rho_{nf}}{\rho_f}\right)^{2m} \tag{127}$$

where the value of *m* depends on the geometry and boundary conditions of the problem. Standard correlations are then used to determine the Nusselt number and heat transfer coefficient of the base fluid. In this way, the computational time reduces significantly.

Figure 19 shows the schematic of different enclosures in which heat transfer enhancement due to natural convection of a homogenous nanofluid was estimated by using Eqs. (126) and (127), and the results were in good agreement with CFD simulation results [162].

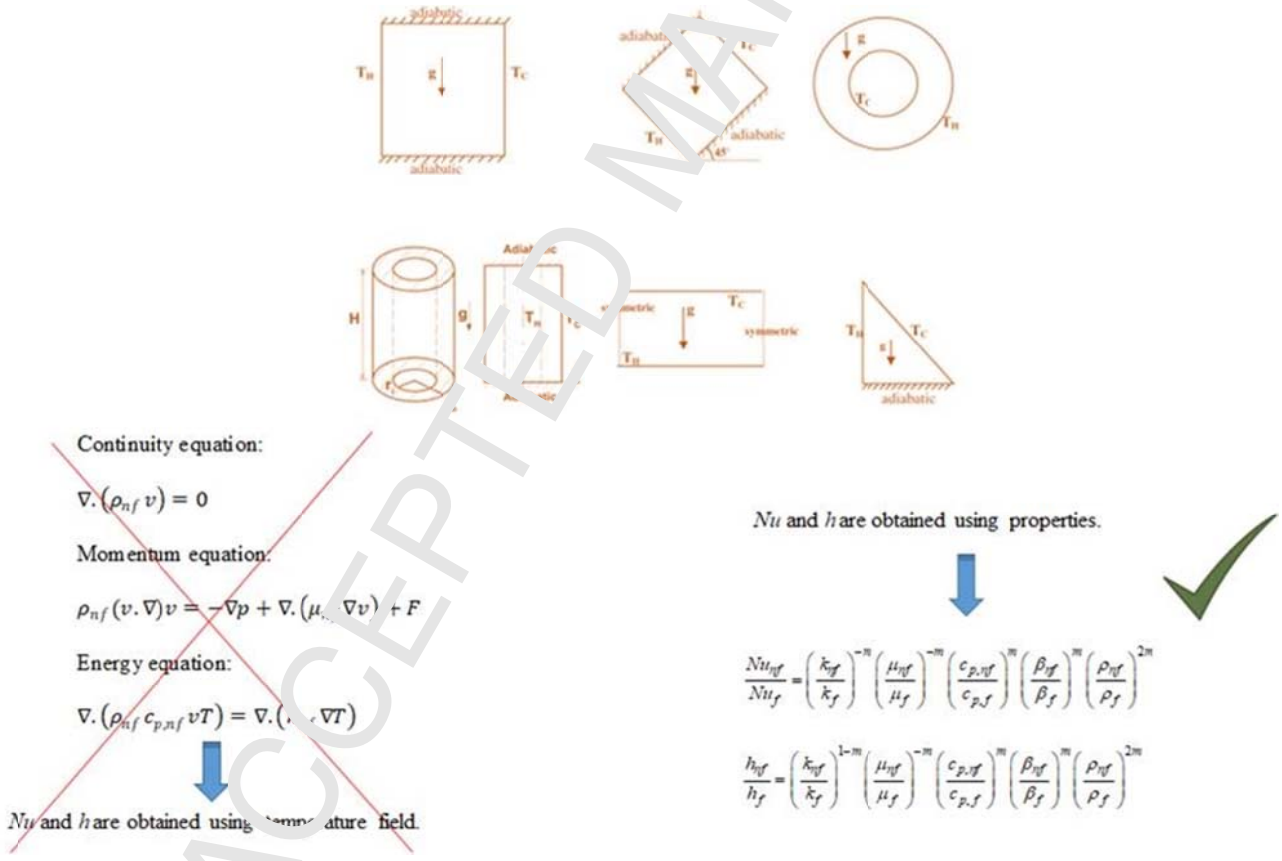

Figure 19. In simple problems, when the nanofluid is assumed as single-phase homogenous, the heat transfer enhancement can be estimated simply by calculating the properties [162] .

4.3.2. Thermal dispersion model

The thermal dispersion model was studied by Xuan and Roetzel [163] by modifying the homogenous single-phase model. Random and irregular motion of nanoparticles raises the energy exchange rate in the nanofluid and induces small perturbations in both velocity and temperature. The intrinsic phase averages are defined in analogy with turbulence, and are given as:

$$\boldsymbol{V} = \overline{\boldsymbol{V}} + \boldsymbol{V}' \tag{128}$$

$$T = \overline{T} + T' \tag{129}$$

where $\boldsymbol{V}'$and T' stand for fluctuations in velocity and temperature due to nanoparticle chaotic movement and mean values are given by $\overline{\boldsymbol{V}} = \frac{1}{\forall_f}\int_{\forall_f} \boldsymbol{V} d\forall$ and $\overline{T} = \frac{1}{\forall_f}\int_{\forall_f} T d\forall$ where $\forall$ is volume of the working fluid. By neglecting the boundary surface between the fluid and the nanoparticles, the energy equation is written as:

$$\nabla \cdot (\rho_{nf} c_{p,nf} \overline{\mathbf{V}}\overline{T}) = \nabla \cdot (k_{nf} \nabla \overline{T}) - \nabla \cdot (\rho_{nf} c_{p,nf} \overline{\mathbf{V}'T'}) \tag{130}$$

The second term on the right side of the above equation demonstrates the perturbation effect of temperature and velocity in enhancing the heat flux in the energy equation. The heat flux generated by the thermal dispersion in the nanofluid flow is computed as follows:

$$q_d = \rho_{nf} c_{p,nf} \overline{\mathbf{V}'T'} = -k_d \nabla \overline{T} \tag{131}$$

where k_d is the dispersion thermal conductivity. The energy equation can be rewritten as:

$$\nabla \cdot (\rho_{nf} c_{p,nf} \overline{\mathbf{V}}\overline{T}) = \nabla \cdot [(k_{nf} + k_d) \nabla \overline{T}] \tag{132}$$

In fact, k_d reveals the thermal dispersion contribution to thermal conductivity enhancement.

Xuan and Roetzel [163] proposed the following model based on a porous media formulation for estimation of dispersion thermal conductivity in nanofluids:

$$k_d = C^* \left(\rho c_p\right)_{nf} VR \tag{133}$$

where R is the radius of a tube in which the nanofluid flows and C^* is a constant that can be obtained by matching the experimental results.

Khanafer et al. [79] suggested the following relation for estimating the dispersion thermal conductivity:

$$k_d = C\left(\rho c_p\right)_{nf} |V| d_p \phi \tag{134}$$

In the above equation, the effects of particle size and nanoparticle volume fraction have been included. Mojarrad et al. [164] proposed a new correlation for determination of dispersion thermal conductivity by investigating the heat transfer performance of Al_2O_3/water nanofluid in a circular tube as follows:

$$k_d = c\left(\rho c_p\right)_{nf} \frac{R\phi}{d_p}\left(\frac{\partial T}{\partial r}\right) \tag{135}$$

Although in the above equation, there is no velocity term "V", its effect has been considered indirectly by involving a temperature gradient in the relation. It should be noted that sides in Eq. (135) are not compatible dimensionally.

A more accurate correlation for the dispersion thermal conductivity in radial direction was presented by Bahiraei and Hosseinalipour [165] as:

$$k_d = c\left(\rho c_p\right)_{nf} \left(\frac{\partial v_x}{\partial r}\right) \phi(r) R d_p \tag{136}$$

In the above relation, which is presented for fully developed flow in a horizontal tube, the nanoparticle distribution has been considered as a function of radius within the tube. The approach for obtaining $\phi(r)$ is not presented here, but the readers can refer to Refs.[165–167] which discuss particle distribution in the tube due to migration. Effective parameters that can be considered for migration are Brownian motion, non-uniform shear rate, viscosity gradient, and thermophoresis.

Several researchers employed the single-phase thermal dispersion model to simulate nanofluid flow and heat transfer. Kumar et al. [168] carried out an analysis of flow and thermal field in Cu/water nanofluid in a thermally driven two-dimensional cavity using a single-phase thermal dispersion model. Özerinç et al. [169] considered homogenous model to simulate the Al_2O_3/water nanofluid inside a tube with various boundary conditions. They found that the estimated values of heat transfer rate with this numerical method are lower than experiments. Therefore, the thermal dispersion model was also examined and good agreement with the experimental data was achieved. Heris et al. [170] showed the high ability of thermal dispersion model to predict the heat transfer rate due to nanofluids flow in circular tubes by comparing the simulation results against tests data. Ameri et al. [171] investigated the capacity of nanofluids for heat transfer enhancement in a metal foam tube where dispersion model was used in the modeling. In this article, the distribution of nanoparticles was assumed to be non-

uniform. In another research, Bahiraei and Vasefi [172] simulated laminar flow of different nanofluids in a horizontal tube using both the homogenous and thermal dispersion models where non-uniform distribution of nanoparticles was included in the dispersion model. They found that with an increase in Re and particle loading, the thermal dispersion model is more suitable than homogenous technique for predicting experimental outcomes. Bahiraei and Hosseinalipour [173] utilized the thermal dispersion model for simulation of convective heat transfer of TiO_2/water nanofluid flow in a circular tube using non-uniform concentration distribution. In another study, Bahiraei and Hosseinalipour [165] compared the efficacy of thermal dispersion (non-uniform concentration distribution) and Euler-Lagrange approaches to predict the heat transfer rate inside a circular tube with alumina/water nanofluid flow. The results revealed that in terms of both computational accuracy and time of calculation, employing the thermal dispersion model is affordable. Akbaridoust et al. [174] investigated nanofluid flow in helically coiled tubes using both the homogenous and thermal dispersion models. The results revealed higher accuracy of thermal dispersion model compared to homogenous model.

4.3.3. Buongiorno model

In 2006, Buongiorno [21] proposed a model to improve the homogenous single phase and thermal dispersion models. Buongiorno studied the effect of seven slip mechanisms including: 1- the inertia, 2- Brownian diffusion, 3- thermophoresis, 4- diffusiophoresis, 5- Magnus effect, 6- fluid drainage, and 7- gravity and concluded that Brownian diffusion and thermophoresis are the most important slip mechanisms in nanofluids, in agreement with our arguments in Section 2 of this article. In this model, the effect of the base fluid and the nanoparticle relative velocity is described more mechanistically than in the thermal dispersion model. Based on the findings of Buongiorno [21], a two-component four-equation nonhomogeneous equilibrium model for transport equations in nanofluids was developed. By taking into account Brownian and the thermophoresis effects, the transport equations in the homogenous model are converted to:

Continuity equation:

$$\nabla \cdot (\rho_{nf} \mathbf{V}) = 0 \tag{137}$$

Momentum equation:

$$\rho_{nf} (\mathbf{V} \cdot \nabla) \mathbf{V} = -\nabla p + \nabla \cdot [\mu_{nf} (\nabla \mathbf{V} + \nabla \mathbf{V}^T)] \tag{138}$$

Energy equation:

$$\nabla\cdot\left(\rho_{nf}c_{p,nf}\boldsymbol{V}T\right)=\nabla\cdot\left(k_{nf}\nabla T\right)+\left(\rho c_p\right)_p\left[D_B\nabla\phi\cdot\nabla T+D_T\frac{\nabla T\cdot\nabla T}{T}\right] \tag{139}$$

Conservation equation for the nanoparticles:

$$\mathbf{V}\cdot\nabla\phi=\nabla\cdot\left[D_B\nabla\phi+D_T\nabla T/T\right] \tag{140}$$

In Eq. (139) Brownian diffusion and thermophoresis (or thermal diffusion coefficient) can be expressed respectively as:

$$D_B=\frac{k_BT}{3\pi\mu_{nf}d_p} \tag{141}$$

$$D_T=0.26\frac{k_{nf}}{2k_{nf}+k_p}\frac{\mu_{nf}}{\rho_{nf}}\phi \tag{142}$$

where k_B is the Boltzmann constant.

Several studies have been conducted regarding the analysis of convection heat transfer of nanofluids based on Buongiorno's model. Sheikholeslami et al. [175] studied heat and mass transfer characteristic of unsteady nanofluid flow between parallel plates under the effect of a magnetic field using Buongiorno model. Sheikholeslami and Rokni [176] applied the Buongiorno model for evaluation of nanofluid flow and radiation and melting heat transfer over a stretching plate in the presence of a magnetic field. Garoosi et al. [177] carried out a numerical simulation of natural convection of water-based Cu, Al_2O_3, and TiO_2 nanofluid in a 2D cavity having several pairs of heater and coolers by Buongiorno approach. In other studies, Garoosi et al. [177,178] analyzed natural convection and mixed convection of Al_2O_3/water nanofluid in a square cavity using Buongiorno model. Malvandi et al. [179] studied the fully-developed mixed convective through an annulus with vertical position. The employed approach for the modelling of nanofluid included the modified two-component four-equation non-homogeneous equilibrium model. Moreover, Malvandi and Ganji [180] evaluated the mixed convective heat transfer of alumina/water nanofluid inside a vertical microchannel and modified Buongiorno's model was employed which fully accounted for the effect of the nanoparticle migration. Shehzad et al. [181] carried out the study of convective heat transfer of nanofluid in a wavy channel and the mathematical formulation was processed utilizing the Buongiorno's model. Sheremet and Pop [182] investigated the steady-state natural convection in a square porous enclosure filled by a nanofluid using Buongiorno model considering the Brownian diffusion and thermophoresis effects.

4.4. Two-phase approaches

Nanofluids act like two-phase fluids. In the two-phase approaches, the base liquid and nanoparticles are modeled as two individual phases with different velocities and possible different temperatures, such that the particles may move relative to the base fluid (the relative velocity of particles through a fluid is called the particle slip velocity, although it is not related to the no-slip boundary condition). Although the two-phase approaches may get more realistic results by considering the movement between the fluid and nanoparticles, but they require longer simulation times for simulation and the models are more complex. The two-phase approaches are categorized in two general groups, known as Eulerian-Eulerian and Eulerian-Lagrangian models. In the Eulerian-Eulerian approach, both the base fluid and the nanoparticles phases are considered as interacting continua. On the other hand, in the Eulerian-Lagrangian approach, the base fluid is considered to be a continuum while the nanoparticles are considered as a discrete phase. (Eulerian-Lagrangian approach sometimes also called discrete-phase approach). In the Eulerian-Lagrangian approach, the path of nanoparticles is determined [183]. Figure 20 illustrates the concept of Eulerian-Eulerian and Eulerian-Lagrangian approaches, where blue arrows indicates the fluid path and red arrow show the particle path. For a given problem, the Eulerian-Lagrangian generally takes a longer time to perform the computation than the Eulerian-Eulerian approach, but the Eulerian-Lagrangian results are more accurate and the model can be used for a much broader range of problems.

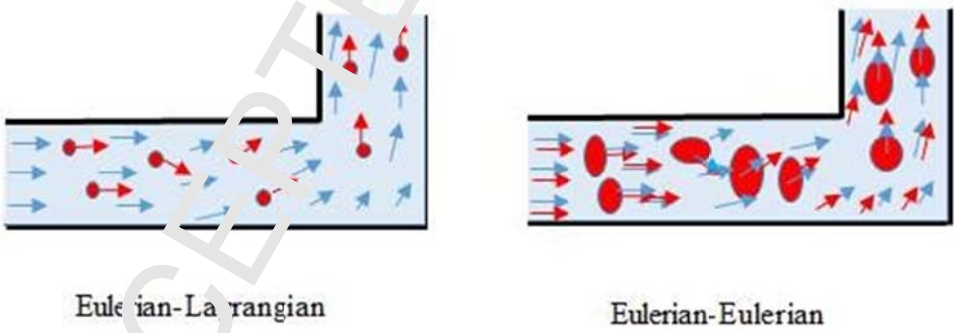

Figure 20. Concept of Eulerian-Lagrangian and Eulerian-Eulerian approaches, blue arrow indicates fluid path and red arrow shows particle path.

4.4.1. Eulerian-Eulerian

Eulerian–Eulerian models (e.g. two-phase approaches) cannot be assigned for tracking the trajectory of suspended particles in fluid [184]. These models can be categorized as (i) volume of fluid (VOF), (ii) mixture, and (iii) Eulerian models. Among them, mixture model is most popular as will be discussed.

4.4.1.1. Volume of fluid (VOF) model

The VOF model is applicable for multiphase immiscible fluid regimes in which the interface between fluid phases should be tracked. Some applications of this model are simulation of bubble growth, free surface flows, stratified flows and liquid-gas surface tracking problems. This model is not most convenient for application to nanofluid flows, since nanoparticles are typically much smaller than the computational cell and are dispersed in the base fluid. Therefore, for nanofluid-flow simulations (typically assuming well-mixed nanoparticle-dispersion) employing the VOF method would be inappropriate, compared to the faster/cheaper Euler-Euler approach (provided that the nanoparticles are <100nm). However, in cases of nanoparticle-stream injection into a moving fluid, VOF approach would be the way to simulate the two-fluid mixing process. Nevertheless, some authors used the VOF for nanofluid flow simulations and therefore it is included here for completeness.

The VOF model has been used to track the nanoparticle concentration by solving the continuity equation for the base fluid over the domain of study using a single set of Navier-Stokes equations for the base liquid and particle phases to determine the values of velocity shared by the two phases. Similarly, a shared temperature is obtained from a single energy equation [185].

The continuity equation can be expressed as:

$$\nabla \cdot (\phi_q \rho_q \mathbf{V}_q) = 0 \tag{143}$$

where q indicates the phase. For example, q is equal to 1 for the base fluid and 2 for the nanoparticles. The summation of the volume fractions of phases is one, or $\sum_{q=1}^{n} \phi_q = 1$.

The momentum and energy equations are identical to the momentum and energy equations for the single-phase homogenous model.

Naphon and Nakharintr [186] considered the flow and heat transfer of TiO_2 nanofluid through mini-channel heat sinks. The model predictions compared well with experimental results, indicating the effectiveness of the VOF model. Akbari et al. [185] compared the accuracy of single-phase and the three Eulerian-Eulerian models in the estimation of experimental data for combined convection and

laminar flow. First, they pointed out that the three two-phase models provide similar predictions of experimental data and are more accurate than single-phase. Second, among two-phase models, VOF was suggested since it needed the lowest computational time.

Rashidi et al. [187] compared two-phase and single-phase approaches for the Cu/water nanofluid flow in a channel with wavy walls. The single-phase model and three different two-phase model predictions (VOF, mixture, and Eulerian) were studied, and their results were compared. Davarnejad and Jamshidzadeh [188] analyzed turbulent heat transfer behavior of the MgO/water nanofluid in a circular tube using three individual models including single phase, VOF and mixture. It was concluded that the VOF model and the mixture model were more accurate than the single-phase model for heat transfer prediction.

4.4.1.2. Mixture model

The mixture model can be implemented for flows with two or more phases, considering n as the number of phases. In this model it is assumed that each phase has different velocity and concentration fields. The mixture model accounts for the coupling between fluid phases and is applicable for dispersed particulate fluids with low interphase coupling, low concentration bubbly flows and separators. Hence, this model has been employed for nanofluid flows when a nanoparticle phase exists and nanoparticles closely track the fluid flow. The base fluid influences the nanoparticles via drag and turbulence, while the nanoparticles affect the base fluid via reduction in mean momentum and enhanced turbulence dissipation. Also, it should be noted that the model requires less run time and CPU usage than some competing models and it sounds precise for a large group of multi-phase flow problems [26]. The mixture model, in contrast to the VOF model, can model the interpenetrating phases and allows the phases to have different velocities. As can be seen in the following equations, the mass conservation and energy equations of the mixture model are similar to those of the single-phase model. However, the momentum equation in the mixture model has an additional term to take into account the relative velocity (also known as drift velocity) between the phases. In addition, the volume fraction equation is also solved for the secondary phases:

Continuity equation.

$$\nabla\cdot(\rho_m \mathbf{V}_m)=0 \tag{144}$$

Momentum equation:

$$\rho_m(\mathbf{V}_m\cdot\nabla)\mathbf{V}_m=-\nabla p+\nabla\cdot[\mu_m(\nabla\mathbf{V}_m+\nabla\mathbf{V}_m^T)]+\nabla\cdot\left(\sum_{k=1}^{n}\phi_k\rho_k\mathbf{V}_{dr,k}\mathbf{V}_{dr,k}\right)+F \tag{145}$$

Energy equation:

$$\nabla\cdot\sum_{k=1}^{n}(\phi_k\rho_k c_{p,k}\mathbf{V}_k T_k)=\nabla\cdot(\sum_{k=1}^{n}k_{eff}\nabla T_k) \tag{146}$$

Volume fraction equation for a secondary phase p:

$$\nabla\cdot(\phi_p\rho_p\mathbf{V}_m)=-\nabla\cdot\left(\phi_p\rho_p\mathbf{V}_{dr,p}\right) \tag{147}$$

where $\mathbf{V}_{dr,k}$ is the drift velocity of phase k, which is defined as $\mathbf{V}_{dr,k}=\mathbf{V}_k-\mathbf{V}_m$. The mixture velocity $V_m$is given by:

$$\boldsymbol{V}_m=\frac{\sum_{k=1}^{n}\phi_k\rho_k\boldsymbol{V}_k}{\rho_m} \tag{148}$$

The other mixture properties such as ρ_m, μ_m and k_{eff} could be evaluated using the common single-phase correlations. The following relations could provide appropriate estimations, as well:

$$\rho_m=\sum_{k=1}^{n}\phi_k\rho_k \tag{149}$$

$$\mu_m=\sum_{k=1}^{n}\phi_k\mu_k \tag{150}$$

$$k_{eff}=\sum_{k=1}^{n}\phi_k(k_k+k_t) \tag{151}$$

where k_t represents the turbulent thermal conductivity.

The above mentioned equations are not closed and another equation is required to find the drift velocity:

$$\boldsymbol{V}_{dr,p}=\boldsymbol{V}_{pq}-\sum_{k=1}^{n}\frac{\phi_k\rho_k}{\rho_m}\boldsymbol{V}_{qk} \tag{152}$$

where $\boldsymbol{V}_{pq}$ is the slip velocity between the secondary phase p and the primary phase q, and for laminar flow can be modeled using the correlation proposed by Manninen et al.[189]:

$$\boldsymbol{V}_{pq}=\boldsymbol{V}_p-\boldsymbol{V}_q=\frac{\tau_p}{f_{drag}}\frac{(\rho_p-\rho_m)}{\rho_p}\boldsymbol{a} \tag{153}$$

In the above equation, τ_p, $\boldsymbol{a}$ and f_{drag} are the particle relaxation time, acceleration vector and drag function, respectively. τ_p and $\boldsymbol{a}$ are defined by:

$$\tau_p = \frac{\rho_p d_p^2}{18\mu_q} \tag{154}$$

$$\boldsymbol{a} = \boldsymbol{g} - (\boldsymbol{V}_m \cdot \nabla)\boldsymbol{V}_m \tag{155}$$

Schiller and Naumann [190] suggested the following relation for f_{drag}:

$$f_{drag} = \begin{cases} 1 + 0.15\, Re^{0.687} & Re \leq 1000 \\ 0.0183\, Re & Re > 1000 \end{cases} \tag{156}$$

Other scientists have also suggested some correlations to account f_{drag}, and among them the work done by Morsi and Alexander [191] can be mentioned.

Most of the numerical nanofluid studies in the literature have employed the mixture model because it is relatively accurate and requires less computational power than many other methods. Labib et al. [192] studied the convective heat transfer coefficient of Al_2O_3/water-ethylene glycol and Al_2O_3-CNTs/water nanofluids flowing in horizontal circular tube using the mixture model. Safikhani et al. [193] used the mixture model to calculate the heat transfer coefficient and pressure drop of Al_2O_3/water nanofluid flow in horizontal flat tubes. The same configuration has been examined for water-based Al_2O_3 and Al_2O_3–Cu hybrid nanofluids by Moghadassi et al. [194]. Mirmasoumi and Behzadmehr [195] evaluated laminar flow (mixed convection) of a nanofluid composed of water and Al_2O_3 nanoparticles flowing in a tube using two-phase mixture model. A two-phase mixture model was employed by Goodarzi et al. [196] to investigate mixed convection of Cu/water nanofluids in a rectangular shallow enclosure. Siavashi and Jamali [197] analyzed entropy generation due to turbulent flow of TiO_2/water dispersions in an annulus by using two-phase mixture model. In another study on the application of two-phase mixture models, Siavashi et al., in three different works [198–200], investigated nanofluid flow inside a porous tube and annulus [198]. Toosi and Siavashi [201] employed the two-phase mixture model for numerical simulation of Cu-water nanofluid flow inside a partially porous cavity. Yaghoubi Emami et al.[202] used the mixture model to simulate two-phase Cu-water nanofluid flow inside an inclined cavity with different hot wall configurations. Siavashi et al. [203] used the same model to solve Cu-water nanofluid natural convection inside an enclosure using porous fins. Later, Siavashi and Rostami [204] employed a two-phase mixture model to model non-Newtonian nanofluid in a porous annulus and presented the mixture equations in the non-dimensional

form. Moraveji and Ardehali [205] performed CFD modeling of laminar forced convection on Al_2O_3 nanofluid in minichannel heat sink by four individual models of single phase, VOF, mixture, Eulerian. It was concluded that the best approach for modeling was the mixture model, considering both accuracy and computational speed. Shariat et al. [206] evaluated the particle size impact on laminar mixed convection of Al_2O_3/water nanofluids in a duct with elliptic cross section employing the two phase mixture model. Recently, Maghsoudi and Siavashi [207] employed a two-phase mixture model for simulating mixed convection of nanofluid flow in a porous lid-driven cavity to find the optimal pore size configuration.

4.4.1.3. Eulerian model

The Eulerian approach is the most complex multi-phase model due to the strong coupling between the phases. The Eulerian model supports volume fraction values ranging from dilute to dense, and can also be used with low to high values of particulate mass loading. In the Eulerian model, the transport equations are solved independently for each phase, which is the primary difference between the Eulerian approach and the mixture model[208]. The pressure and interphase exchange coefficients are utilized for coupling of the equations, depending on the type of fluid phases (such as fluid-fluid or fluid-solid). This model is appropriate for simulation of bubbly flows, fluidized beds and particulate flows, and can also be implemented for nanofluid flow simulation.

Ignoring the interphase mass transfer, the governing equations of a particulate laminar flow (fluid-solid) for the Eulerian model is presented as follows.

The continuity equation for phase q can be expressed as:

$$\nabla\cdot(\phi_q\rho_q\mathbf{V}_q)=0 \tag{157}$$

Obviously, the summation of volume fraction of all the n phases is $\sum_{q=1}^{n}\phi_q=1$.

The momentum equation is given by:

$$\rho_q\phi_q(\mathbf{V}_q\cdot\nabla)\mathbf{V}_q=-\phi_q\nabla p+\nabla\cdot[\mu_q\phi_q(\nabla\mathbf{V}_q+\nabla\mathbf{V}_q^T)]+\sum_{p=1}^{n}R_{pq}+(F+F_L+F_{wl}+F_A)_q \tag{158}$$

where $\boldsymbol{R}_{pq}$ is the interaction force between the fluid phase q and the particulate phase p, $\boldsymbol{F}$, $\boldsymbol{F}_L$, $\boldsymbol{F}_{wl}$ and $\boldsymbol{F}_A$ are body, lift, wall lubrication and virtual mass forces, respectively. It should be noted other forces may be putted in the above equation as explained in section 2. The interaction force $\boldsymbol{R}_{pq}$ is calculated by:

$$\boldsymbol{R}_{pq} = \sum_{p=1}^{n} K_{pq}\left(\boldsymbol{V}_p - \boldsymbol{V}_q\right) \tag{159}$$

in which, K_{pq} is the interphase momentum exchange coefficient.

For a nanofluid flow, K_{pq} should be defined according to the relation proposed by Wen and Yu [209] for dilute fluid-solid flows.

$$K_{pq} = \frac{3}{4} C_d \frac{\phi_p \phi_q \rho_q \left|\boldsymbol{V}_p - \boldsymbol{V}_q\right|}{d_p} \phi_q^{-265} \tag{160}$$

The drag coefficient, C_d, is given by:

$$C_D = \frac{24\left(1 + 0.15\left(\phi_q Re_p\right)^{0.678}\right)}{\phi_q Re_p} \tag{161}$$

where $Re_p = \rho_q d_p \left|\boldsymbol{V}_p - \boldsymbol{V}_q\right| / \mu_q$.

The lift force, $\boldsymbol{F}_L$, acting on the particles is caused by the velocity gradient inside the primary phase q, and for nanofluids with nano-scale particles is not significant. The wall lubricant force, $\boldsymbol{F}_{wl}$, is a force acting on the secondary phase p and takes it away from the wall. This force is important in gas-liquid flows and has negligible effect on nanofluid flows. The virtual mass force, $\boldsymbol{F}_A$, should be included when the particulate phase p accelerates with respect to the fluid phase q. This force should not be respected for steady flows or nanofluid flows since the nanoparticle density is much greater than the base fluid density [210].

The energy equation is given by:

$$\nabla \cdot \left(\phi_q \rho_q c_{p,q} \mathbf{V}_q T_q\right) = \nabla \cdot \left(k_q \nabla T_q\right) - \left[\mu_q \phi_q \left(\nabla \mathbf{V}_q + \nabla \mathbf{V}_q^T\right)\right] : \nabla \mathbf{V}_q + \sum_{p=1}^{n} Q_{pq} \tag{162}$$

where $Q_{pq} = h_{pq}\left(T_p - T_q\right)$ is the interphase heat exchange coefficient. h_{pq} is the heat transfer coefficeint between phases and can be specified as a constant value or be defined as a function of Nusselt number, $h_{pq} = \left(6k_q \phi_q \phi_p Nu_p\right)/d_p^2$. Nu_p can also be calculated from the Ranz and Marshall [211] model as:

$$Nu_p = 2 + 0.6 {Re_p}^{0.5} Pr^{0.333} \tag{163}$$

Pr is the Prandtl number of phase q and is given by:

$$Pr = \frac{c_{p,q}\mu_q}{k_q} \quad (164)$$

As can be seen in the above mentioned equations, the Eulerian model considers different temperatures for the particulate and fluid phases. Concerning nanofluid flows, nanoparticles have very small size and could be considered to be in local thermal equilibrium with the base fluid. Hence, the solution of an additional energy equation for nanoparticles is not beneficial and does not improve the simulation accuracy. Anyway, the Eulerian method has been used in a few investigations of nanofluid flows. Kalteh et al. [210] studied the prediction of Cu/water nanofluid flow in an isothermally heated microchannel using the Eulerian approach. Using the same approach, Bag et al. [212] studied the flow and heat transfer of bio-nanofluid in circular channel. Predictions showed that the difference between results of Eulerian approach and experiments was only 7% while it was 35% for single phase model. Lotfi et al. [213] examined alumina nanofluid flow with forced convection in horizontal conduits employing two-phase Eulerian model. It was shown that both single-phase and the Eulerian models underestimate the Nu number. Hejazian et al. [214] performed a comparative study of Euler and mixture models for nanofluid turbulent flow inside a horizontal conduit. They found that the two models almost showed the same results. Sabaghan et al. [215] employed Eulerian two-phase model for the simulation of TiO_2 nanofluid flow in microchannels with six longitudinal vortex generators. Ebrahimnia-Bajestan et al.[216] analyzed the heat transfer characteristics of water-based TiO_2 nanofluid for application in solar heat exchangers using single-phase, Eulerian-Eulerian, and mixture models. They revealed that Eulerian model is not able to predict the experimental data accurately, so they modified the common mixture model. Behroyan et al. [217] compared the predictions of numerical models to evaluate turbulent flow(gravity influence was neglected) of Cu/water nanofluid in a pipe under fixed value of heat flux and illustrated that the Eulerian model gives inaccurate results.

4.4.2. Eulerian-Lagrangian

In the Eulerian–Lagrangian model, the fluid phase is considered as a continuum medium by solving the momentum equations and the particle phase is modeled by solving for individual particle motion using the particle motion theory in the Lagrangian reference frame [208]. The influence of particles in the fluid is introduced as source terms in the momentum and energy equations. The dispersed phase can exchange momentum, mass, and energy with the fluid phase. Our presentation of the Eulerian-Lagrangian method makes the common assumption that the dispersed second phase occupies a small

volume fraction; however, the model can be easily extended to dense flows. A limitation of this model is that it requires high memory and computational time. Not only are the number of nanoparticles very large, but the small value of Stokes number for nanoparticle flows introduces numerical stiffness that necessitates use of small time steps, which is a stability requirement in explicit numerical methods and necessary for accurate computation of particle drift in implicit numerical methods. The governing equations are written for the base liquid as follows.

Continuity equation:

$$\nabla \cdot (\rho_f \mathbf{V}_f) = 0 \tag{165}$$

Momentum equation:

$$\rho_f (\mathbf{V}_f \cdot \nabla)\mathbf{V}_f = -\nabla p + \nabla \cdot [\mu_f (\nabla \mathbf{V}_f + \nabla \mathbf{V}_f^T)] + S_m \tag{166}$$

Energy equation:

$$\nabla \cdot (\rho_f c_{p,f} \mathbf{V}_f T_f) = \nabla \cdot (k_f \nabla T_f) + S_e \tag{167}$$

where $\boldsymbol{S}_m$ is the momentum source term vector which represents the momentum transfer between fluid and particles, and S_e is the energy source term which gives the energy transfer between fluid and particles. These source terms can be computed by averaging over a grid cell as

$$\boldsymbol{S}_m = \frac{1}{\delta V} \sum_{p=1}^{n_p} m_p \boldsymbol{F_p} \tag{168}$$

$$S_e = \frac{1}{\delta V} \sum_{p}^{n_p} m_p c_{p,p} \frac{dT_p}{dt} \tag{169}$$

where the subscript p refers to particle, m_p and $\boldsymbol{F_p}$ respectively denote mass of the particle and the total force per unit mass of the particle acting on the fluid, δV represents the grid cell volume and n_p is the number of solid particles within a cell volume. The particle force on the fluid (i.e. F) in Eq. (168) is the negative of the sum of the various hydrodynamic forces acting on the particle, including Brownian motion, drag, Saffman and Magnus lift, pressure gradient force, thermophoretic force, and virtual mass force, which were discussed in Section 2.

The energy equation for the particle can be written as

$$m_p c_{p,p} \frac{dT_p}{dt} = Nu_p \pi d_p k_f (T_f - T_p) \tag{170}$$

where the Nusselt number Nu_p for heat transfer to the particle was evaluated using the Ranz and Marshall correlation presented in Eq. (163).

Particle trajectory motion equation could also be written as follows to find the particle position:

$$m_p \frac{d\boldsymbol{V}_p}{dt} = \boldsymbol{F}_p \tag{171}$$

A large number of research studies have been conducted to simulate nanofluid flow and heat transfer using the Eulerian-Lagrangian approach. Due to the limitation on the number of particles that can be handled, this method is particularly well suited for modeling the micromechanics of a nanofluid flow field for problems on a scale of up to about one million particles.

Rashidi et al. [218] employed Eulerian- Lagrangian approach (two- way coupling) to simulate fluid flow and heat transfer inside a channel equipped with two square blocks where the working fluid was a mixture of water and alumina particles (sizes between 30 nm and 0.5 μm and a concentration of 1%). They used ANSYS-Fluent software to solve the problem. Figure 21 displays the algorithm for the CFD simulation of the mixture fluid flow in the channel using Eulerian-Lagrangian approach.

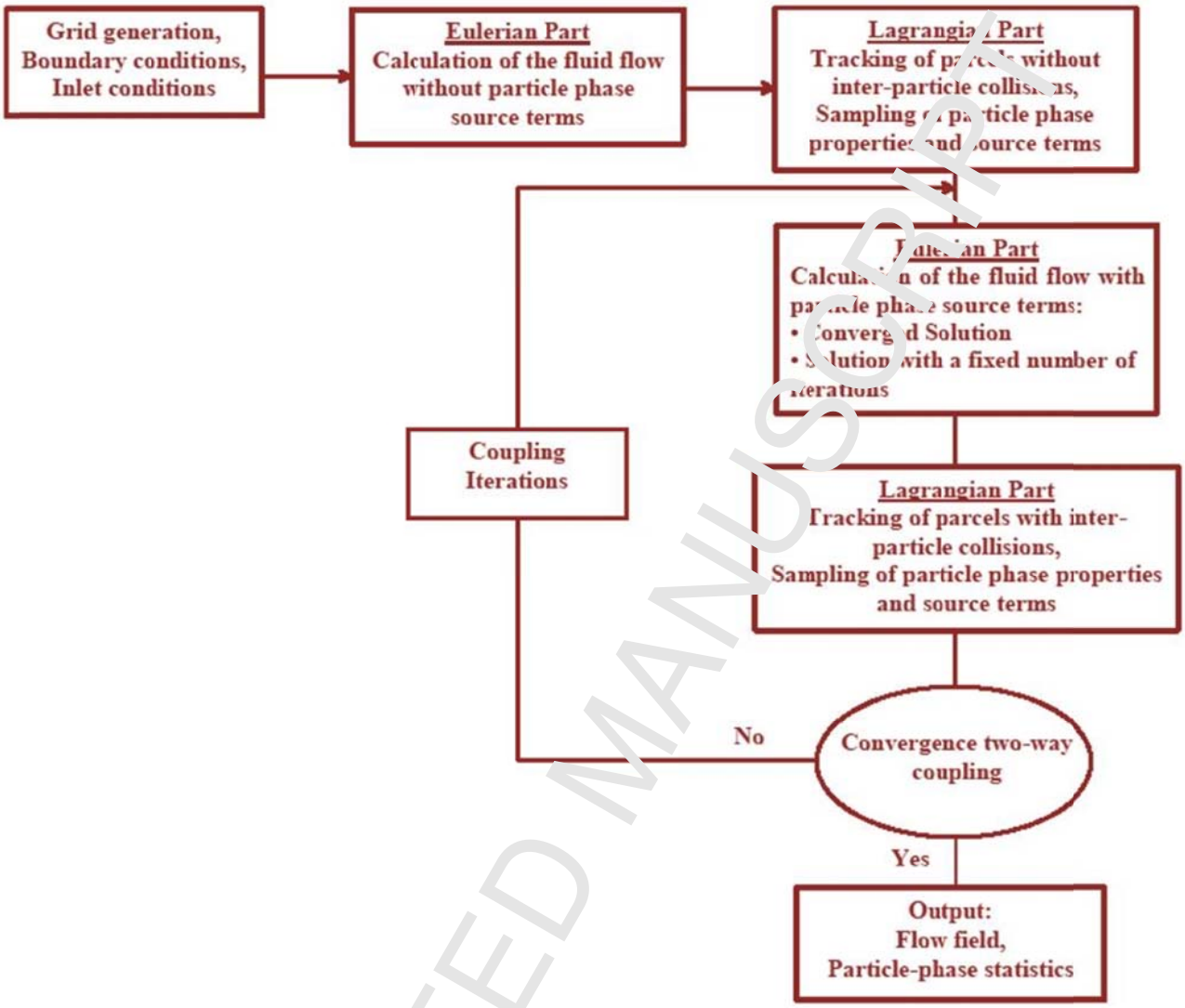

Figure 21. Numerical procedure to solve mixture flow using Eulerian-Lagrangian approach [218].

He et al. [219] studied TiO_2 nanofluid flow(laminar regime) through a tube using both the single phase method and the Eulerian-Lagrangian method. The numerical results were compared with experimental data and reasonably good agreement was achieved. Bianco et al. [220] used the same model to study the laminar forced convection of Al_2O_3 nanofluid in a tube and mentioned that there is a difference of 11% comparing the heat transfer coefficient resulting of the Eulerian–Lagrangian model and that of the single phase model. Bahiraei [221] used two-phase Eulerian-Lagrangian method to evaluate the effects of adding CuO nanoparticles to pure water on the rate of heat transfer in a straight tube. It was found that the Euler-Lagrange method gives more accurate predictions of heat transfer rate compared to the single-phase homogenous approach. In another study, Bahiraei [222] focused on particle

migration effects on heat transfer rate through simulations done by Eulerian–Lagrangian simulation. By employing the Eulerian-Lagrangian approach, Kumar and Puranik [223] simulated forced convection heat transfer of Al_2O_3, TiO_2 and Cu nanoparticles dispersed in water under fully-developed turbulent flow in a circular tube where its surface was heated uniformly. Their results were also compared with the single phase model. The comparison indicated that the Eulerian-Lagrangian approach was more precise. Bahiraei et al. [224] assessed the hydrothermal characteristics of Mn-Zn ferrite nanofluid under a magnetic field using the Eulerian-Lagrangian method. Ghasemi et al. [225] evaluated the laminar forced convection heat transfer of the water-based nanofluid inside a minichannel heat sink using the Eulerian–Eulerian two-phase model. Their simulation results were in excellent agreement with the experimental data and the maximum deviation from experimental data was 5%. Sonawane et al. [226] employed Eulerian–Lagrangian model to study turbulent forced convection flow using nanofluids at low concentration and its precision was confirmed. Rostami and Abbassi [227] studied conjugate heat transfer of nanofluid in wavy microchannels using Eulerian–Lagrangian approach. The results again showed a good agreement with experimental results.

In earlier studies on the Eulerian-Lagrangian approach for nanofluid flow and heat transfer analysis, the boundary conditions for nanoparticle interaction with the wall are not typically discussed. In some cases reflection boundary conditions were assumed, while not explicitly stated. The influence of particle-wall boundary condition on the nanofluid flows was studied by Rashidi et al. [228] and Bovand et al. [229] where both reflection and trapping boundary conditions were used. It was shown that the particle-wall boundary condition significantly affects the near-wall flow behavior of the nanofluids and the nanoparticle concentrations.

4.5. Comparison of different approaches

In the majority of numerical studies on the flow and convective heat transfer of nanofluids, the slip velocity between nanoparticles and the bulk fluid is neglected and accordingly the effective single-phase model is used. However, it is clear that the corresponding results of this model have some errors, such as underestimation of the heat transfer rate, which has been widely reported for studies using the homogeneous model. These errors, of course, can be significantly reduced by employing the temperature-dependent thermophysical properties. Regarding the more advanced models like the two-phase, Buongiorno, and thermal dispersion, the thermal dispersion model is more preferred due to its

lower computational time. However, two-phase models provide most reliable results by considering major influential parameters including thermophoresis, Brownian motion, and slip velocity concepts. Two-phase models comprise of different approaches, including the Eulerian-Eulerian, Eulerian-Lagrangian, mixture, and VOF models. The Eulerian-Lagrangian and mixture models are mostly used in heat transfer studies of nanofluids compared to VOF and Eulerian models, since there are numerous investigations indicating the superiority of these models regarding the provision of more precise results. It should be noted that the CPU and memory requirement is much higher, and consequently the computational time is much longer in the Eulerian-Lagrangian model due to requirement of computing the trajectories of each particle, which affects its range of application for numerical investigations. Due to the complexity of nanofluid flow and heat transfer behavior, there is still a lot to do to reach a final conclusion on the precision of different models for different cases.

Table 3 provides a collection of comparative studies in which the results of different modeling approaches have been compared with experimental data for nanofluid flow in a circular tube under various regimes and boundary conditions.

As can be seen, there are inconsistencies among the results of the researchers and it is not clear at this time which model is the best choice. However, the following notes can be considered when modeling approaches are compared with each other and with experimental data:

- Using temperature-dependent thermophysical relations for properties may increase the accuracy of the homogenous model so that the deviation with experimental data decreases.
- Two-phase models involve more physical phenomena compared to the single-phase homogenous model, so naturally their corresponding results should be closer to experimental data. In some cases that has been reported results of the homogenous model are closer to experimental data; however, we note that both the experimental data and the numerical model are subject to uncertainties of various types. Some factors such as sedimentation of nanoparticles, aggregation of nanoparticles and uncertainties in measurements which are not considered in the mathematical modeling may be the reason for high deviation of two-phase model results from experimental data.

Table 3 Comparison of various nanofluid modeling approaches in a circular tube.

Researcher	Nanofluids	Flow regime	BC	Findings

Kumar and Puranik [223]	Al_2O_3/water TiO_2/water Cu/water	Fully developed turbulent forced convection	Constant wall heat flux	Euler-Lagrange > Homogenous for lower volume fractions (<0.5%) Homogenous > Euler-Lagrange for higher volume fractions (>0.5%)
Moraveji and Esmaeili [230]	Al_2O_3/water	Fully developed laminar forced convection	Constant wall heat flux	Euler-Lagrange > Homogenous
Bianco et al. [220]	Al_2O_3/water	Developing laminar forced convection	Constant wall heat flux	Euler-Lagrange > Homogenous
Moghadassi et al. [194]	Al_2O_3/water Al_2O_3-Cu/water	Fully developed laminar forced convection	Constant wall heat flux	Mixture > Homogenous
Akbari et al. [185]	Al_2O_3/water	Fully developed laminar mixed convection	Constant wall heat flux	-Eulerian, Mixture, VOF > Homogenous -VOF is the best since lowest running expense
Akbari et al. [231]	Al_2O_3/water Cu/water	Fully developed turbulent forced convection	Constant wall heat flux	Homogenous > Eulerian, Mixture, VOF
Albojamal and Vafai [232]	Al_2O_3/water	Developing laminar forced convection	Constant wall heat flux	Homogenous > Euler-Lagrange > Mixture
Bahiraei and Hosseinalipour [165]	Al_2O_3/water	Developing laminar forced convection	Constant wall heat flux	Euler-Lagrange > Dispersion > Homogenous
Bahiraei [233]	CuO/water	Developing laminar forced convection	Constant wall heat flux	Euler-Lagrange > Homogenous
Göktepe et al. [234]	Al_2O_3/water	Developing laminar forced convection	Constant wall heat flux	Eulerian > Mixture > Dispersion > Homogenous
Hejazian and Moraveji [235]	TiO_2/water	Developing turbulent forced convection	Constant wall temperature	Mixture > Homogenous
Hejazian et al. [236]	TiO_2/water	Developing turbulent forced convection	Constant wall heat flux	VOF > Mixture > Homogenous > Eulerian
Haghshenas Fard et al. [237]	Al_2O_3/water Cu/water CuO/water	Developing laminar forced convection	Constant wall temperature	Euler-Lagrange > Homogenous
Lotfi et al. [213]	Al_2O_3/water	Developing turbulent forced convection	Constant wall heat flux	Mixture > Homogenous, Eulerian
Mojarrad et al. [164]	Al_2O_3/water	Developing laminar forced convection	Constant wall temperature	Dispersion > Euler-Lagrange > Mixture > Homogenous

5. Conclusions

It has been more than two decades since the discovery of nanofluids. As a type of colloidal suspension, nanofluids are typically employed as heat transfer fluids due to their higher thermal

conductivity compared conventional liquids. Many numerical studies have been done on nanofluids in recent years. In this paper, a comprehensive review (in two parts) was presented covering the latest developments in modeling of nanofluid flows in different passages and flow regimes, with emphasis on the underlying physical aspects and three dimensional studies. In the first section of Part I, general descriptions of nanofluids, their applications and the research trends in this field were described. In the second section, various forces and physical phenomena in nanofluid flows were reviewed. Next, the main models for properties of nanofluids, including thermal conductivity, viscosity, density, heat capacity, and thermal expansion coefficient, were presented. In the fourth section, physical models that are used for prediction of flow and heat transfer characteristics of nanofluids were reviewed by dividing these models into two general groups: single-phase and two-phase approaches. In the following, the main points of Part I are summarized:

- In nanofluid flow, forces including Brownian motion and thermophoretic force play a primary role in balancing the drag force to determine particle motion and bulk fluid heat transfer rate. Other forces, such as lift and Basset history force, are negligible because of the ultrafine particle sizes.
- Typically the two-phase approaches give results that are generally closer to experimental data than the single-phase model. Uncertainty in the experimental studies, due to phenomena such as sedimentation of nanoparticles, aggregation of particles, and errors in measurements, must also be considered when using such data to evaluate the accuracy of computational models.
- In geometrically simple problems such as natural convection in cavities, instead of employing a single-phase homogenous approach, the heat transfer rate can be estimated easily just by using accurate models for the nanofluid thermophysical properties in the classical correlations.
- Review of the literature suggests that the two-phase mixture model is the easiest approach to apply among two-phase models.
- In a single-phase approach, using novel models for thermophysical properties instead of classic models can reduce errors in predictions of heat and mass flow characteristics.
- Adding nanoparticles and using nanoparticles with a smaller size usually provides higher heat transfer enhancement rates.

In Part II, the primary CFD approaches for solution of the governing equations given in Part I will be investigated. Next, three dimensional studies on modeling of nanofluid flow will be reviewed by

indicating the flow regime and geometry, the nanofluid type, the method of solution, and the physical phenomena responsible for heat transfer enhancement.

Acknowledgment

Omid Mahian and Somchai Wongwises acknowledge the support provided by the "Research Chair Grant" National Science and Technology Development Agency (NSTDA), the Thailand Research Fund (TRF), and King Mongkut's University of Technology Thonburi through the "KMUTT 55th Anniversary Commemorative Fund". Patrice Estellé wishes to acknowledge the King Mongkut's University of Technology Thonburi as well as Professor Wongwises for support during his visit as an invited Professor from the university. R.A.T. would like to acknowledge support financial support from the Australian Research Council in the form of a Discovery Early Career Researcher Award (DE160100131). The authors also would like to thank Professor Lian-Ping Wang from Southern University of Science and Technology, China and Dr. Ehsan Ebrahimnia Bajestan from University of Calgary, Canada for their valuable comments.

Appendix A: Extended form of transport equations

Extended form of governing equations for conventional fluids in different coordinate systems shown in Fig. 1.A.

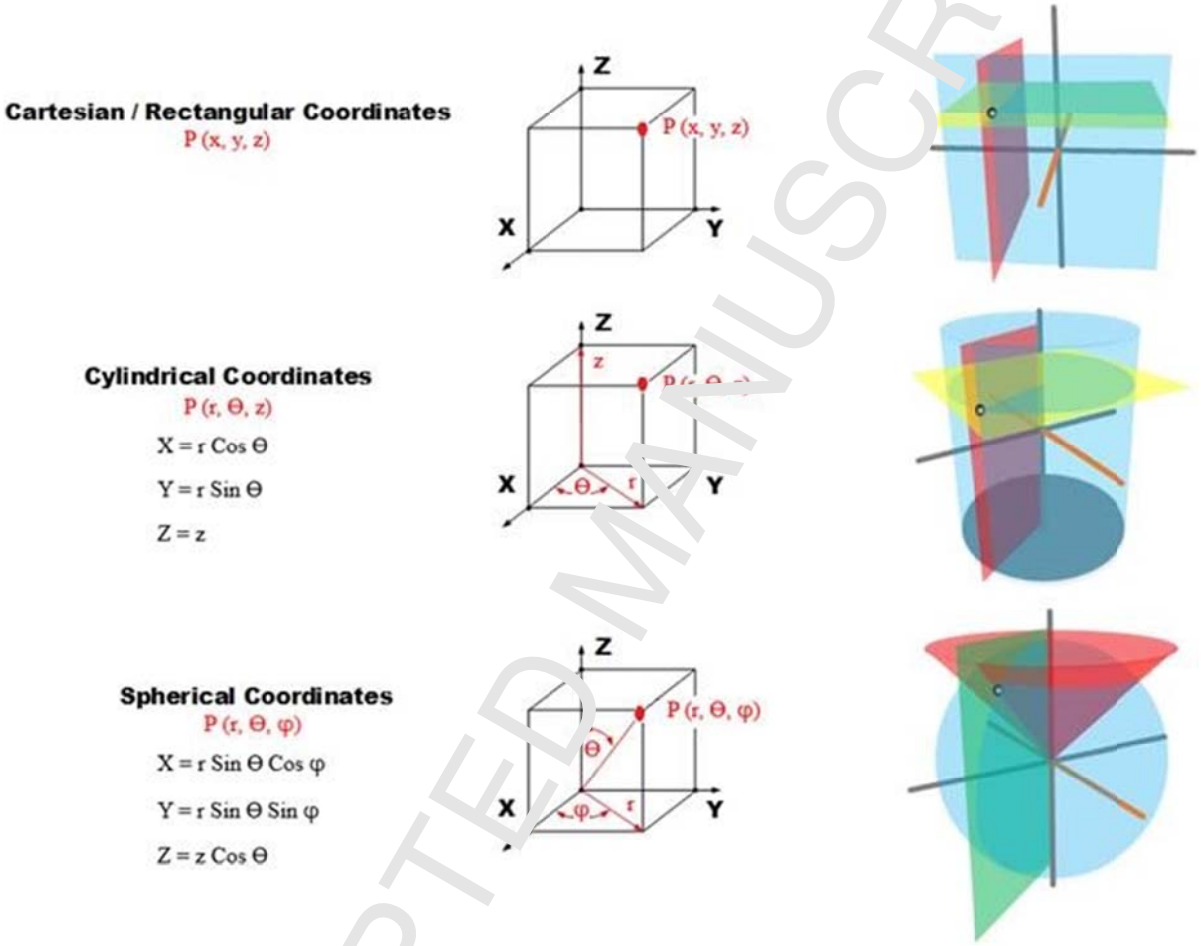

Figure 1 A. Cartesian, cylindrical, and spherical coordinate systems.

in Cartesian coordinate system:

Continuity:

$$\frac{\partial v_x}{\partial x}+\frac{\partial v_y}{\partial y}+\frac{\partial v_z}{\partial z}=0 \qquad (1\text{-A})$$

Momemtum in x direction:

$$\rho\left(\frac{\partial v_x}{\partial t}+v_x\frac{\partial v_x}{\partial x}+v_y\frac{\partial v_x}{\partial y}+v_z\frac{\partial v_x}{\partial z}\right)=-\frac{\partial p}{\partial x}+\mu\left(\frac{\partial^2 v_x}{\partial x^2}+\frac{\partial^2 v_x}{\partial y^2}+\frac{\partial^2 v_x}{\partial z^2}\right)+F_x \tag{2-A}$$

Momemtum in *y* direction:

$$\rho\left(\frac{\partial v_y}{\partial t}+u\frac{\partial v_y}{\partial x}+v\frac{\partial v_y}{\partial y}+w\frac{\partial v_y}{\partial z}\right)=-\frac{\partial p}{\partial y}+\mu\left(\frac{\partial^2 v_y}{\partial x^2}+\frac{\partial^2 v_y}{\partial y^2}+\frac{\partial^2 v_y}{\partial z^2}\right)+F_y \tag{3-A}$$

Momemtum in *z* direction:

$$\rho\left(\frac{\partial v_z}{\partial t}+u\frac{\partial v_z}{\partial x}+v\frac{\partial v_z}{\partial y}+w\frac{\partial v_z}{\partial z}\right)=-\frac{\partial p}{\partial z}+\mu\left(\frac{\partial^2 v_z}{\partial x^2}+\frac{\partial^2 v_z}{\partial y^2}+\frac{\partial^2 v_z}{\partial z^2}\right)+F_z \tag{4-A}$$

Energy equation:

$$\rho c_p\left(\frac{\partial T}{\partial t}+v_x\frac{\partial T}{\partial x}+v_y\frac{\partial T}{\partial y}+v_z\frac{\partial T}{\partial z}\right)= \frac{\partial}{\partial x}\left(k\frac{\partial T}{\partial x}\right)+\frac{\partial}{\partial y}\left(k\frac{\partial T}{\partial y}\right)+\frac{\partial}{\partial z}\left(k\frac{\partial T}{\partial z}\right)+\mu\Phi \tag{5-A}$$

Where

$$\Phi=2\left[\left(\frac{\partial v_x}{\partial x}\right)^2+\left(\frac{\partial v_y}{\partial y}\right)^2+\left(\frac{\partial v_z}{\partial z}\right)^2\right]+\left[\left(\frac{\partial v_x}{\partial y}+\frac{\partial v_y}{\partial x}\right)^2+\left(\frac{\partial v_y}{\partial z}+\frac{\partial v_z}{\partial y}\right)^2+\left(\frac{\partial v_z}{\partial x}+\frac{\partial v_x}{\partial z}\right)^2\right]-\frac{2}{3}\left(\frac{\partial v_x}{\partial x}+\frac{\partial v_y}{\partial y}+\frac{\partial v_z}{\partial z}\right)^2 \tag{6-A}$$

in Cylindrical coordinate system:

Continuity:

$$\frac{1}{r}\frac{\partial}{\partial r}\left(rv_r\right)+\frac{1}{r}\frac{\partial}{\partial\theta}\left(v_\theta\right)+\frac{\partial}{\partial z}\left(v_z\right)=0 \tag{7-A}$$

Momemtum in *r* direction:

$$\rho\left(\frac{\partial v_r}{\partial t}+v_r\frac{\partial v_r}{\partial r}+\frac{v_\theta}{r}\frac{\partial v_\theta}{\partial \theta}-\frac{v_\theta^2}{r}+v_z\frac{\partial v_r}{\partial \mathbf{z}}\right)= \tag{8-A}$$
$$-\frac{\partial p}{\partial r}+\mu\left[\frac{\partial}{\partial r}\left(\frac{1}{r}\frac{\partial}{\partial r}(rv_r)\right)+\frac{1}{r^2}\frac{\partial^2 v_r}{\partial \theta^2}-\frac{2}{r^2}\frac{\partial v_r}{\partial \theta}+\frac{\partial^2 v_r}{\partial z^2}\right]+F_r$$

Momemtum in θ direction:

$$\rho\left(\frac{\partial v_\theta}{\partial t}+v_r\frac{\partial v_\theta}{\partial r}+\frac{v_\theta}{r}\frac{\partial v_\theta}{\partial \theta}-\frac{v_r v_\theta}{r}+v_z\frac{\partial v_\theta}{\partial z}\right)= \tag{9-A}$$
$$\rho g_\theta-\frac{1}{r}\frac{\partial p}{\partial \theta}+\mu\left[\frac{\partial}{\partial r}\left(\frac{1}{r}\frac{\partial}{\partial r}(rv_\theta)\right)+\frac{1}{r^2}\frac{\partial^2 v_\theta}{\partial \theta^2}+\frac{2}{r^2}\frac{\partial v_r}{\partial \theta}+\frac{\partial^2 v_\theta}{\partial z^2}\right]+F_\theta$$

Momemtum in *z* direction:

$$\rho\left(\frac{\partial v_z}{\partial t}+v_r\frac{\partial v_z}{\partial r}+\frac{v_\theta}{r}\frac{\partial v_z}{\partial \theta}+v_z\frac{\partial v_z}{\partial z}\right)= \tag{10-A}$$
$$-\frac{\partial p}{\partial z}+\mu\left[\frac{1}{r}\frac{\partial}{\partial r}\left(r\frac{\partial v_z}{\partial r}\right)+\frac{1}{r^2}\frac{\partial^2 v_z}{\partial \theta^2}+\frac{\partial^2 v_z}{\partial z^2}\right]+F_z$$

Energy equation:

$$\rho c_P\left(\frac{\partial T}{\partial t}+v_r\frac{\partial T}{\partial r}+\frac{v_\theta}{r}\frac{\partial T}{\partial \theta}+v_z\frac{\partial T}{\partial z}\right)= \tag{11-A}$$
$$\left[\frac{1}{r}\frac{\partial}{\partial r}\left(k\,r\frac{\partial T}{\partial r}\right)+\frac{1}{r^2}\frac{\partial}{\partial \theta}\left(k\frac{\partial T}{\partial \theta}\right)+\frac{\partial}{\partial z}\left(k\frac{\partial T}{\partial z}\right)\right]+\mu\Phi$$

where:

$$\Phi=2\left(\frac{\partial v_r}{\partial r}\right)^2+2\left(\frac{1}{r}\frac{\partial v_\theta}{\partial \theta}+\frac{v_r}{r}\right)^2+2\left(\frac{\partial v_z}{\partial z}\right)^2+ \tag{12-A}$$
$$\left(\frac{\partial v_\theta}{\partial r}-\frac{v_\theta}{r}+\frac{1}{r}\frac{\partial v_r}{\partial \theta}\right)^2+\left(\frac{1}{r}\frac{\partial v_z}{\partial \theta}+\frac{\partial v_\theta}{\partial z}\right)^2+\left(\frac{\partial v_r}{\partial z}+\frac{\partial v_z}{\partial r}\right)^2$$

In spherical coordinate system:

Continuity:

$$\frac{\partial \rho}{\partial t}+\frac{1}{r^2}\frac{\partial}{\partial r}\left(\rho r^2 v_r\right)+\frac{1}{r\sin\theta}\frac{\partial}{\partial \theta}\left(\rho v_\theta \sin\theta\right)+\frac{1}{r\sin\theta}\frac{\partial}{\partial \varphi}\left(\rho v_\varphi\right)=0 \tag{13-A}$$

Momemtum in *r* direction:

$$\rho\left(\frac{\partial v_r}{\partial t}+v_r\frac{\partial v_r}{\partial r}+\frac{v_\theta}{r}\frac{\partial v_r}{\partial \theta}+\frac{v_\varphi}{r\sin\theta}\frac{\partial v_r}{\partial \varphi}-\frac{v_\theta^{\,2}+v_\phi^{\,2}}{r}\right)= \tag{14-A}$$
$$F_r-\frac{\partial p}{\partial r}+\mu\left(\nabla^2 v_r-\frac{2}{r^2}v_r-\frac{2}{r^2}\frac{\partial v_\theta}{\partial \theta}-\frac{2v_\theta\cot\theta}{r^2}-\frac{2}{r^2\sin\theta}\frac{\partial v_\varphi}{\partial \varphi}\right)$$

Momemtum in θ direction:

$$\rho\left(\frac{\partial v_\theta}{\partial t}+v_r\frac{\partial v_\theta}{\partial r}+\frac{v_\theta}{r}\frac{\partial v_\theta}{\partial \theta}-\frac{v_\varphi}{r\sin\theta}\frac{\partial v_\theta}{\partial \varphi}+\frac{v_r v_\theta}{r}-\frac{v_\varphi^{\,2}\cot\theta}{r}\right)= \tag{15-A}$$
$$F_\theta-\frac{1}{r}\frac{\partial p}{\partial \theta}+\mu\left(\nabla^2 v_\theta+\frac{2}{r^2}\frac{\partial v_r}{\partial \theta}-\frac{v_\theta}{r^2\sin^2\theta}-\frac{2\cos\theta}{r^2\sin^2\theta}\frac{\partial v_\varphi}{\partial \varphi}\right)$$

Momemtum in φ direction:

$$\rho\left(\frac{\partial v_\theta}{\partial t}+v_r\frac{\partial v_\varphi}{\partial r}+\frac{v_\theta}{r}\frac{\partial v_\varphi}{\partial \theta}+\frac{v_\varphi}{r\sin\theta}\frac{\partial v_\varphi}{\partial \varphi}+\frac{v_\varphi v_r}{r}+\frac{v_\theta v_\varphi}{r}\cot\theta\right)= \tag{16-A}$$
$$F_\varphi-\frac{1}{r\sin\theta}\frac{\partial p}{\partial \varphi}+$$
$$\mu\left(\nabla^2 v_\varphi-\frac{v_\varphi}{r^2\sin^2\theta}-\frac{2}{r^2\sin^2\theta}\frac{\partial v_r}{\partial \varphi}+\frac{2\cos\theta}{r^2\sin^2\theta}\frac{\partial v_\theta}{\partial \varphi}\right)$$

Energy equation:

$$\rho c_p\left(\frac{\partial T}{\partial t}+v_r\frac{\partial T}{\partial r}+\frac{v_\varphi}{r}\frac{\partial T}{\partial \varphi}+\frac{v_\theta}{r\sin\varphi}\frac{\partial T}{\partial \theta}\right)=\frac{1}{r^2}\frac{\partial}{\partial r}\left(k\,r^2\frac{\partial T}{\partial r}\right)+ \frac{1}{r^2\sin^2\theta}\frac{\partial}{\partial \varphi}\left(k\frac{\partial T}{\partial \varphi}\right)+\frac{1}{r^2\sin\theta}\frac{\partial}{\partial \theta}\left(k\sin\theta\frac{\partial T}{\partial \theta}\right)+\mu\Phi \tag{17-A}$$

where:

$$\Phi=2\left[\left(\frac{\partial v_r}{\partial r}\right)^2+\left(\frac{1}{r}\frac{\partial v_\varphi}{\partial \varphi}+\frac{v_r}{r}\right)^2+\left(\frac{1}{r\sin\varphi}\frac{\partial v_\theta}{\partial \theta}+\frac{v_r}{r}+\frac{v_\varphi\cot\varphi}{r}\right)^2\right]+ \left[r\frac{\partial}{\partial r}\left(\frac{v_\varphi}{r}\right)+\frac{1}{r}\frac{\partial v_r}{\partial \varphi}\right]^2+ \left[\frac{\sin\varphi}{r}\frac{\partial}{\partial \varphi}\left(\frac{v_\theta}{r\sin\varphi}\right)+\frac{1}{r\sin\varphi}\frac{\partial v_\theta}{\partial \theta}\right]^2+\left[\frac{1}{r\sin\varphi}\frac{\partial v_r}{\partial \varphi}+r\frac{\partial}{\partial r}\left(\frac{v_\theta}{r}\right)\right]^2 \tag{18-A}$$

References

[1] H. Masuda, A. Ebata, K. Teramae, N. Hishinuma, Alteration of Thermal Conductivity and Viscosity of Liquid by Dispersing Ultra-Fine Particles. Dispersion of Al_2O_3, SiO_2 and TiO_2 Ultra-Fine Particles, Netsu Bussei. 7 (1993) 227–233. doi:10.2963/jjtp.7.227.

[2] S.U.S. Choi, J.A. Eastman, Enhancing thermal conductivity of fluids with nanoparticles, ASME Int. Mech. Eng. Congr. Expo. 66 (1995) 99–105. doi:10.1115/1.1532008.

[3] A. Ghadimi, R. Saidur, H.S.C. Metselaar, A review of nanofluid stability properties and characterization in stationary conditions, Int. J. Heat Mass Transf. 54 (2011) 4051–4068. doi:10.1016/j.ijheatmasstransfer.2011.04.014.

[4] R. Saidur, K.Y. Leong, H.A. Mohammad, A review on applications and challenges of nanofluids, Renew. Sustain. Energy Rev. 15 (2011) 1646–1668. doi:10.1016/j.rser.2010.11.035.

[5] R. Taylor, S. Coulombe, T. Otanicar, P. Phelan, A. Gunawan, W. Lv, G. Rosengarten, R. Prasher, H. Tyagi, Small particles, big impacts: A review of the diverse applications of

nanofluids, J. Appl. Phys. 113 (2013). doi:10.1063/1.4754271.

[6] Z. Zhien, C. Jianchao, C. Feng, L. Hao, Z. Wenxian, Q. Wenjie, Progress in enhancement of CO_2 absorption by nanofluids: A mini review of mechanisms and current status, Renew. Energy. 118 (2018) 527–535. doi:10.1016/j.renene.2017.11.031.

[7] O. Mahian, A. Kianifar, S.Z. Heris, D. Wen, A.Z. Sahin, S. Wongwises, Nanofluids effects on the evaporation rate in a solar still equipped with a heat exchanger, Nano Energy. 36 (2017) 134–155. doi:10.1016/j.nanoen.2017.04.025.

[8] D.K. Devendiran, V.A. Amirtham, A review on preparation, characterization, properties and applications of nanofluids, Renew. Sustain. Energy Rev. 60 (2016) 21–40. doi:10.1016/j.rser.2016.01.055.

[9] G. Colangelo, E. Favale, M. Milanese, A. de Risi, D. Laforgia, Cooling of electronic devices: Nanofluids contribution, Appl. Therm. Eng. 127 (2017) 421–435. doi:10.1016/j.applthermaleng.2017.08.042.

[10] A. Kasaeian, A.T. Eshghi, M. Sameti, A review on the applications of nanofluids in solar energy systems, Renew. Sustain. Energy Rev. 43 (2015) 584–598. doi:10.1016/j.rser.2014.11.020.

[11] S. Rashidi, O. Mahian, E.M. Languri, Applications of nanofluids in condensing and evaporating systems: A review, J. Therm. Anal. Calorim. (2017). doi:10.1007/s10973-017-6773-7.

[12] S. Rashidi, M. Eskandarian, O. Mahian, S. Poncet, Combination of nanofluid and inserts for heat transfer enhancement, J. Therm. Anal. Calorim. (2018). doi:10.1007/s10973-018-7070-9.

[13] A. Kasaeian, R.D. Azarian, O. Mahian, L. Kolsi, A.J. Chamkha, S. Wongwises, I. Pop, Nanofluid flow and heat transfer in porous media: A review of the latest developments, Int. J. Heat Mass Transf. 107 (2017). doi:10.1016/j.ijheatmasstransfer.2016.11.074.

[14] M. Ramezanpour, M. Siavashi, Application of SiO_2–water nanofluid to enhance oil recovery: A new hybrid optimization approach using pattern search and PSO algorithms, J. Therm. Anal. Calorim. (2018) 1–16. doi:10.1007/s10973-018-7156-4.

[15] O. Mahian, A. Kianifar, A.Z. Sahin, S. Wongwises, Heat Transfer, Pressure Drop, and Entropy Generation in a Solar Collector Using SiO_2/Water Nanofluids: Effects of Nanoparticle Size and pH, J. Heat Transfer. 137 (2015). doi:10.1115/1.4029870.

[16] S.S. Meibodi, A. Kianifar, O. Mahian, S. Wongwises, Second law analysis of a nanofluid-based solar collector using experimental data, J. Therm. Anal. Calorim. 126 (2016) 617–625.

[17] A. Kasaeian, S.M. Hosseini, M. Sheikhpour, O. Mahian, W.M. Yan, S. Wongwises, Applications of eco-friendly refrigerants and nanorefrigerants: A review, Renew. Sustain. Energy Rev. 96 (2018) 91–99. doi:10.1016/j.rser.2018.07.033.

[18] M.S. Kamel, F. Lezsovits, A.M. Hussein, O. Mahian, S. Wongwises, Latest developments in boiling critical heat flux using nanofluids: A concise review, Int. Commun. Heat Mass Transf. 98 (2018) 59–66. doi:https://doi.org/10.1016/j.icheatmasstransfer.2018.08.009.

[19] O. Mahian, A. Kianifar, S.A. Kalogirou, I. Pop, S. Wongwises, A review of the applications of nanofluids in solar energy, Int. J. Heat Mass Transf. 57 (2013) 582–594. doi:10.1016/j.ijheatmasstransfer.2012.10.037.

[20] W. Daungthongsuk, S. Wongwises, A critical review of convective heat transfer of nanofluids, Renew. Sustain. Energy Rev. 11 (2007) 797–817. doi:10.1016/j.rser.2005.06.005.

[21] J. Buongiorno, Convective Transport in Nanofluids, J. Heat Transfer. 128 (2006) 240. doi:10.1115/1.2150834.

[22] M. Sheikholeslami, D.D. Ganji, eds., Front matter, in: Appl. Nanofluid Heat Transf. Enhanc., William Andrew Publishing, 2017: p. iii-. doi:https://doi.org/10.1016/B978-0-08-102172-9.00011-3.

[23] M.R. Safaei, A. Jahanbin, A. Kianifar, S. Gharehkhani, A.S. Kherbeet, M. Goodarzi, M. Dahari, Mathematical Modeling for Nanofluids Simulation: A Review of the Latest Works, in: N.S. Akbar, O.A. Beg (Eds.), Model. Simul. Eng. Sci., InTech, Rijeka, 2016. doi:10.5772/64154.

[24] M. Bahiraei, A Comprehensive Review on Different Numerical Approaches for Simulation in Nanofluids: Traditional and Novel Techniques, J. Dispers. Sci. Technol. 35 (2014) 984–996. doi:10.1080/01932691.2013.825210.

[25] N.A.C. Sidik, M.N.A.W.M. Yazid, S. Samion, M.N. Musa, R. Mamat, Latest development on computational approaches for nanofluid flow modeling: Navier-Stokes based multiphase models, Int. Commun. Heat Mass Transf. 74 (2016) 114–124. doi:10.1016/j.icheatmasstransfer.2016.03.007.

[26] S.M. Vanaki, P. Ganesan, H.A. Mohammed, Numerical study of convective heat transfer of nanofluids: A review, Renew. Sustain. Energy Rev. 54 (2016) 1212–1239. doi:10.1016/j.rser.2015.10.042.

[27] S. Kakaç, A. Pramuanjaroenkij, Single-phase and two-phase treatments of convective heat transfer enhancement with nanofluids - A state-of-the-art review, Int. J. Therm. Sci. 100 (2016) 75–97. doi:10.1016/j.ijthermalsci.2015.09.021.

[28] G. Ahmadi, J.B. McLaughlin, Transport, Deposition and Removal of Fine Particles - Biomedical Applications, in: E. Matijević (Ed.) Med. Appl. Colloids, Springer US, New York, NY, 2008: pp. 92–173. doi:10.1007/978-0-387-76921-9_4.

[29] J.S. Marshall, S. Li, Adhesive Particle Flow: A Discrete-Element Approach, Cambridge University Press, 2014. doi:10.1017/CBO9781139424547.

[30] R. Clift, J.R. Grace, M.E. Weber, Bubbles, Drops, and Particles, Academic Press, 1978. https://books.google.co.th/books?id=n8gKAQAAIAAJ.

[31] G. Sekrani, S. Poncet, P. Proulx, Conjugated heat transfer and entropy generation of Al2O3--water nanofluid flows over a heated wall-mounted obstacle, J. Therm. Anal. Calorim. (2018). doi:10.1007/s10973-018-7340-x.

[32] M.A. E. Cunningham, On the velocity of steady fall of spherical particles through fluid medium, Proc. R. Soc. London A Math. Phys. Eng. Sci. 83 (1910) 357–365. doi:10.1098/rspa.1910.0024.

[33] H. Brenner, The slow motion of a sphere through a viscous fluid towards a plane surface, Chem. Eng. Sci. 16 (1961) 242–251. doi:10.1016/0009-2509(61)80035-3.

[34] P.G. Saffman, The lift on a small sphere in a slow shear flow, J. Fluid Mech. 22 (1965) 385–400. doi:10.1017/S0022112065000824.

[35] P.G. Saffman, Corrigendum to "The lift force on a small sphere in a slow shear flow.," J. Fluid Mech. (1968).

[36] S.I. Rubinow, J.B. Keller, The transverse force on a spinning sphere moving in a viscous fluid, J. Fluid Mech. 11 (1961) 447–459. doi:10.1017/S0022112061000640.

[37] O. Mahian, A. Kianifar, A.Z. Sahin, S. Wongwises, Performance analysis of a minichannel-based solar collector using different nanofluids, Energy Convers. Manag. 88 (2014) 129–138. doi:10.1016/j.enconman.2014.08.021.

[38] R.I.A.V.P.L.S. Robert Brown, XXVII. A brief account of microscopical observations made in the months of June, July and August 1827, on the particles contained in the pollen of plants; and on the general existence of active molecules in organic and inorganic bodies, Philos. Mag. 4 (1828) 161–173. doi:10.1080/14786442808674769.

[39] E.E.S. Michaelides, Heat and Mass Transfer in Particulate Suspensions, Springer-Verlag New York, 2013.

[40] A. Li, G. Ahmadi, Dispersion and deposition of spherical particles from point sources in a turbulent channel flow, Aerosol Sci. Technol. 16 (1992) 209–226. doi:10.1080/02786829208959550.

[41] A. Einstein, Über die von der molekularkinetischen Theorie der Wärme geforderte Bewegung von in ruhenden Flüssigkeiten suspendierten Teilchen, Ann. Phys. 322 (1905) 549–560. doi:10.1002/andp.19053220806.

[42] M. von Smoluchowski, Zur kinetischen Theorie der Brownschen Molekularbewegung und der Suspensionen, Ann. Phys. 326 (1906) 756–780. doi:10.1002/andp.19063261405.

[43] O. Abouali, A. Nikbakht, G. Ahmadi, S. Saadabadi, Three-dimensional simulation of Brownian motion of nano-particles in aerodynamic lenses, Aerosol Sci. Technol. 43 (2009) 205–215. doi:10.1080/02786820802587888.

[44] E.E. Michaelides, Transport properties of nanofluids. A critical review, J. Non-Equilibrium Thermodyn. 38 (2013) 1–79. doi:10.1515/jnetdy-2012-0023.

[45] P.S. Epstein, Zur Theorie des Radiometers, Zeitschrift Für Phys. 54 (1929) 537–563. doi:10.1007/BF01338485.

[46] J.R. Brock, On the theory of thermal forces acting on aerosol particles, J. Colloid Sci. 17 (1962) 768–780. doi:10.1016/0095-8522(62)90051-X.

[47] L. Talbot, R.K. Cheng, R.W. Schefer, D.R. Willis, Thermophoresis of particles in a heated boundary layer, J. Fluid Mech. 101 (1980) 737–758. doi:10.1017/S0022112080001905.

[48] C. He, G. Ahmadi, Particle Deposition with Thermophoresis in Laminar and Turbulent Duct Flows, Aerosol Sci. Technol. 29 (1998) 525–546. doi:10.1080/02786829808965588.

[49] E.E. Michaelides, Brownian movement and thermophoresis of nanoparticles in liquids, Int. J. Heat Mass Transf. 81 (2015) 179–187. doi:10.1016/j.ijheatmasstransfer.2014.10.019.

[50] S. Savithiri, A. Pattamatta, S.K. Das, Scaling analysis for the investigation of slip mechanisms in nanofluids, Nanoscale Res. Lett. 6 (2011) 1–13. doi:10.1186/1556-276X-6-471.

[51] S. Elghobashi, On predicting particle-laden turbulent flows, Appl. Sci. Res. 52 (1994) 309–329. doi:10.1007/BF00936835.

[52] C.T. Crowe, J.D. Schwarzkopf, M. Sommerfeld, Y. Tsuji, Multiphase Flow with Droplets and Particles, CRC Press Taylor Fr. Gr. (2011) 209.

[53] C. Tropea, A.L. Yarin, J.F. Foss, Springer Handbook of Experimental Fluid Mechanics, AIAA J. 46 (2007) 2653–2655. doi:10.2514/1.38773.

[54] J.N. Israelachvili, Intermolecular and Surface Forces: Third Edition, 2011. doi:10.1016/C2011-0-05119-0.

[55] D. Guo, G. Xie, J. Luo, Mechanical properties of nanoparticles: Basics and applications, J. Phys. D. Appl. Phys. 47 (2014). doi:10.1088/0022-3727/47/1/013001.

[56] H.C. Hamaker, The London-van der Waals attraction between spherical particles, Physica. 4 (1937) 1058–1072.

[57] R. Hogg, T.W. Healy, D.W. Fuerstenau, Mutual coagulation of colloidal dispersions, Trans.

Faraday Soc. 62 (1966) 1638–1651.

[58] J.A. Lewis, Colloidal Processing of Ceramics, J. Am. Ceram. Soc. 83 (n.d.) 2341–2359. doi:10.1111/j.1151-2916.2000.tb01560.x.

[59] L.P. Aoki, H.E. Schulz, M.G. Maunsell, An MHD Study of the Behavior of an Electrolyte Solution using 3D Numerical Simulation and Experimental results, in: Proceeding COMSOL Conf., 2013: pp. 1–7. doi:10.13140/2.1.1398.6082.

[60] A.A. Doinikov, Radiation force due to a spherical sound field on a rigid sphere in a viscous fluid, J. Acoust. Soc. Am. 96 (1994) 3100–3105. doi:10.1121/1.410247.

[61] M. Settnes, H. Bruus, Forces acting on a small particle in an acoustical field in a viscous fluid, Phys. Rev. E - Stat. Nonlinear, Soft Matter Phys. 85 (2012). doi:10.1103/PhysRevE.85.016327.

[62] Y. Zhao, J.S. Marshall, Spin coating of a colloidal suspension, Phys. Fluids. 20 (2008) 43302. doi:10.1063/1.2896601.

[63] J.D.S. Efstathios Michaelides, Clayton T. Crowe ed., Multiphase Flow Handbook, Second, CRC Press, 2016.

[64] C. Jin, I. Potts, M.W. Reeks, A simple stochastic quadrant model for the transport and deposition of particles in turbulent boundary layers, Phys. Fluids. 27 (2015). doi:10.1063/1.4921490.

[65] K. Khanafer, K. Vafai, A critical synthesis of thermophysical characteristics of nanofluids, Int. J. Heat Mass Transf. 54 (2011) 4410–4428. doi:10.1016/j.ijheatmasstransfer.2011.04.048.

[66] J.C. Maxwell, A treatise on electricity and magnetism Vol.II, Oxford Clarendon Press. (1873) 360–366. doi:10.1016/0016-0032(54)90053-8.

[67] Bruggema, D.A.G. N. Berechnung von verschiedener physikalischer Konstanten von Heterogener Substanzen, Ann. Phys. 24 (1935) 636–664. doi:10.1115/1.4006796.

[68] R.L. Hamilton, Thermal conductivity of heterogeneous two-component systems, Ind. Eng. Chem. Fundam. 1 (1962) 187–191. doi:10.1021/i160003a005.

[69] W. Yu, S.U.S. Choi, The role of interfacial layers in the enhanced thermal conductivity of nanofluids: A renovated Maxwell model, J. Nanoparticle Res. 5 (2003) 167–171. doi:10.1023/A:1024438603801.

[70] Y. Xuan, Q. Li, W. Hu, Aggregation structure and thermal conductivity of nanofluids, AIChE J. 49 (2003) 1038–1043. doi:10.1002/aic.690490420.

[71] J. Koo, C. Kleinstreuer, A new thermal conductivity model for nanofluids, J. Nanoparticle Res. 6 (2004) 577–588. doi:10.1007/s11051-004-3170-5.

[72] U. Lee, J. (NC State University, Raleigh, NC, Computational analysis of nanofluid flow in microchannels with applications to micro-heat sinks and bio-MEMS, NC State University, Raleigh, NC, USA, 2008.

[73] Y. Feng, C. Kleinstreuer, Nanofluid convective heat transfer in a parallel-disk system, Int. J. Heat Mass Transf. 53 (2010) 4619–4628. doi:10.1016/j.ijheatmasstransfer.2010.06.031.

[74] Z. Xu, C. Kleinstreuer, Concentration photovoltaic-thermal energy co-generation system using nanofluids for cooling and heating, Energy Convers. Manag. 87 (2014) 504–512. doi:10.1016/j.enconman.2014.07.047.

[75] C.-W. Nan, R. Birringer, D.R. Clarke, H. Gleiter, Effective thermal conductivity of particulate composites with interfacial thermal resistance, J. Appl. Phys. 81 (1997) 6692–6699. doi:10.1063/1.365209.

[76] R. Prasher, P. Bhattacharya, P.E. Phelan, Thermal conductivity of nanoscale colloidal solutions (nanofluids), Phys. Rev. Lett. 94 (2005). doi:10.1103/PhysRevLett.94.025901.

[77] S.K. Das H.E. Patel, T. Pradeep, T. Sundararajan, A. Dasgupta, N. Dasgupta, A microconvection model for thermal conductivity of nanofluid, Pramana-Journal Phys. 65 (2005) 863–869.

[78] A. Amiri, K. Vafai, Analysis of dispersion effects and non-thermal equilibrium, non-Darcian, variable porosity incompressible flow through porous media, Int. J. Heat Mass Transf. 37 (1994) 939–954. doi:10.1016/0017-9310(94)90219-4.

[79] K. Khanafer, K. Vafai, M. Lightstone, Buoyancy-driven heat transfer enhancement in a two-dimensional enclosure utilizing nanofluids, Int. J. Heat Mass Transf. 46 (2003) 3639–3653. doi:10.1016/S0017-9310(03)00156-X.

[80] Q.Z. Xue, Model for thermal conductivity of carbon nanotube-based composites, Phys. B Condens. Matter. 368 (2005) 302–307. doi:10.1016/j.physb.2005.07.024.

[81] H.E. Patel, K.B. Anoop, T. Sundararajan, S.K. Das, Model for thermal conductivity of CNT-nanofluids, in: Bull. Mater. Sci., 2008: pp. 387–390. doi:10.1007/s12034-008-0060-y.

[82] C.-W. Nan, G. Liu, Y. Lin, M. Li, Interface effect on thermal conductivity of carbon nanotube composites, Appl. Phys. Lett. 85 (2004) 3549–3551. doi:10.1063/1.1808874.

[83] B. Lamas, B. Abreu, A. Fonseca, N. Martins, M. Oliveira, Critical analysis of the thermal conductivity models for CNT based nanofluids, Int. J. Therm. Sci. 78 (2014) 65–76. doi:10.1016/j.ijthermalsci.2013.11.017.

[84] S.M.S. Murshed, K.C. Leong, C. Yang, Investigations of thermal conductivity and viscosity of nanofluids, Int. J. Therm. Sci. 47 (2008) 560–568. doi:10.1016/j.ijthermalsci.2007.05.004.

[85] S.M.S. Murshed, C.A. Nieto De Castro, Superior thermal features of carbon nanotubes-based nanofluids - A review, Renew. Sustain. Energy Rev. 37 (2014) 155–167. doi:10.1016/j.rser.2014.05.017.

[86] P. Estellé, S. Halelfadl, T. Maré, Thermal Conductivity of CNT Water Based Nanofluids: Experimental Trends and Models Overview, J. Therm. Enginnering. 1 (2015) 381–390. doi:10.13140/2.1.2173.9841.

[87] S. El Bécaye Maïga, S.J. Palm, C.T. Nguyen, G. Roy, N. Galanis, Heat transfer enhancement by using nanofluids in forced convection flows, Int. J. Heat Fluid Flow. 26 (2005) 530–546. doi:10.1016/j.ijheatfluidflow.2005.02.004.

[88] M. Corcione, Heat transfer features of buoyancy-driven nanofluids inside rectangular enclosures differentially heated at the sidewalls, Int. J. Therm. Sci. 49 (2010) 1536–1546. doi:10.1016/j.ijthermalsci.2010.05.005.

[89] C.H. Chon, K.D. Kihm, S.P. Lee, S.U.S. Choi, Empirical correlation finding the role of temperature and particle size for nanofluid (Al_2O_3) thermal conductivity enhancement, Appl. Phys. Lett. 87 (2005) 1–3. doi:10.1063/1.2093936.

[90] C.J. Ho, W.K. Liu, Y.S. Chang, C.C. Lin, Natural convection heat transfer of alumina-water nanofluid in vertical square enclosures: An experimental study, Int. J. Therm. Sci. 49 (2010) 1345–1353. doi:10.1016/j.ijthermalsci.2010.02.013.

[91] K. V Sharma, P.K. Sarma, W.H. Azmi, R. Mamat, K. Kadirgama, Correlations To Predict Friction and Forced Convection Heat Transfer Coefficients of Water Based Nanofluids for Turbulent Flow in a Tube, Int. J. Microscale Nanoscale Therm. Fluid Transp. Phenomena, Suppl. Spec. Issue Heat Mass Transf. Nanofluids; Hauppauge. 3 (2012) 283–307.

[92] W.H. Azmi, K. V. Sharma, R. Mamat, S. Anuar, Turbulent forced convection heat transfer of nanofluids with twisted tape insert in a plain tube, in: Energy Procedia, 2014: pp. 296–307. doi:10.1016/j.egypro.2014.07.081.

[93] G. Zyła, J. Fal, Experimental studies on viscosity, thermal and electrical conductivity of aluminum nitride-ethylene glycol (AlN-EG) nanofluids, Thermochim. Acta. 637 (2016) 11–16. doi:10.1016/j.tca.2016.05.006.

[94] G. Zyła, Thermophysical properties of ethylene glycol based yttrium aluminum garnet ($Y_3Al_5O_{12}$-EG) nanofluids, Int. J. Heat Mass Transf. 92 (2016) 751–756. doi:10.1016/j.ijheatmasstransfer.2015.09.045.

[95] G. Żyła, J. Fal, Viscosity, thermal and electrical conductivity of silicon dioxide–ethylene glycol transparent nanofluids. An experimental studies, Thermochim. Acta. 650 (2017) 106–113. doi:10.1016/j.tca.2017.02.001.

[96] G. Żyła, J. Fal, J. Traciak, M. Gizowska, K. Perkowski, Huge thermal conductivity enhancement in boron nitride – ethylene glycol nanofluids, Mater. Chem. Phys. 180 (2016) 250–255. doi:10.1016/j.matchemphys.2016.06.003.

[97] G. Żyła, J. Fal, P. Estellé, The influence of ash content on thermophysical properties of ethylene glycol based graphite/diamonds mixture nanofluids, Diam. Relat. Mater. 74 (2017) 81–89.

doi:10.1016/j.diamond.2017.02.008.

[98] G. Żyła, J. Fal, P. Estellé, Thermophysical and dielectric profiles of ethylene glycol based titanium nitride (TiN–EG) nanofluids with various size of particles, Int. J. Heat Mass Transf. 113 (2017) 1189–1199. doi:10.1016/j.ijheatmasstransfer.2017.06.032.

[99] G. Żyła, J.P. Vallejo, J. Fal, L. Lugo, Nanodiamonds – Ethylene Glycol nanofluids: Experimental investigation of fundamental physical properties, Int. J. Heat Mass Transf. 121 (2018) 1201–1213. doi:10.1016/j.ijheatmasstransfer.2018.01.07[illegible]

[100] M.H. Ahmadi, M.A. Ahmadi, M.A. Nazari, O. Mahian, R. Ghasempour, A proposed model to predict thermal conductivity ratio of Al_2O_3/EG nanofluid by applying least squares support vector machine (LSSVM) and genetic algorithm as a connectionist approach, J. Therm. Anal. Calorim. (2018). doi:10.1007/s10973-018-7035-z.

[101] M. Hemmat Esfe, S. Saedodin, M. Bahiraei, D. Toghraie, O. Mahian, S. Wongwises, Thermal conductivity modeling of MgO/EG nanofluids using experimental data and artificial neural network, J. Therm. Anal. Calorim. 118 (2014). doi:10.1007/s10973-014-4002-1.

[102] M. Hemmat Esfe, P.M. Behbahani, A.A.A. Arani, M.R. Sarlak, Thermal conductivity enhancement of SiO_2–MWCNT (85:15 %)- EG hybrid nanofluids□: ANN designing, experimental investigation, cost performance and sensitivity analysis, J. Therm. Anal. Calorim. 128 (2017) 249–258. doi:10.1007/s10973-016-5893-9.

[103] M. Hemmat Esfe, H. Rostamian, D. Toghraie, W.-M. Yan, Using artificial neural network to predict thermal conductivity of ethylene glycol with alumina nanoparticle, J. Therm. Anal. Calorim. (2016) 1–6. doi:10.1007/s10973-016-5506-7.

[104] M. Vakili, M. Karami, S. Delfani, S. Khosrojerdi, K. Kalhor, Experimental investigation and modeling of thermal conductivity of CuO–water/EG nanofluid by FFBP-ANN and multiple regressions, J. Therm. Anal. Calorim. 129 (2017) 629–637. doi:10.1007/s10973-017-6217-4.

[105] M.H. Esfe, S. Saedodin, O. Mahian, S. Wongwises, Thermal conductivity of Al_2O_3/water nanofluids. Measurement, correlation, sensitivity analysis, and comparisons with literature reports, J. Therm. Anal. Calorim. 117 (2014). doi:10.1007/s10973-014-3771-x.

[106] M. Hemmat Esfe, S. Saedodin, O. Mahian, S. Wongwises, Thermophysical properties, heat transfer and pressure drop of COOH-functionalized multi walled carbon nanotubes/water nanofluids, Int. Commun. Heat Mass Transf. 58 (2014). doi:10.1016/j.icheatmasstransfer.2014.08.037.

[107] M. Hemmat Esfe, S. Saedodin, O. Mahian, S. Wongwises, Heat transfer characteristics and pressure drop of of COOH-functionalized DWCNTs/water nanofluid in turbulent flow at low concentrations, Int. J. Heat Mass Transf. 73 (2014). doi:10.1016/j.ijheatmasstransfer.2014.01.069.

[108] M. Amani, P. Amani, A. Kasaeian, O. Mahian, S. Wongwises, Thermal conductivity measurement of spinel-type ferrite $MnFe_2O_4$ nanofluids in the presence of a uniform magnetic field, J. Mol. Liq. 230 (2017) 121–128. doi:10.1016/j.molliq.2016.12.013.

[109] M. Amani, P. Amani, A. Kasaeian, O. Mahian, I. Pop, S. Wongwises, Modeling and optimization of thermal conductivity and viscosity of $MnFe_2O_4$ nanofluid under magnetic field using an ANN, Sci. Rep. 7 (2017) 17369. doi:10.1038/s41598-017-17444-5.

[110] S.M.S. Murshed, K.C. Leong, C. Yang, Enhanced thermal conductivity of TiO_2- Water based nanofluids, Int. J. Therm. Sci. 44 (2005) 367–373. doi:10.1016/j.ijthermalsci.2004.12.005.

[111] A. Turgut, I. Tavman, M. Chirtoc, H.P. Schuchmann, C. Sauter, S. Tavman, Thermal Conductivity and Viscosity Measurements of Water-Based TiO_2 Nanofluids, Int. J. Thermophys. 30 (2009) 1213–1226. doi:10.1007/s10765-009-0594-2.

[112] S. Wang, Y. Li, H. Zhang, Y. Lin, Z. Li, W. Wang, Q. Wu, Y. Qian, H. Hong, C. Zhi, Enhancement of thermal conductivity in water-based nanofluids employing TiO_2 reduced graphene oxide composites, J. Mater. Sci. 51 (2016) 10104–10115. doi:10.1007/s10853-016-0239-3.

[113] M. Zadkhast, D. Toghraie, A. Karimipour, Developing a new correlation to estimate the thermal conductivity of MWCNT-CuO/water hybrid nanofluid via an experimental investigation, J. Therm. Anal. Calorim. 129 (2017) 859–867. doi:10.1007/s10973-017-6213-8.

[114] P.K. Singh, D. Khandelwal, C. Sidhant, A. Shubham, N. Priyanshu, G. Rasu, Nanofluid heat

transfer mechanism and thermo-physical properties: A review, Int. J. Mech. Eng. Technol. 8 (2017) 156–164.

[115] K.Y. Leong, K.Z. Ku Ahmad, H.C. Ong, M.J. Ghazali, A. Baharum, Synthesis and thermal conductivity characteristic of hybrid nanofluids – A review, Renew. Sustain. Energy Rev. 75 (2017) 868–878. doi:10.1016/j.rser.2016.11.068.

[116] A. Kotia, S. Borkakoti, P. Deval, S.K. Ghosh, Review of interfacial layer's effect on thermal conductivity in nanofluid, Heat Mass Transf. Und Stoffuebertragung. 53 (2017) 2199–2209. doi:10.1007/s00231-016-1963-6.

[117] M.I. Pryazhnikov, A. V Minakov, V.Y. Rudyak, D. V Guzei, Thermal conductivity measurements of nanofluids, Int. J. Heat Mass Transf. 104 (2017) 1275–1282. doi:10.1016/j.ijheatmasstransfer.2016.09.080.

[118] P.C. Mishra, S.K. Nayak, S. Mukherjee, Thermal Conductivity of Nanofluids-An Extensive Literature Review, Int. J. Eng. Res. Technol. 2 (2013) 734–745.

[119] H. Younes, G. Christensen, D. Li, H. Hong, A. Al Ghaferi, Thermal Conductivity of Nanofluids: Review, J. Nanofluids. 4 (2015) 107–132. doi:10.1166/jon.2015.1151.

[120] P.M. Kumar, J. Kumar, R. Tamilarasan, S. Sendhilnathan, S. Suresh, Review on nanofluids theoretical thermal conductivity models, Eng. J. 19 (2015) 67–83. doi:10.4186/ej.2015.19.1.67.

[121] S.A. Angayarkanni, J. Philip, Review on thermal properties of nanofluids: Recent developments, Adv. Colloid Interface Sci. 225 (2015) 146–176. doi:10.1016/j.cis.2015.08.014.

[122] M.H. Ahmadi, A. Mirlohi, M.A. Nazari, R. Ghasempour, A review of thermal conductivity of various nanofluids, J. Mol. Liq. 265 (2018) 181–188. doi:https://doi.org/10.1016/j.molliq.2018.05.124.

[123] C. Kleinstreuer, Y. Feng, Experimental and theoretical studies of nanofluid thermal conductivity enhancement: a review, Nanoscale Res. Lett. 6 (2011) 439. doi:10.1186/1556-276X-6-439.

[124] H.C. Birkman, The viscosity of concentrated suspensions and solution, J. Chem. Phys. 20

(1952) 571. doi:doi: 10.1063/1.1700493.

[125] I.M. Krieger, T.J. Dougherty, A Mechanism for Non□Newtonian Flow in Suspensions of Rigid Spheres, Trans. Soc. Rheol. 3 (1959) 137–152. doi:10.1122/1.548848.

[126] S.H. Maron, P.E. Pierce, Application of ree-eyring generalized flow theory to suspensions of spherical particles, J. Colloid Sci. 11 (1956) 80–95. doi:10.1016/0095-8522(56)90023-X.

[127] S. Halelfadl, P. Estellé, B. Aladag, N. Doner, T. Maré, Viscosity of carbon nanotubes water-based nanofluids: Influence of concentration and temperature, Int. J. Therm. Sci. 71 (2013) 111–117. doi:10.1016/j.ijthermalsci.2013.04.013.

[128] H. Chen, Y. Ding, C. Tan, Rheological behaviour of nanofluids, New J. Phys. 9 (2007). doi:10.1088/1367-2630/9/10/367.

[129] J. Chevalier, O. Tillement, F. Ayela, Structure and rheology of SiO_2 nanoparticle suspensions under very high shear rates, Phys. Rev. E - Stat. Nonlinear, Soft Matter Phys. 80 (2009). doi:10.1103/PhysRevE.80.051403.

[130] N. Masoumi, N. Sohrabi, A. Behzadmehr, A new model for calculating the effective viscosity of nanofluids, J. Phys. D. Appl. Phys. 42 (2009). doi:10.1088/0022-3727/42/5/055501.

[131] P.K. Singh, K.B. Anoop, T. Sundararajan, S.K. Das, Entropy generation due to flow and heat transfer in nanofluids, Int. J. Heat Mass Transf. 53 (2010) 4757–4767. doi:10.1016/j.ijheatmasstransfer.2010.06.016.

[132] U. Rea, T. McKrell, L. Wen Hu, J. Buongiorno, Laminar convective heat transfer and viscous pressure loss of alumina-water and zirconia-water nanofluids, Int. J. Heat Mass Transf. 52 (2009) 2042–2048. doi:10.1016/j.ijheatmasstransfer.2008.10.025.

[133] W. Williams, J. Buongiorno, L.-W. Hu, Experimental Investigation of Turbulent Convective Heat Transfer and Pressure Loss of Alumina/Water and Zirconia/Water Nanoparticle Colloids (Nanofluids) in Horizontal Tubes, J. Heat Transfer. 130 (2008) 42412. doi:10.1115/1.2818775.

[134] S.P. Jang, J.Y. Lee, K.S. Hwang, S.U.S. Choi, Particle concentration and tube size dependence of viscosities of Al_2O_3 -water nanofluids flowing through micro- and minitubes, Appl. Phys.

Lett. 91 (2007). doi:10.1063/1.2824393.

[135] K. Bashirnezhad, S. Bazri, M.R. Safaei, M. Goodarzi, M. Dahari, O. Mahian, A.S. Dalkiliça, S. Wongwises, Viscosity of nanofluids: A review of recent experimental studies, Int. Commun. Heat Mass Transf. 73 (2016) 114–123. doi:10.1016/j.icheatmasstransfer.2016.02.005.

[136] S.M.S. Murshed, P. Estellé, A state of the art review on viscosity of nanofluids, Renew. Sustain. Energy Rev. 76 (2017) 1134–1152. doi:10.1016/j.rser.2017.03.113.

[137] J.P. Meyer, S.A. Adio, M. Sharifpur, P.N. Nwosu, The Viscosity of Nanofluids: A Review of the Theoretical, Empirical, and Numerical Models, Heat Transf. Eng. 37 (2016) 387–421. doi:10.1080/01457632.2015.1057447.

[138] H.D. Koca, S. Doganay, A. Turgut, I.H. Tavman, R. Saidur, I.M. Mahbubul, Effect of particle size on the viscosity of nanofluids: A review, Renew. Sustain. Energy Rev. 82 (2018) 1664–1674. doi:10.1016/j.rser.2017.07.016.

[139] M. Amani, P. Amani, A. Kasaeian, O. Mahian, F. Kasaeian, S. Wongwises, Experimental study on viscosity of spinel-type manganese ferrite nanofluid in attendance of magnetic field, J. Magn. Magn. Mater. 428 (2017) 457–463.

[140] T. Yiamsawas, A.S. Dalkilic, O. Mahian, S. Wongwises, Measurement and Correlation of the Viscosity of Water-Based Al_2O_3 and TiO_2 Nanofluids in High Temperatures and Comparisons with Literature Reports, J. Dispers. Sci. Technol. 34 (2013) 1697–1703. doi:10.1080/01932691.2013.764403.

[141] T. Yiamsawas, O. Mahian, A.S. Dalkilic, S. Kaewnai, S. Wongwises, Experimental studies on the viscosity of TiO2 and Al2O3 nanoparticles suspended in a mixture of ethylene glycol and water for high temperature applications, Appl. Energy. 111 (2013) 40–45. doi:10.1016/j.apenergy.2013.04.068.

[142] G.M. Moldoveanu, A.A. Minea, M. Iacob, C. Ibanescu, M. Danu, Experimental study on viscosity of stabilized Al_2O_3 , TiO_2 nanofluids and their hybrid, Thermochim. Acta. 659 (2018). doi:10.1016/j.tca.2017.12.008.

[143] G.M. Moldoveanu, C. Ibanescu, M. Danu, A.A. Minea, Viscosity estimation of Al_2O_3 , SiO_2

nanofluids and their hybrid: An experimental study, J. Mol. Liq. 253 (2018). doi:10.1016/j.molliq.2018.01.061.

[144] G. Zyła, M. Cholewa, On unexpected behavior of viscosity of diethylene glycol-based MgAl2O4nanofluids, RSC Adv. 4 (2014) 26057–26062. doi:10.1039/c4ra03143a.

[145] O. Mahian, A. Kianifar, C. Kleinstreuer, M.A. Al-Nimr, I. Pop, A.Z. Sahin, S. Wongwises, A review of entropy generation in nanofluid flow, Int. J. Heat Mass Transf. 65 (2013). doi:10.1016/j.ijheatmasstransfer.2013.06.010.

[146] P. Estellé, D. Cabaleiro, G. Żyła, L. Lugo, S.M.S. Murshed, Current trends in surface tension and wetting behavior of nanofluids, Renew. Sustain. Energy Rev. 94 (2018) 931–944. doi:https://doi.org/10.1016/j.rser.2018.07.006.

[147] N. Ahammed, L.G. Asirvatham, S. Wongwises, Effect of volume concentration and temperature on viscosity and surface tension of graphene-water nanofluid for heat transfer applications, J. Therm. Anal. Calorim. 123 (2016). doi:10.1007/s10973-015-5034-x.

[148] D. Cabaleiro, P. Estellé, H. Navas, A. Desforges, B. Vigolo, Dynamic Viscosity and Surface Tension of Stable Graphene Oxide and Reduced Graphene Oxide Aqueous Nanofluids, J. Nanofluids. 7 (2018) 1081–1088. doi:10.1166/jon.2018.1539.

[149] J. Chinnam, D.K. Das, R.S. Vajjha, S.R. Satti, Measurements of the surface tension of nanofluids and development of a new correlation, Int. J. Therm. Sci. 98 (2015) 68–80. doi:10.1016/j.ijthermalsci.2015.07.008.

[150] O. Mahian, A. Kianifar, A.Z. Sahin, S. Wongwises, Entropy generation during Al_2O_3/water nanofluid flow in a solar collector: Effects of tube roughness, nanoparticle size, and different thermophysical models, Int. J. Heat Mass Transf. 78 (2014). doi:10.1016/j.ijheatmasstransfer.2014.06.051.

[151] O. Mahian, A. Mahmud, S. Zeinali Heris, Effect of Uncertainties in Physical Properties on Entropy Generation Between Two Rotating Cylinders With Nanofluids, J. Heat Transfer. 134 (2012) 101704. doi:10.1115/1.4006662.

[152] O. Mahian, A. Kianifar, S.Z. Heris, S. Wongwises, Natural convection of silica nanofluids in

square and triangular enclosures: Theoretical and experimental study, Int. J. Heat Mass Transf. 99 (2016). doi:10.1016/j.ijheatmasstransfer.2016.03.045.

[153] E. Abu-Nada, A.J. Chamkha, Effect of nanofluid variable properties on natural convection in enclosures filled with a CuO-EG-Water nanofluid, Int. J. Therm. Sci. 49 (2010) 2339–2352. doi:10.1016/j.ijthermalsci.2010.07.006.

[154] E. Abu-Nada, Effects of variable viscosity and thermal conductivity of Al_2O_3-water nanofluid on heat transfer enhancement in natural convection, Int. J. Heat Fluid Flow. 30 (2009) 679–690. doi:10.1016/j.ijheatfluidflow.2009.02.003.

[155] G. Saha, M.C. Paul, Investigation of the characteristics of nanofluids flow and heat transfer in a pipe using a single phase model, Int. Commun. Heat Mass Transf. 93 (2018) 48–59. doi:https://doi.org/10.1016/j.icheatmasstransfer.2018.02.001.

[156] H. Demir, A.S. Dalkilic, N.A. Kürekci, W. Duangthongsuk, S. Wongwises, Numerical investigation on the single phase forced convection heat transfer characteristics of TiO_2 nanofluids in a double-tube counter flow heat exchanger, Int. Commun. Heat Mass Transf. 38 (2011) 218–228. doi:10.1016/j.icheatmasstransfer.2010.12.009.

[157] P.K. Namburu, D.K. Das, K.M. Tanguturi, R.S. Vajjha, Numerical study of turbulent flow and heat transfer characteristics of nanofluids considering variable properties, Int. J. Therm. Sci. 48 (2009) 290–302. doi:10.1016/j.ijthermalsci.2008.01.001.

[158] M.K. Moraveji, M. Darabi, S.M.H. Haddad, R. Davarnejad, Modeling of convective heat transfer of a nanofluid in the developing region of tube flow with computational fluid dynamics, Int. Commun. Heat Mass Transf. 38 (2011) 1291–1295. doi:10.1016/j.icheatmasstransfer.2011.06.011.

[159] O. Manca, S. Nardini, D. Ricci, A numerical study of nanofluid forced convection in ribbed channels, Appl. Therm. Eng. 37 (2012) 280–292. doi:10.1016/j.applthermaleng.2011.11.030.

[160] M.A. Ahmed, M.M. Yaseen, M.Z. Yusoff, Numerical study of convective heat transfer from tube bank in cross flow using nanofluid, Case Stud. Therm. Eng. 10 (2017) 560–569. doi:10.1016/j.csite.2017.11.002.

[161] R.S. Vajjha, D.K. Das, P.K. Namburu, Numerical study of fluid dynamic and heat transfer performance of Al_2O_3 and CuO nanofluids in the flat tubes of a radiator, Int. J. Heat Fluid Flow. 31 (2010) 613–621. doi:10.1016/j.ijheatfluidflow.2010.02.016.

[162] O. Abouali, G. Ahmadi, Computer simulations of natural convection of single phase nanofluids in simple enclosures: A critical review, Appl. Therm. Eng. 36 (2012) 1–13. doi:10.1016/j.applthermaleng.2011.11.065.

[163] Y. Xuan, W. Roetzel, Conceptions for heat transfer correlation of nanofluids, Int. J. Heat Mass Transf. 43 (2000) 3701–3707. doi:10.1016/S0017-9310(99)00369-5.

[164] M.S. Mojarrad, A. Keshavarz, A. Shokouhi, Nanofluids thermal behavior analysis using a new dispersion model along with single-phase, Heat Mass Transf. Und Stoffuebertragung. 49 (2013). doi:10.1007/s00231-013-1182-3.

[165] M. Bahiraei, S.M. Hosseinalipour, Thermal Dispersion Model Compared with Euler-Lagrange Approach in Simulation of Convective Heat Transfer for Nanoparticle Suspensions, J. Dispers. Sci. Technol. 34 (2013) 1778–1789. doi:10.1080/01932691.2012.751339.

[166] M. Amani, P. Amani, A. Kasaeian, O. Mahian, W.-M. Yan, Two-phase mixture model for nanofluid turbulent flow and heat transfer: Effect of heterogeneous distribution of nanoparticles, Chem. Eng. Sci. 167 (2017). doi:10.1016/j.ces.2017.03.065.

[167] Y. Ding, D. Wen, Particle migration in a flow of nanoparticle suspensions, Powder Technol. 149 (2005) 84–92. doi:10.1016/j.powtec.2004.11.012.

[168] S. Kumar, S.K. Prasad, J. Banerjee, Analysis of flow and thermal field in nanofluid using a single phase thermal dispersion model, Appl. Math. Model. 34 (2010) 573–592. doi:10.1016/j.apm.2009.06.026.

[169] S. Özerinç, A.G. Yazıcıoğlu, S. Kakaç, Numerical analysis of laminar forced convection with temperature-dependent thermal conductivity of nanofluids and thermal dispersion, in: Int. J. Therm. Sci., 2012: pp. 138–148. doi:10.1016/j.ijthermalsci.2011.10.007.

[170] S.Z. Heris, M.N. Esfahany, G. Etemad, Numerical investigation of nanofluid laminar convective heat transfer through a circular tube, Numer. Heat Transf. Part A Appl. 52 (2007)

1043–1058. doi:10.1080/10407780701364411.

[171] M. Ameri, M. Amani, P. Amani, Thermal performance of nanofluids in metal foam tube: Thermal dispersion model incorporating heterogeneous distribution of nanoparticles, Adv. Powder Technol. 28 (2017) 2747–2755. doi:10.1016/j.apt.2017.07.028.

[172] M. Bahiraei, S.I. Vasefi, A novel thermal dispersion model to improve prediction of nanofluid convective heat transfer, Adv. Powder Technol. 25 (2014) 1772–1779 doi:10.1016/j.apt.2014.07.005.

[173] M. Bahiraei, S.M. Hosseinalipour, Accuracy enhancement of thermal dispersion model in prediction of convective heat transfer for nanofluids considering the effects of particle migration, Korean J. Chem. Eng. 30 (2013) 1552–1558. doi:10.1007/s11814-013-0087-7.

[174] F. Akbaridoust, M. Rakhsha, A. Abbassi, M. Saffar-Avval, Experimental and numerical investigation of nanofluid heat transfer in helically coiled tubes at constant wall temperature using dispersion model, Int. J. Heat Mass Transf. 58 (2013) 480–491. doi:https://doi.org/10.1016/j.ijheatmasstransfer.2012.11.064.

[175] M. Sheikholeslami, D.D. Ganji, M.M. Rashidi, Magnetic field effect on unsteady nanofluid flow and heat transfer using Buongiorno model, J. Magn. Magn. Mater. 416 (2016) 164–173. doi:10.1016/j.jmmm.2016.05.026.

[176] M. Sheikholeslami, H.B. Rokni, Effect of melting heat transfer on nanofluid flow in existence of magnetic field considering Buongiorno Model, Chinese J. Phys. 55 (2017) 1115–1126. doi:10.1016/j.cjph.2017.04.019.

[177] F. Garoosi, L. Jahanshaloo, M.M. Rashidi, A. Badakhsh, M.E. Ali, Numerical simulation of natural convection of the nanofluid in heat exchangers using a Buongiorno model, Appl. Math. Comput. 254 (2015) 183–203. doi:10.1016/j.amc.2014.12.116.

[178] F. Garoosi, F. Garoosi, K. Hooman, Numerical simulation of natural convection and mixed convection of the nanofluid in a square cavity using Buongiorno model, Powder Technol. 268 (2014) 279–292. doi:10.1016/j.powtec.2014.08.006.

[179] A. Malvandi, S.A. Moshizi, E.G. Soltani, D.D. Ganji, Modified Buongiorno's model for fully

developed mixed convection flow of nanofluids in a vertical annular pipe, Comput. Fluids. 89 (2014) 124–132. doi:10.1016/j.compfluid.2013.10.040.

[180] A. Malvandi, D.D. Ganji, Mixed convective heat transfer of water/alumina nanofluid inside a vertical microchannel, Powder Technol. 263 (2014) 37–44. doi:https://doi.org/10.1016/j.powtec.2014.04.084.

[181] N. Shehzad, A. Zeeshan, R. Ellahi, K. Vafai, Convective heat transfer of nanofluid in a wavy channel: Buongiorno's mathematical model, J. Mol. Liq. 222 (2016) 446–455. doi:10.1016/j.molliq.2016.07.052.

[182] M.A. Sheremet, I. Pop, Conjugate natural convection in a square porous cavity filled by a nanofluid using Buongiorno's mathematical model, Int. J. Heat Mass Transf. 79 (2014) 137–145. doi:10.1016/j.ijheatmasstransfer.2014.07.092.

[183] Z. Zhang, Q. Chen, Comparison of the Eulerian and Lagrangian methods for predicting particle transport in enclosed spaces, Atmos. Environ. 41 (2007) 5236–5248. doi:10.1016/j.atmosenv.2006.05.086.

[184] S. Kakaç, A. Pramuanjaroenkij, Analysis of Convective Heat Transfer Enhancement by Nanofluids: Single-Phase and Two-Phase Treatments, J. Eng. Phys. Thermophys. 89 (2016) 758–793. doi:10.1007/s10891-016-1437-1.

[185] M. Akbari, N. Galanis, A. Behzadmehr, Comparative analysis of single and two-phase models for CFD studies of nanofluid heat transfer, Int. J. Therm. Sci. 50 (2011) 1343–1354. doi:10.1016/j.ijthermalsci.2011.03.008.

[186] P. Naphon, L. Nakharintr, Turbulent two phase approach model for the nanofluids heat transfer analysis flowing through the minichannel heat sinks, Int. J. Heat Mass Transf. 82 (2015) 388–395. doi:10.1016/j.ijheatmasstransfer.2014.11.024.

[187] M.M. Rashidi, A. Hosseini, I. Pop, S. Kumar, N. Freidoonimehr, Comparative numerical study of single and two-phase models of nanofluid heat transfer in wavy channel, Appl. Math. Mech. (English Ed.) 35 (2014) 831–848. doi:10.1007/s10483-014-1839-9.

[188] R. Davarnejad, M. Jamshidzadeh, CFD modeling of heat transfer performance of MgO-water

nanofluid under turbulent flow, Eng. Sci. Technol. an Int. J. 18 (2015) 536–542. doi:10.1016/j.jestch.2015.03.011.

[189] M. Manninen, V. Taivassalo, S. Kallio, On the mixture model for multiphase flow, Vtt Publ. (1996) 1–67.

[190] L. Schiller, Z. Naumann, A drag coefficient correlation, Z.Ver.Deutsch.Ing. 77 (1933) 318–320. doi:10.1016/j.ijheatmasstransfer.2009.02.006.

[191] S.A. Morsi, A.J. Alexander, An investigation of particle trajectories in two-phase flow systems, J. Fluid Mech. 55 (1972) 193–208. doi:10.1017/S0022112072001806.

[192] M. Nuim Labib, M.J. Nine, H. Afrianto, H. Chung, H. Jeong, Numerical investigation on effect of base fluids and hybrid nanofluid in forced convective heat transfer, Int. J. Therm. Sci. 71 (2013) 163–171. doi:10.1016/j.ijthermalsci.2013.04.003.

[193] H. Safikhani, A. Abbassi, A. Khalkhali, M. Kalteh, Modeling and Optimization of Nanofluid Flow in Flat Tubes Using a Combination of CFD and Response Surface Methodology, Heat Transf. Res. (2014) n/a-n/a. doi:10.1002/htj.21125.

[194] A. Moghadassi, E. Ghomi, F. Parvizian, A numerical study of water based Al_2O_3 and Al_2O_3–Cu hybrid nanofluid effect on forced convective heat transfer, Int. J. Therm. Sci. 92 (2015) 50–57.

[195] S. Mirmasoumi, A. Behzadmehr, Numerical study of laminar mixed convection of a nanofluid in a horizontal tube using two-phase mixture model, Appl. Therm. Eng. 28 (2008) 717–727. doi:10.1016/j.applthermaleng.2007.06.019.

[196] M. Goodarzi, M.R. Safaei, K. Vafai, G. Ahmadi, M. Dahari, S.N. Kazi, N. Jomhari, Investigation of nanofluid mixed convection in a shallow cavity using a two-phase mixture model, Int. J. Therm. Sci. 75 (2014) 204–220. doi:10.1016/j.ijthermalsci.2013.08.003.

[197] M. Siavashi, M. Jamali, Heat transfer and entropy generation analysis of turbulent flow of TiO_2-water nanofluid inside annuli with different radius ratios using two-phase mixture model, Appl. Therm. Eng. 100 (2016) 1149–1160. doi:10.1016/j.applthermaleng.2016.02.093.

[198] M. Siavashi, H.R. Talesh Bahrami, H. Saffari, Numerical investigation of flow characteristics,

heat transfer and entropy generation of nanofluid flow inside an annular pipe partially or completely filled with porous media using two-phase mixture model, Energy. 93 (2015). doi:10.1016/j.energy.2015.10.100.

[199] M. Siavashi, H.R. Talesh Bahrami, E. Aminian, Optimization of heat transfer enhancement and pumping power of a heat exchanger tube using nanofluid with gradient and multi-layered porous foams, Appl. Therm. Eng. 138 (2018) 465–474. doi:10.1016/j.applthermaleng.2018.04.066.

[200] M. Siavashi, H.R.T. Bahrami, H. Saffari, Numerical investigation of porous rib arrangement on heat transfer and entropy generation of nanofluid flow in an annulus using a two-phase mixture model, Numer. Heat Transf. Part A Appl. 71 (2017) 1251–1271. doi:10.1080/10407782.2017.1345270.

[201] M.H. Toosi, M. Siavashi, Two-phase mixture numerical simulation of natural convection of nanofluid flow in a cavity partially filled with porous media to enhance heat transfer, J. Mol. Liq. 238 (2017) 553–569. doi:10.1016/j.molliq.2017.05.015.

[202] R. Yaghoubi Emami, M. Siavashi, G. Shahriari Moghaddam, The effect of inclination angle and hot wall configuration on Cu-water nanofluid natural convection inside a porous square cavity, Adv. Powder Technol. 29 (2018) 519–536. doi:10.1016/j.apt.2017.10.027.

[203] M. Siavashi, R. Yousofvand, S. Rezanejad, Nanofluid and porous fins effect on natural convection and entropy generation of flow inside a cavity, Adv. Powder Technol. 29 (2018) 142–156. doi:10.1016/j.apt.2017.10.021.

[204] M. Siavashi, A. Rostami, Two-phase simulation of non-Newtonian nanofluid natural convection in a circular annulus partially or completely filled with porous media, Int. J. Mech. Sci. 133 (2017) 689–703. doi:10.1016/j.ijmecsci.2017.09.031.

[205] M.K. Moraveji, R.M. Ardehali, CFD modeling (comparing single and two-phase approaches) on thermal performance of Al_2O_3/water nanofluid in mini-channel heat sink, Int. Commun. Heat Mass Transf. 44 (2013) 157–164. doi:10.1016/j.icheatmasstransfer.2013.02.012.

[206] M. Shariat, R.M. Moghari, A. Akbarinia, R. Rafee, S.M. Sajjadi, Impact of nanoparticle mean

diameter and the buoyancy force on laminar mixed convection nanofluid flow in an elliptic duct employing two phase mixture model, Int. Commun. Heat Mass Transf. 50 (2014) 15–24. doi:10.1016/j.icheatmasstransfer.2013.11.003.

[207] P. Maghsoudi, M. Siavashi, Application of nanofluid and optimization of pore size arrangement of heterogeneous porous media to enhance mixed convection inside a two-sided lid-driven cavity, J. Therm. Anal. Calorim. (2018) 1–15. doi:10.1007/s10973-018-7335-3.

[208] R.M.C. Mourad Rebay, Sadik Kakaç, Microscale and Nanoscale Heat Transfer: Analysis, Design, and Application, 1st ed., CRC Press, 2016.

[209] C.Y. Wen, Y.H. Yu, Mechanics of fluidization, Chem. Eng. Progress, Symp. Ser. 62 (1966) 100–111. doi:10.1016/S0032-0633(98)00014-2.

[210] M. Kalteh, A. Abbassi, M. Saffar-Avval, J. Harting, Eulerian-Eulerian two-phase numerical simulation of nanofluid laminar forced convection in a microchannel, Int. J. Heat Fluid Flow. 32 (2011) 107–116. doi:10.1016/j.ijheatfluidflow.2010.08.001.

[211] W.E. Ranz, W.R. Marshall, Evaporation from drops - Part 1, Chem. Eng. Prog. 48 (1952) 141–148. doi:10.1016/S0924-7963(01)00032-X.

[212] O.A. Beg, M.M. Rashidi, M. Akbari, A. Hosseini, Comparative Numerical Study of Single-Phase and Two-Phase Models for Bio-Nanofluid Transport Phenomena, J. Mech. Med. Biol. 14 (2014) 1450011. doi:10.1142/S0219519414500110.

[213] R. Lotfi, Y. Saboohi, A.M. Rashidi, Numerical study of forced convective heat transfer of Nanofluids: Comparison of different approaches, Int. Commun. Heat Mass Transf. 37 (2010) 74–78. doi:10.1016/j.icheatmasstransfer.2009.07.013.

[214] M. Hejazian, M.K. Moraveji, A. Beheshti, Comparative study of Euler and mixture models for turbulent flow of Al_2O_3 nanofluid inside a horizontal tube, Int. Commun. Heat Mass Transf. 52 (2014) 152–158. doi:10.1016/j.icheatmasstransfer.2014.01.022.

[215] A. Sabaghan, M. Edalatpour, M.C. Moghadam, E. Roohi, H. Niazmand, Nanofluid flow and heat transfer in a microchannel with longitudinal vortex generators: Two-phase numerical simulation, Appl. Therm. Eng. 100 (2016) 179–189. doi:10.1016/j.applthermaleng.2016.02.020.

[216] E. Ebrahimnia-Bajestan, M. Charjouei Moghadam, H. Niazmand, W. Daungthongsuk, S. Wongwises, Experimental and numerical investigation of nanofluids heat transfer characteristics for application in solar heat exchangers, Int. J. Heat Mass Transf. 92 (2016) 1041–1052. doi:10.1016/j.ijheatmasstransfer.2015.08.107.

[217] I. Behroyan, P. Ganesan, S. He, S. Sivasankaran, Turbulent forced convection of Cu-water nanofluid: CFD model comparison, Int. Commun. Heat Mass Transf. 67 (2015) 163–172. doi:10.1016/j.icheatmasstransfer.2015.07.014.

[218] S. Rashidi, J.A. Esfahani, R. Ellahi, Convective heat transfer and particle motion in an obstructed duct with two side by side obstacles by means of DPM model, Appl. Sci. 7 (2017). doi:10.3390/app7040431.

[219] Y. He, Y. Men, Y. Zhao, H. Lu, Y. Ding, Numerical investigation into the convective heat transfer of TiO_2 nanofluids flowing through a straight tube under the laminar flow conditions, Appl. Therm. Eng. 29 (2009) 1965–1972. doi:10.1016/j.applthermaleng.2008.09.020.

[220] V. Bianco, F. Chiacchio, O. Manca, S. Nardini, Numerical investigation of nanofluids forced convection in circular tubes, Appl. Therm. Eng. 29 (2009) 3632–3642. doi:10.1016/j.applthermaleng.2009.05.013.

[221] M. Bahiraei, A numerical study of heat transfer characteristics of CuO-water nanofluid by Euler-Lagrange approach, J. Therm. Anal. Calorim. 123 (2016) 1591–1599. doi:10.1007/s10973-015-5019-9.

[222] M. Bahiraei, Studying nanoparticle distribution in nanofluids considering the effective factors on particle migration and determination of phenomenological constants by Eulerian-Lagrangian simulation, Adv. Powder Technol. 26 (2015) 802–810. doi:10.1016/j.apt.2015.02.005.

[223] N. Kumar, B.P. Puranik, Numerical study of convective heat transfer with nanofluids in turbulent flow using a Lagrangian-Eulerian approach, Appl. Therm. Eng. (2016).

[224] M. Bahiraei, M. Hangi, A. Monavari, Assessment of hydrothermal characteristics of Mn-Zn ferrite nanofluid as a functional material under quadrupole magnetic field, Powder Technol. 305 (2017) 174–182. doi:10.1016/j.powtec.2016.10.009.

[225] S.E. Ghasemi, A.A. Ranjbar, M.J. Hosseini, Numerical study on the convective heat transfer of nanofluid in a triangular minichannel heat sink using the Eulerian–Eulerian two-phase model, Numer. Heat Transf. Part A Appl. 72 (2017) 185–196. doi:10.1080/10407782.2017.1358990.

[226] S. Sonawane, U. Bhandarkar, B. Puranik, Modeling Forced Convection Nanofluid Heat Transfer Using an Eulerian–Lagrangian Approach, J. Therm. Sci. Eng. Appl. 8 (2016) 31001. doi:10.1115/1.4032734.

[227] J. Rostami, A. Abbassi, Conjugate heat transfer in a wavy microchannel using nanofluid by two-phase Eulerian-Lagrangian method, Adv. Powder Technol. 27 (2016) 9–18. doi:10.1016/j.apt.2015.10.003.

[228] S. Rashidi, M. Bovand, J. Abolfazli Esfahani, G. Ahmadi, Discrete particle model for convective AL_2O_3-water nanofluid around a triangular obstacle, Appl. Therm. Eng. 100 (2016) 39–54. doi:10.1016/j.applthermaleng.2016.01.076.

[229] M. Bovand, S. Rashidi, G. Ahmadi, J.A. Esfahani, Effects of trap and reflect particle boundary conditions on particle transport and convective heat transfer for duct flow - A two-way coupling of Eulerian-Lagrangian model, Appl. Therm. Eng. 108 (2016) 368–377. doi:10.1016/j.applthermaleng.2016.07.124.

[230] M. Keshavarz Moraveji, E. Esmaeili, Comparison between single-phase and two-phases CFD modeling of laminar forced convection flow of nanofluids in a circular tube under constant heat flux, Int. Commun. Heat Mass Transf. 39 (2012) 1297–1302. doi:10.1016/j.icheatmasstransfer.2012.07.012.

[231] M. Akbari, N. Galanis, A. Behzadmehr, Comparative assessment of single and two-phase models for numerical studies of nanofluid turbulent forced convection, Int. J. Heat Fluid Flow. 37 (2012) 136–146. doi:10.1016/j.ijheatfluidflow.2012.05.005.

[232] A. Albojamal, K. Vafai, Analysis of single phase, discrete and mixture models, in predicting nanofluid transport, Int. J. Heat Mass Transf. 114 (2017) 225–237. doi:10.1016/j.ijheatmasstransfer.2017.06.030.

[233] M. Bahiraei, A numerical study of heat transfer characteristics of CuO–water nanofluid by

Euler–Lagrange approach, J. Therm. Anal. Calorim. 123 (2016) 1591–1599. doi:10.1007/s10973-015-5031-0.

[234] S. Göktepe, K. Atalık, H. Ertürk, Comparison of single and two-phase models for nanofluid convection at the entrance of a uniformly heated tube, Int. J. Therm. Sci. 80 (2014) 83–92. doi:10.1016/j.ijthermalsci.2014.01.014.

[235] M. Hejazian, M.K. Moraveji, A Comparative Analysis of Single and Two-Phase Models of Turbulent Convective Heat Transfer in a Tube for TiO_2 Nanofluid with CFD, Numer. Heat Transf. Part A Appl. 63 (2013) 795–806. doi:10.1080/10407782.2013.756759.

[236] M. Hejazian, M.K. Moraveji, A. Beheshti, Comparative Numerical Investigation on TiO_2/Water Nanofluid Turbulent Flow by Implementation of Single Phase and Two Phase Approaches, Numer. Heat Transf. Part A Appl. 66 (2014) 330–348. doi:10.1080/10407782.2013.873271.

[237] M. Haghshenas Fard, M.N. Esfahany, M.R. Talaie, Numerical study of convective heat transfer of nanofluids in a circular tube two-phase model versus single-phase model, Int. Commun. Heat Mass Transf. 37 (2010) 91–97. doi:10.1016/j.icheatmasstransfer.2009.08.003.